

**GDR1 GEOMECH**

*Directed by Olivier Millet and François Nicot*

**Multi-Physics and Multiscale Couplings in  
Geo-environmental Mechanics**

**Workshop on multiscaled approaches  
towards degradation, damage and  
aging in geomaterials**

*Organised by Frédéric Grondin and Pierre-Yves Hicher*

*Nantes, January 23-24 2017*

**Book of extended abstracts**

**Edited by Pierre-Yves Hicher and Pearl-Angelika Lee**



## **Workshop GDRI GeoMech**

**Nantes, 23-24 January 2017**

The GDRI (Groupement De Recherche International) GeoMech was created in January 2016, in the immediate aftermath of the GDR MeGe. For 8 years, the GDR assembled the main French research groups involved in the broad field of geomechanics, with a special focus on environmental applications.

Benefitting from different collaborations and connections that the partners had developed with foreign academic and research institutions, it was a natural step to extend the network to an international level. The goal of the new network (GDRI) is thus to promote the research possibilities of the French community in geomechanics and to strengthen its national and international visibility.

Today, the GDRI GeoMech is composed of more than 25 partners from many countries including Netherland, Italy, Spain, Canada and China.

Within the existing community working on Multi-Physics and Multiscaled Couplings in Geo-environmental Mechanics, the main lines of research are:

- Catastrophic failures and triggering mechanisms
- Safety of storage reservoirs
- Energetic geomechanics.

The aim of the GDRI is to collect and to share state of the art research information on geomechanical subjects by extending international collaborations through the organisation of bi-annual international scientific meetings and other related events.

In this context, the first international workshop organised in Nantes (France) presented the following programme:

## **Multi-scaled approaches towards degradation, damage and aging in geomaterials (soil, rock, concrete)**

The durability of geostructures, be they natural sites or constructions in the environment, and of civil engineering materials and structures, all require a scientific approach which takes into account the coupling of multi-physical phenomena, i.e. thermo-hydro-chemico-mechanical coupling, at different scales. As time evolves, the processes of aging in a material at the nano or micro-structural scale will have an impact on the mechanical behaviour of the structures at their elemental scale. The aim of this workshop was therefore to confront experimental approaches, theoretical developments and multi-scaled numerical methods.

With a focus upon the microstructure of natural materials such as soils and rocks as well as man-made materials such as cement, a special focus was given to the mechanisms of degradation, the onset and development of damage, all of which can lead to the propagation of fractures within quasi fragile materials, and to the erosion of geotechnical constructions under the effect of the circulating pore fluids.

With more than 50 attendees, coming from 7 different countries, and 22 oral presentations giving rise to extremely stimulating discussions, this first international workshop was a real success.

In acknowledgment of their organisation of this event, the directors of the GDRI GeoMech would like to express their high gratitude to Professors Pierre-Yves Hicher and Frederic Grondin.

The following set of extended abstracts constitutes an up-to-date picture of the research activities of the GDRI, spanning the different scales of interest from the elementary grain to the structures.

This piece of work will contribute to an excellent promotion of the GDRI over the forthcoming years!

Olivier Millet & François Nicot

Directors of GDRI GeoMech

# Contents

E. E. ALONSO and M. TAPIAS

Degradation of coarse granular aggregates

X. LI

The stress-strain behaviour of granular materials at the meso-scale

C. ZHAO, Z.Y. YIN and P.Y. HICHER

Numerical modelling of geotechnical problems based on a static micromechanical approach

A.P.S. SELVADURAI

Stress-induced permeability evolution in a heterogeneous rock

Ö. DINÇ and L. SCHOLTÈS

Failure processes and damage evolution in transversely isotropic rocks by DEM

H. SOULI

The effect of chemical solutions upon the hydromechanical properties and the structure of two clays

A. WAUTIER, S. BONELLI and F. NICOT

Mechanical stability of granular materials subjected to suffusion

L.H. LUU, P. PHILIPPE, G. NOURY, J. PERRIN and O. BRIVOIS

Numerical modelling of sinkhole formation by means of a coupled LBM-DEM model

L. SIBILLE, F. LOMINÉ, I. G. TEJADA, B. CHAREYRE and D. MAROT

Soil erosion by suffusion: various attempts at describing different mechanisms

J. YANG, Z.Y. YIN, P.Y. HICHER and F. LAOUAFA

Numerical modelling of the hydro-mechanical internal erosion process

R. WAN and J. DURIEZ

Micromechanical aspects of partially saturated granular media with reference to capillary and effective stresses

G. SCIARRA, F. CASINI and J. VAUNAT

Modelling gravity-driven segregation in porous media by a phase field approach to unsaturated poromechanics

J. DESRUES

First results from a new tomographic survey of early localisation in triaxial tests on sand

J. SANAHUJA and S. HUANG

Influence of microstructural evolutions on macroscopic mechanical behaviour: contributions of mean-field homogenisation

V.Q. TRAN and A. SOIVE

The advantages of using a geochemical transport model to simulate the durability of concretes exposed to seawater and sulphates

M. ACHOUR, O. AMIRI, F. BIGNONNET and E. ROZIÈRE

Modelling the coupling of chloride and carbonation in concrete

S.Y. ALAM and A. LOUKILI

Transition from energy dissipative processes to displacement discontinuities during concrete failure

B. HILLOULIN, D. HILLOULIN, A. SOIVE, M. MATALLAH, F. GRONDIN, A. LOUKILI

Multi-scale modelling of healing mechanism in cementitious materials

F. DELL'ISOLA

Modelling mechanical interactions in granular media with generalised continua: towards granular metamaterials

# Degradation of coarse granular aggregates

E. E. Alonso and M. Tapias

Civil Engineering School, UPC, Barcelona  
eduardo.alonso@upc.edu

## Introduction. Lessons from simple tests

A fundamental mechanism capable of explaining the stress-strain-time behaviour of gravels and rockfill is the breakage of particles under external stress and the subsequent re-arrangement of the granular structure. When the external stress increase or, equivalently, when the irreversible work input increases, the initial grain size distribution evolves towards stable configurations. This phenomenon was illustrated by the results of oedometer tests on a singular coarse granular material: an aggregation of sugar cubes. Their regular geometry (a parallelepiped) allows preparing samples of widely different void ratios. The cubes are made of welded saccharose crystals having mean dimensions of the order of 1 mm. Therefore, the samples tested are an example of a gap-graded material made of two different sizes: the sugar cube (27.4 x 17.6 x 12.2 mm) and the saccharose crystal. When testing in the oedometer samples of widely different void ratios ( $e=0.78$ ;  $e=0.18$ ) under vertical stresses of 400-600 kPa, a most unexpected result was to obtain a common grain size distribution (gsd) (Figure 1). Moreover, the final gsd was a combination of two ‘degraded’ curves, each one of them starting at the initial grain size of the two ‘particles’ defining the aggregate: the ‘big’ sugar cube and the small saccharose crystal.

The results highlight the relevance of a final gsd attractor, which is independent of the initial soil structure even for extremely different granular arrangements.

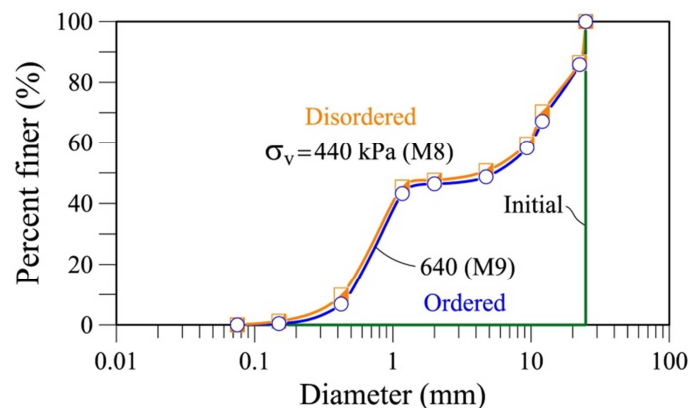


Figure 1. Grain size distributions at the maximum vertical stress of two samples of sugar cubes.

The set of tests performed (Tapias et al, 2016) was also useful to reach other conclusions very relevant for the understanding of breakage mechanisms and its effect at the larger scale of aggregates of individual particles.

They are summarized as follows:

- Two breakage mechanisms are identified: local crushing around contacts and particle splitting
- A unified breakage mechanism explains load-induced and time-induced gsd evolution.

## Suction controlled oedometer and triaxial tests on gravels

Oldecop and Alonso (2001); Chavez and Alonso (2003) and Alonso et al (2016) describe a series of large diameter (25 cm – 30 cm) oedometer and triaxial tests on two lithologies: a quartzitic slate used in the construction of Lechago Dam (Alonso et al, 2011) and a hard limestone ballast-like aggregate. Figure 2 shows the results of multistage triaxial tests on compacted limestone gravels equilibrated at two Relative Humidities,  $RH = 100\%$  and  $RH = 50\%$ . The plots show the relevance of volumetric yielding and the shape of the yield locus in  $[p=(\sigma_1+2\sigma_3)/3; q=\sigma_1-\sigma_3]$  triaxial space. Note also the effect of applied suction to enhance the dilatant behaviour of this soil. The rest of tests performed revealed a few additional features of rockfill behaviour:

- Isotropic yielding (cap) is very significant
- Critical states are difficult to find
- RH controls the stress-strain-time behaviour
- Scale effects are very significant

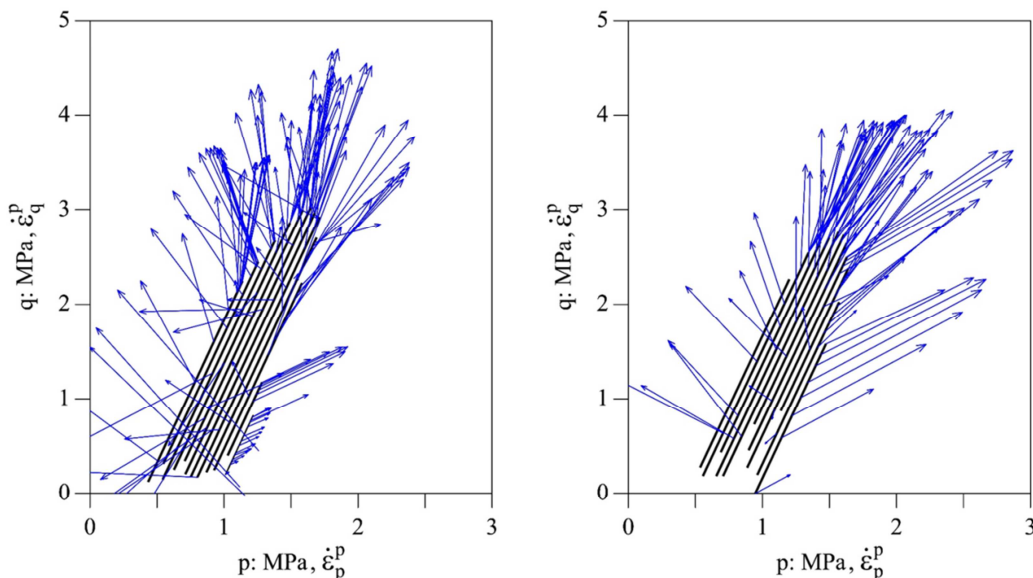


Figure 2. Incremental plastic strain vectors measured in multistage tests on compacted limestone gravels.

## DEM Modelling

DEM is a useful tool to gain understanding of rockfill deformation. It may be viewed as a virtual laboratory because it may realistically simulate the number of particles (and their divisions) involved in laboratory testing of gravel-like materials. Tapias et al (2015) describe a DEM model based on the following ideas:

- Particle geometry is approximated by ‘clumps’ of spherical particles
- Particle breakage is introduced through fracture mechanics concepts. Particle breaks when an existing crack propagates. The velocity of propagation is a function of crack size, water energy, time and stress state. In this manner, long-term deformations, water and scale effects are automatically accounted for.
- Two analytical solutions are introduced at particle level:
  - The stress distribution inside the particle (Russell and Wood, 2009)
  - The propagation of crack in a disk under Mode I tensile fracture (Oldecop and Alonso, 2007)
- A breakage protocol distinguishing local breakage and particle splitting is defined.

Model predictions were compared with suction controlled oedometric and triaxial tests in Tapias et al (2015).

Figure 3 shows a comparison between calculations and deformations measured in an oedometer test for a sequence of increasing loading steps. The initial loading sequence was performed under dry conditions (RH = 10%). The final step is a full wetting under a vertical confining stress of 2.8 MPa. Sample collapse is well captured by the model.

Figure 4 illustrates the capability of the DEM model to reproduce size effects. It shows the compressibility index in terms of the mean diameter of particles. Some test results for particle sizes in the range 1.5 – 4 cm are also shown in the plot. The model rightly predicts an increase in compressibility with particle size.

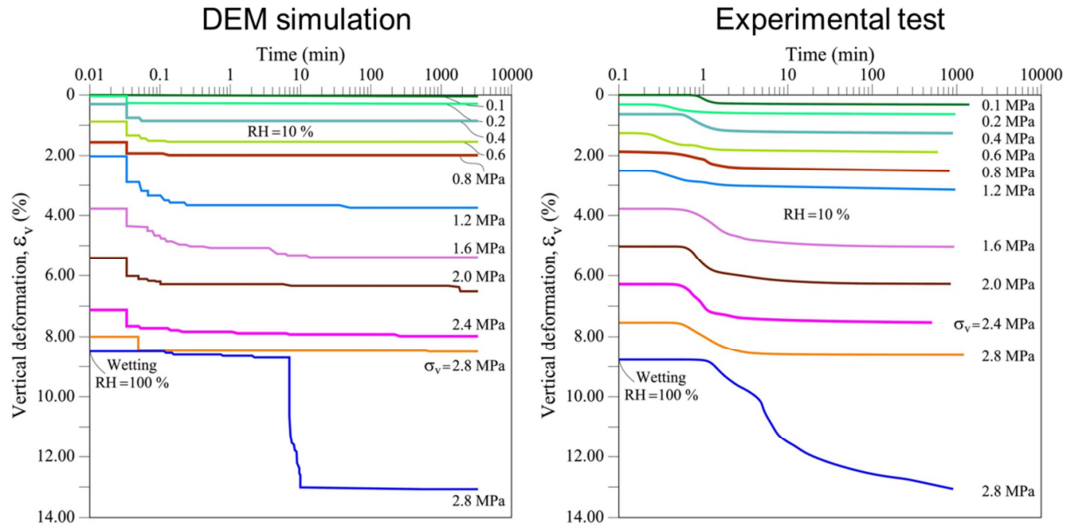


Figure 3. Simulation of oedometer tests.

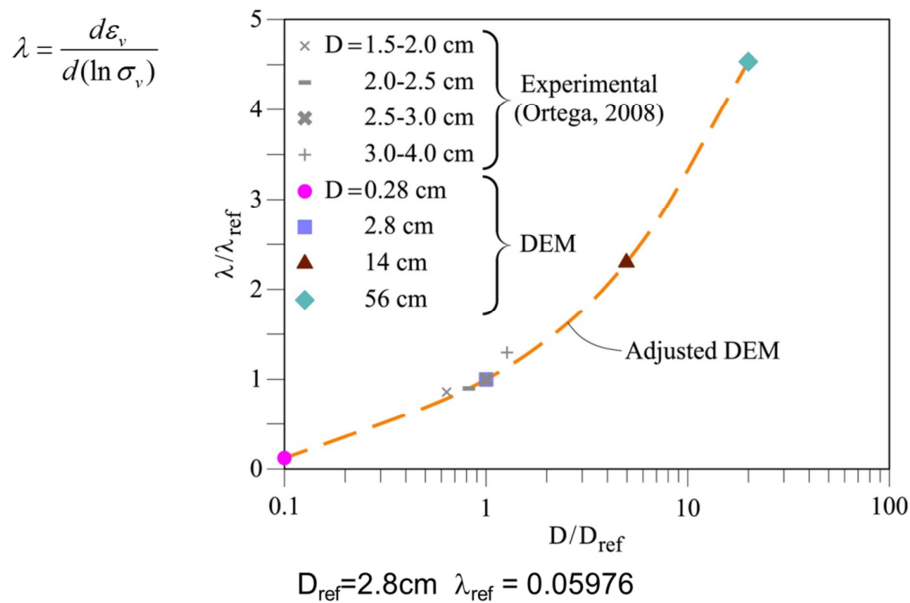


Figure 4. Size effects. Experimental vs. DEM results.

The DEM model developed captures most of the features observed in testing coarse granular aggregates. It only requires a small number of constitutive parameters: contact stiffness, contact friction and particle toughness, which are all amenable to laboratory determination. Advances in the characterization of particle geometry and the protocol of particle breakage would hopefully increase the accuracy and capabilities of the model developed.

## References

- Alonso E.E., Olivella S., Soriano A., Pinyol N.M. & Esteban F. (2011) Modelling the response of Lechago earth and rockfill dam. *Géotechnique* 61, 5; 387-407.
- Alonso E.E., Romero E. & Ortega E. (2016) Yielding of rockfill in relative humidity-controlled triaxial experiments *Acta Geotechnica* 11; 455-477.
- Chávez, C. & Alonso, E. E. (2003). A constitutive model for crushed granular aggregates, which includes suction effects. *Soils and Foundations*, Vol. 43(4), 215-227.
- Oldecop, L. & Alonso, E. E. (2001). A model for rockfill compressibility. *Géotechnique*, Vol.51 (2), 127-139.
- Oldecop, L. & Alonso, E. E. (2007). Theoretical investigation of the time-dependent behaviour of rockfill. *Géotechnique*, Vol. 57(3), 289–301.
- Russell, A. & MuirWood, D. (2009). Point load tests and strength measurements for brittle spheres. *Int. J. Rock Mechanics & Mining Sciences* 46, 272–280.
- Tapias M., Alonso E.E. & Gili J. (2016) Compressibility, grain breakage and time-dependent behaviour of gap-graded aggregates of sugar cubes. *Soils and Foundations* 56, 5; 805-817.
- Tapias M., Alonso E.E. & Gili J. (2015) A particle model for rockfill behaviour. *Géotechnique* 65, 12; 975-994.

# The stress-strain behaviour of granular materials at the meso-scale

X. Li<sup>1,2</sup>

<sup>1</sup> Faculty of Engineering, University of Nottingham, Nottingham, UK

<sup>2</sup> School of Civil Engineering, Southeast University, Nanjing, China

Email: xia\_li@hotmail.com

## Introduction

Granular materials are assemblies of discrete particles interacting with each other and displacing themselves by contact sliding and particle rotation. They demonstrate a wide range of interesting phenomena, such as memory effect, self-organisation, etc. Over time, extensive laboratory investigations have been carried out, and a good description of the experimental data on the stress-strain behaviour of granular materials may be found in Hicher, 1998.

The mathematical formulation of their stress-strain relationship is evidently challenging. Macroscopic approaches treat a granular material on a macro-scale as an equivalent continuum, and study its constitutive relationship between macro-quantities (stress and strain), while microscopic approaches consider it on a micro-scale as an assembly of individual particles interacting with each other, where the physical quantities under study are forces and displacements. Both approaches have led to significant achievements in the last few decades. Following other research work on this topic, this paper studies the macro-micro relations so as to connect the findings from the two scales.

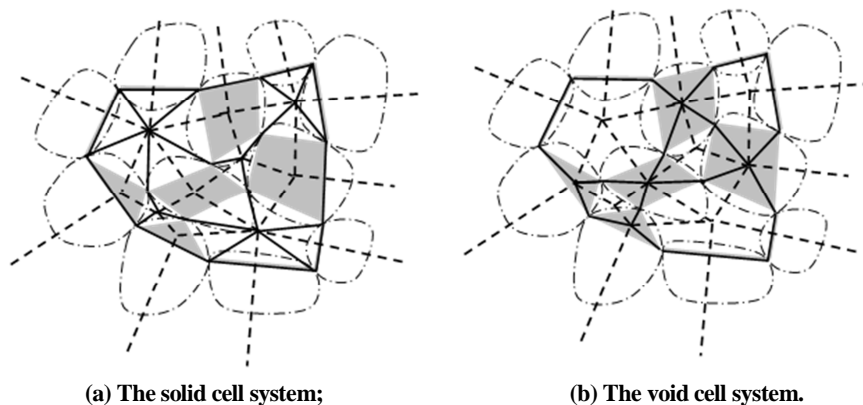


Figure 1. The solid and void cell systems for granular materials (after (Li and Li 2009))

## Homogenisation theory

Microstructure has long been identified as the key missing factor in the mathematical formulation. Following Satake's graph theory (Satake 1985) and Bagi's dual cell system (Bagi 1999, Li and Li 2009) proposed the tessellation systems, including a solid cell system and a void cell system, by a modification of the Voronoi-Denauay tessellations based on contact points, which serve as the mathematical description of material internal structure. The proposed algorithm is valid for both the two dimensional and the three dimensional granular materials, although only two dimensional results are given in Fig. 1 for simple illustration.

Building upon the description of the material internal structure, researchers have sought for the linkages between the classical continuum mechanics variables, stress and strain, and the particle-scale quantities, contact forces and particle displacement, to improve understanding of the complicated macro scale material behaviour from particle-scale interactions.

The expression of the stress tensor in terms of its micro counterpart, the contact forces, has been well established under static conditions (Christoffersen 1981, Rothenburg and Selvadurai 1981, Bagi 1996, Kruyt and Rothenburg 1996). Li, Yu et al. (2009) derived, based on the basis of Newton's law of motion, that in a stress field uniform on the macro scale, denoting the solid vector  $v_i^{Pc} = X_i^P - x_i^c$  as the vector from the contact point  $c$  to the particle centre  $P$ , and  $f_i^{Pc}$  as the contact force acting on particle  $P$  at the contact point  $c$ , the stress tensor can be expressed as

$$\bar{\sigma}_{ij} = \frac{1}{V} \sum_{P \in V} \sum_{c \in P} v_i^{Pc} f_j^{Pc} + \sum_{P \in V} R_{ij}^P \quad (1)$$

The expression is different from the conventional expression with the additional term  $\sum_{P \in V} R_{ij}^P$  due to particle rotation.

The linkage between the strain tensor and the particle displacements is more versatile, including the micro-structural expressions based on geometrical description of the internal structure (Bagi 1996, Kruyt and Rothenburg 1996, Kuhn 1999, Satake 2004) and the best-fit results corresponding to the smallest deviation from the characteristic displacements of the system (Liao et al., 1997; Cambou et al. 2000). An overview and comparison of different micro-structural strain expressions were given in Bagi (2006). By defining a complementary area vector,  $\chi_i^{Mc} = \phi_{ijk} h_j^{Mc} v_k^{Mc} / 2$ , where  $\phi_{ijk}$  is the permutation tensor, and  $\chi_i^{Mc}$  is an area-like variable determined from the positions of the contact point  $c$  relative to the void cell center and the surface center, Li, Yu et al. (2009) derived the 3D micro-structural expression of the displacement gradient tensor:

$$\bar{e}_{ij} = \frac{1}{V} \sum_{M \in V} \sum_{L \in M} \sum_{c \in L} \chi_i^{Mc} \Delta u_j^{Mc} \quad (2)$$

of which the micro-structural expression of the strain tensor can be obtained by considering the symmetric part. In 2D space, the void cells degenerate into polygons. Eq. (2) becomes

$\bar{e}_{ij} = \frac{1}{V} \sum_{M \in V} \sum_{c \in M} \chi_i^{Mc} \Delta u_j^{Mc}$ , in which  $\chi_i^{Mc} = \phi_{ij} v_j^{Mc}$ . The expression is similar to the results of Kruyt and Rothenburg (1996).

### Micro-scale interpretation of material strength

To explore further the micro-mechanisms of granular materials, a series of numerical experiments using the Discrete Element method (Cundall and Strack 1979, Cundall and Strack 1983) has been conducted to study how the particle friction coefficient affects the material stress-strain responses (Li 2017). Examining the statistical feature of the solid vectors and the contact forces, Li (2017) demonstrated that the following simplified form of the stress-force-fabric relationship gives almost exact matches to the continuum-scale stress:

$$\sigma_{ij} = \frac{\omega^p N^p}{2V} \zeta v_0 f_0 \left[ (1+h) \delta_{ij} + G_{ji}^f + \frac{1}{2} D_{ij}^c \right] \quad (3)$$

where  $\omega^p$  is the particle coordination number,  $N^p$  is the number of particles,  $v_0$  is the directional average of mean contact vector and  $f_0$  is the directional average of mean contact force,  $\zeta$  reflects the statistical dependence between contact vectors and contact forces, and  $h$  is a scalar accounting for the contribution from the joint products which increases slightly from 0 to around 0.01 during shearing.  $G_{ji}^f$  and  $D_{ij}^c$  are the direction tensors for contact force anisotropy and contact normal density, respectively. These are the key contributors to stress anisotropy, plotted in Fig. 2. No matter what the particle friction coefficient is, the anisotropy in contact force is of similar magnitude as the contact normal anisotropy, which is better shown when the two anisotropies are plotted against each other, although the reason is not yet known.

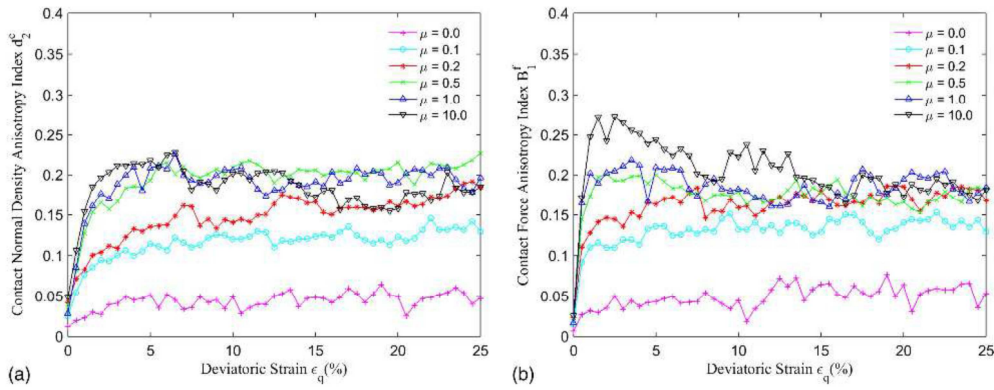


Figure 2. Micromechanical contributors to material strength: (a) contact normal anisotropy degree and (b) contact force anisotropy degree

### Meso-scale observation of internal structure and material strain

With different particle friction coefficients, the internal structures formed from a deposition process are evidently different as shown in Fig. 3 in terms of the void cell system, where the colour scheme indicates the void cell area

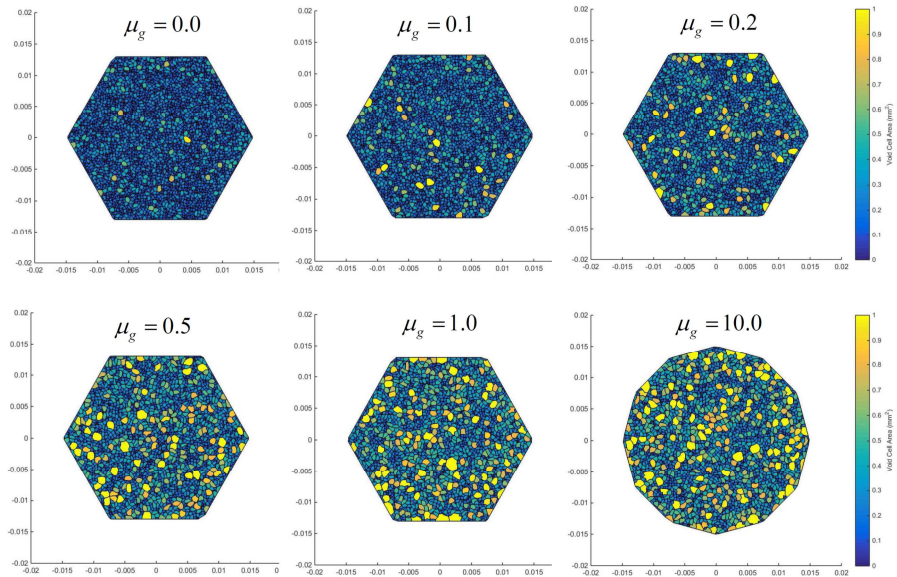


Figure 3. The void cell system

Take the configuration when the void cell system is constructed as the reference undeformed configuration. The relative displacements occurring during the subsequent 0.5% deviatoric strain increments are extracted from the DEM simulations and used to calculate the

displacement gradient tensor of each void cell as per Eq. (2). Fig. 4 shows the local displacement gradients of each void cell when the sample was sheared from 15 to 15.5% deviatoric strain.

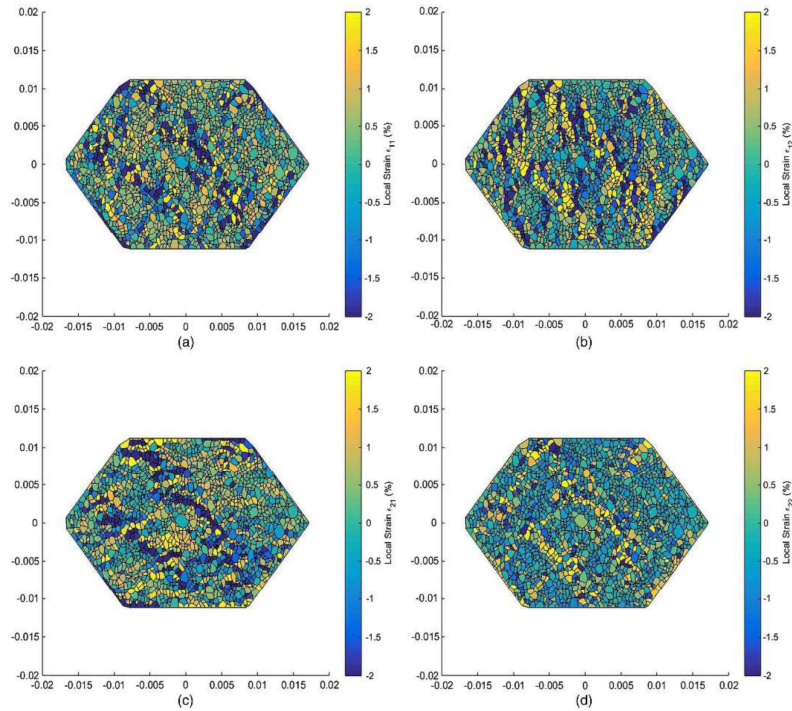


Figure 4. Spatial distribution of non-affined deformation gradient

The four components of non-affined displacement gradient tensor, defined as the deviation of the local strain from the sample average displacement gradient tensor for the sample with a friction coefficient 0.5, are plotted in Figs. 4(a – d). Localised banding structures are observed where the strain is much more significant than within the remaining areas. This is similar to the observation made in Kuhn (1999) that slip deformation was most intense within thin oblique micro bands. Different from the periodic boundaries used in Kuhn (1999), the sample boundaries are rigid walls that impose a uniform displacement gradient field. These banding structures do not persist during shearing. Subsequent loading continuously destroys the existing banding structures and promotes the formation of new bands in other locations. Although certain banding features are commonly observed in the four plots, the patterns for the two shear-strain components are observed to be different from those for the two normal-strain components.

### Concluding remarks

Due to its ubiquitous existence in nature as geo-materials, the study of granular materials has attracted long-term interest and efforts, and has increasingly been promoted by recent developments in numerical simulation capacities and particle-scale experimental techniques (Wakabayashi 1957, Drescher and De Josselin de Jong 1972, Hall, Bornert et al. 2010). This paper has summarised the homogenisation theory and presented the particle-scale observations guided by the homogenisation theory. It has demonstrated clearly that internal structures formed by granular particles with different friction coefficients are different and the micro-banding structure, when the sample is sheared, has been evidenced. The formation,

characteristics and impact of this strong strain heterogeneity is an interesting area for future research work.

## References

- Bagi, K. (1996). "Stress and strain in granular assemblies." *Mechanics of Materials* **22**(3): 165-177.
- Bagi, K. (1999). "Microstructural Stress Tensor of Granular Assemblies With Volume Forces." *Journal of Applied Mechanics* **66**(4): 934-936.
- Christoffersen, J., Mehrabadi, M.M., Nemat-Nasser, S. (1981). "A micromechanical description of granular material behaviour." *Journal of Applied Mechanics, ASME* **48**(2): 339-344.
- Cundall, P. A. and O. D. L. Strack (1979). "A discrete numerical model for granular assemblies." *Geotechnique* **29**(1): 47-65.
- Cundall, P. A. and O. D. L. Strack (1983). Modeling of microscopic mechanisms in granular materials. *Mechanics of Granular Materials: New Model and Constitutive Relations*. J. T. Jenkins and M. Satake. Amsterdam, Elsevier: 137-149.
- Drescher, A. and G. De Josselin de Jong (1972). "Photoelastic verification of a mechanical model for the flow of a granular material." *Journal of the Mechanics and Physics of Solids* **20**: 337-351.
- Hall, S. A., M. Bornert, J. Desrues, Y. Pannier, N. Lenoir, G. Viggiani and P. Besuelle (2010). "Discrete and continuum analysis of localised deformation in sand using X-ray micro CT and volumetric digital image correlation." *Geotechnique* **60**(5): 315-322.
- Hicher, P. Y. (1998). Experimental behaviour of granular materials. *Behaviour of granular materials*. B. Cambou. Printed in Italy, Springer-Verlag Wien New York: 1-97.
- Kruyt, N. P. and L. Rothenburg (1996). "Micromechanical definition of the strain tensor for granular materials." *Journal of Applied Mechanics* **63**(3): 706-711.
- Kuhn, M. R. (1999). "Structured deformation in granular materials." *Mechanics of Materials* **31**(6): 407-429.
- Li, X. (2017). "Internal structure quantification for granular constitutive modeling." *Journal of Engineering Mechanics*.
- Li, X. and X.-S. Li (2009). "Micro-macro quantification of the internal structure of granular materials." *Journal of Engineering Mechanics* **135**(7): 641-656.
- Li, X., H.-S. Yu and X.-S. Li (2009). "Macro-micro relations in granular mechanics." *International Journal of Solids and Structures* **46**(25-26): 4331-4341.
- Rothenburg, L. and A. P. S. Selvadurai (1981). A micromechanical definition of the Cauchy stress tensor for particulate media. *Proceedings of the International Symposium on Mechanical Behaviour of Structured Media*. A. P. S. Selvadurai. Ottawa, Canada: 469-486.
- Satake, M. (1985). Graph-theoretical approach to the mechanics of granular materials. *Continuum Models of Discrete Systems: Proceedings of the Fifth International Symposium*. Nottingham, A A Balkema Publishers: 163-173.
- Satake, M. (2004). "Tensorial form definition of discrete-mechanical quantities for granular assemblies." *International Journal of Solids and Structures* **41**: 5775-5791.
- Wakabayashi, T. (1957). Photoelastic method for determination of stress in powdered mass. *Proceedings of the 7th Japan National Congress for Applied Mechanics*.

# Numerical modelling of geotechnical problems based on a static micromechanical approach

C. Zhao, Z.Y. Yin and P.Y. Hicher

*Ecole Centrale de Nantes, UMR CNRS GeM, Nantes, France.  
chaofa.zhao/zhenyu.yin/pierre-yves.hicher@ec-nantes.fr*

Constructing constitutive models is one of the most important tasks in geotechnical engineering. Generally, the favoured models are those which reveal the physics of soils and can predict their behaviour correctly with a limited number of parameters. Based on continuum mechanics, phenomenological models have been proposed to describe the granular soil behaviour obtained from elementary tests. More recently, micromechanical models have been developed which consider force-displacement relationships at the interparticle contacts. These models are thus able to take into account the fundamentals of granular physics and to reproduce basic soil behaviour (Chang and Hicher, 2005; Nicot and Darve, 2005; Yin and Chang, 2009; Nicot and Darve, 2011). It would, therefore, benefit multiscale modelling of geotechnical problems to implement these models into finite element codes.

Micromechanical models based on the static hypothesis have proved to perform well in predicting soil behaviour (Chang and Hicher, 2005; Hicher and Chang, 2007; Hicher *et al.*, 2008; Yin and Chang, 2009; Yin *et al.*, 2009; Yin *et al.*, 2011; Yin *et al.*, 2012; Yin *et al.*, 2014). However, these particular models cannot easily integrate the stress at the macro level, since the displacement at the contact level is not directly obtained from the global strain. In order to analyse boundary value problems with these models, this study proposes an efficient implicit method to integrate stress-strain relationship with consideration both the micro and macro levels. For this purpose, the Chang-Hicher micromechanical model has been adopted. A predictor-corrector scheme is first proposed to solve the linearised mixed control constrains. An iteration procedure then implements the macro-micro relations. Additionally, two return mapping schemes including the closest point projection method (CPPM) and the cutting plane algorithm (CPA) are adopted to integrate the inter-particle force-displacement relations. The studies on elementary tests and boundary value problems have shown the accuracy and efficiency of the proposed implicit algorithms. The results show that the proposed linearized method can successfully perform stress-controlled or strain-controlled loadings. The proposed implicit algorithm for the macro-micro relations expresses the static hypothesis consistently with the stress integration tensor.

CPPM on integrating local laws for the micromechanical model provides a more significant computational cost efficiency without any loss of accuracy, compared to CPA. Simulations on several conventional loading paths, i.e. drained and undrained triaxial compression tests, are conducted for investigating numerical accuracy and efficiency. Finally, the model has been implemented into a finite element code and validated by elementary tests. Three typical boundary value problems, i.e. a biaxial test, a square footing and the excavation of a tunnel, were numerically performed and the results analysed to evaluate the applicability of the numerical approach (Figure 1).

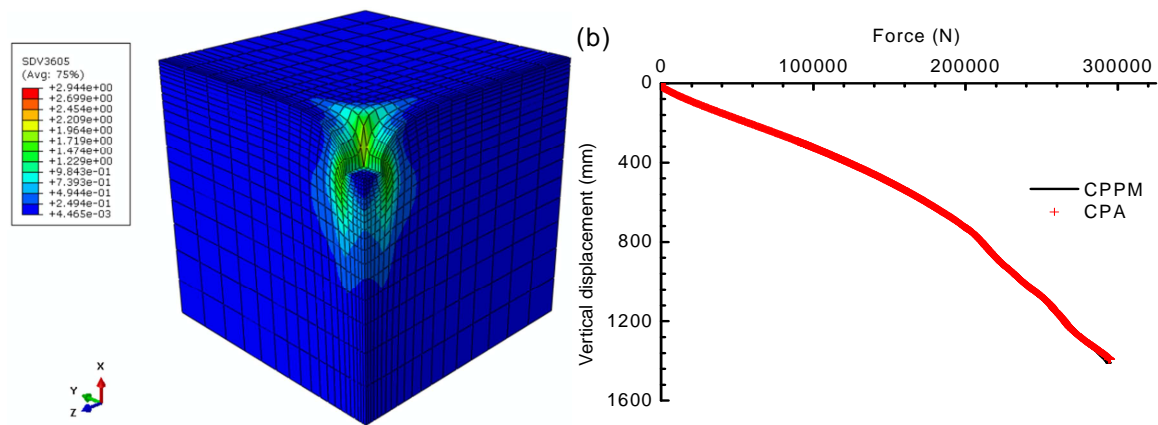


Figure 1. Multi-scale modelling of a square footing: (a) deviatoric plastic strain; (b) force-displacement relationship

**Keywords:** micromechanical approach, geotechnical problems, finite element method, multiscale modelling

## References

- Chang, C. S. and Hicher, P. Y., 2005. An Elasto-plastic Model for Granular Materials with Microstructural Consideration. *International Journal of Solids and Structures*, 42(14), pp. 4258-4277.
- Hicher, P.Y. and Chang, C.S., 2007. A microstructural elastoplastic model for unsaturated granular materials. *International Journal of Solids and Structures*, 44(7), pp.2304-2323.
- Hicher, P.Y., Chang, C.S. and Dano, C., 2008. Multi-scale modeling of grouted sand behavior. *International Journal of Solids and Structures*, 45(16), pp.4362-4374.
- Nicot, F. and Darve, F., 2005. A multi-scale approach to granular materials. *Mechanics of Materials*, 37(9), pp.980-1006.
- Nicot, F. and Darve, F., 2011. The H-microdirectional model: accounting for a mesoscopic scale. *Mechanics of Materials*, 43(12), pp.918-929.
- Yin, Z.Y. and Chang, C.S., 2009. Microstructural modelling of stress-dependent behaviour of clay. *International Journal of Solids and Structures*, 46(6), pp.1373-1388.
- Yin, Z.Y., Chang, C.S., Hicher, P.Y. and Karstunen, M., 2009. Micromechanical analysis of kinematic hardening in natural clay. *International Journal of Plasticity*, 25(8), pp.1413-1435.
- Yin, Z.Y., Hattab, M. and Hicher, P.Y., 2011. Multiscale modeling of a sensitive marine clay. *International Journal for Numerical and Analytical Methods in Geomechanics*, 35(15), pp.1682-1702.
- Yin, Z.Y., Xu, Q. and Chang, C.S., 2012. Modeling cyclic behavior of clay by micromechanical approach. *Journal of Engineering Mechanics*, 139(9), pp.1305-1309.
- Yin, Z.Y., Zhao, J. and Hicher, P.Y., 2014. A micromechanics-based model for sand-silt mixtures. *International Journal of Solids and Structures*, 51(6), pp.1350-1363.

# Stress-induced permeability evolution in a heterogeneous rock

A.P.S. Selvadurai

Department of Civil Engineering and Applied Mechanics, McGill University, Montréal, QC,  
Canada H3A 0C3

E-mail: [patrick.selvadurai@mcgill.ca](mailto:patrick.selvadurai@mcgill.ca); Web page:

<http://www.mcgill.ca/civil/people/selvadurai>

## Abstract

The paper presents results of recent research to investigate the role of stress states on permeability evolution in a heterogeneous argillaceous rock. The fabric of the rock, that consists of light grey nodular regions of calcite, dolomite and quartz interspersed with dark grey regions of calcite, dolomite with a clay fraction, contributes to unconventional results relating to the evolution of permeability with the stress state.

## Introduction

The general consensus in many countries is that deep geological disposal presents the most environmentally benign form of disposal and containment of the hazardous nuclear wastes. A major factor to be considered when constructing an underground repository is the *in situ* stress-assisted alteration of the fluid transport characteristics of the repository rock due to the development of defects such as micro-cracks and other defects. Fluid flow patterns in the vicinity of an underground repository will be the main source for the migration of radionuclides that can be released either accidentally or during the natural degradation of the waste containers. In most applications involving groundwater hydrology and water resources development, the permeability characteristics of geologic media are assumed to remain constant throughout the effective lifetime of the environmental geosciences activity. This is in contrast to environmental geomechanics activities associated with geologic disposal where the stress state in the ground can be altered by the engineering activity, which can in turn lead to alterations in the permeability of the rock mass. Canadian proposals for the deep geologic disposal of all levels of radioactive waste involve two types of host rocks. The granitic option for storing heat-emitting high level nuclear waste considers the siting of repositories in plutonic rock masses of the tectonically stable Canadian Shield. This option has been examined over the past six decades and presents a viable option for geologic storage of hazardous nuclear waste; the excavation related to the construction of the Underground Research Laboratory in the Canadian Shield at Pinawa, Manitoba has emphasized the role of *in situ* stress states in initiating excavation damage zones and excessive deformations around the galleries constructed at typical repository depths of 450m. The Canadian proposals for the geologic storage of low- and intermediate-level nuclear waste focus on siting a repository in the Ordovician Limestone sequences located in southern Ontario. The geologic formations are nearly horizontally stratified and the approximately 45 m thick Middle Ordovician Lindsay formation is located about 630 m below ground level. The Cobourg formation is overlain by Upper Ordovician Siltstone and Gray Shale extending to a depth of 200 m and underlain by Argillaceous Limestone and Gray Shale, approximately 150 m thick. The entire sequence of Paleozoic rocks rests on a Pre-Cambrian Granitic Gneiss basement rock. The Cobourg Limestone, located at a depth of 660m, is the sedimentary sequence which has been targeted for the siting of a geologic repository. The Cobourg Limestone displays heterogeneity resulting from the interspersed fabric of a calcite, dolomite-rich light gray, nodular limestone separated by argillaceous partings. There is some visual evidence of a nominal plane of stratification but this can vary from sample to sample depending on the spatial arrangement of the fabric (Figure 1). In terms of mineralogy, the light gray nodular limestone is composed of carbonates (84%) calcite and dolomite, quartz (8%) with traces of clays (0.3%), whereas the

argillaceous partings contain carbonates (66%) calcite and dolomite, quartz (22%), with a clay content of (2.4%) (Illite, Kaolinite and a trace of Montmorillonite).

### **Damage and Permeability**

Damage development in rocks can be complex and several theories based on damage mechanics concepts have been adopted to describe the evolution of permeability and elasticity properties that ultimately describe the poromechanical response (Mahyari and Selvadurai, 1998; Selvadurai and Shirazi, 2004; Selvadurai, 2004; Pellet and Selvadurai, 2016). A further aspect of damage evolution is the transition of the damaged region to an extensively fractured rock mass that can significantly alter the fluid transport characteristics within the rock mass. This research deals with the experimental study of the evolution of permeability with stress in a heterogeneous rock (Cobourg Limestone) consisting of a nodular fabric of calcite-dolomite and quartz interspersed with partings that are also composed of calcite and dolomite but with a less than a five percent clay fraction. In its intact unstressed state, the heterogeneous argillaceous rock is highly impervious with permeabilities ranging from  $10^{-22} \text{ m}^2$  to  $10^{-20} \text{ m}^2$ . This is a major reason for the choice of the Cobourg Limestone as a candidate for a repository setting. Furthermore, in regions where the in situ stress state is altered, the rock will have the potential to accommodate straining without the development of extensive damage. In this research program, the influence of the stress state on permeability evolution was first assessed by subjecting the Cobourg Limestone to isotropic compression followed by permeability measurements conducted using hydraulic pulse tests (Selvadurai and Najari, 2016). The results of the isotropic compression testing are given in Selvadurai et al (2011). In relatively homogeneous materials, such as sandstone and granite, pore compression can lead to reductions in permeability. However, in the case of the Cobourg Limestone, the application of isotropic compression can lead to an increase in the measured permeability. In addition, the application of a cycle of isotropic compression and unloading can lead to permanent increases in the permeability (Figure 2). It is conjectured that the application of external isotropic stress states can induce heterogeneous stress states within the fabric of the rock that can lead to the development of damage along the argillaceous partings, which can alter the permeability. The experiments conducted on 100 mm diameter samples were repeated on 85 mm diameter and 130 mm long samples tested in an Obert-Hoek Cell (Selvadurai and Głowacki, 2017) and identical results were obtained (Figure 3). The research was extended to examine the influence of discrete fracture development on the estimation of bulk permeability of the Cobourg Limestone. Cylindrical samples of the Cobourg Limestone were subjected to stress states that simulated geostatic conditions and the radial principal stresses were reduced to simulate conditions that can arise during the stress relief following excavation of an underground opening. The variation of permeability with the failure stress state was estimated from steady state permeability tests (Figure 4). With the attainment of failure, distinct fractures were observed in the argillaceous partings (Figure 5), which leads to an overall increase in the permeability of the heterogeneous rock by approximately four orders of magnitude (i.e.  $\sim 10^{-18} \text{ m}^2$  to  $10^{-16} \text{ m}^2$ ) (Selvadurai and Głowacki, 2017).

### **Concluding Remarks**

The evolution of irreversible permeability increases during isotropic compression is a characteristic response resulting from micro-mechanical damage that causes an increase in the permeability. In the post-failure range, the permeability is controlled by damage and failure in the partings that contain an argillaceous component. In the modelling of the stress-assisted evolution of permeability in the heterogeneous Cobourg Limestone, greater attention can therefore be devoted to modelling damage and failure in the argillaceous phase. In this regard, more non-invasive techniques such as CT-scans and AE measurements can be used to supplement traditional mechanical testing.

## Acknowledgements

The author is grateful to the Nuclear Waste Management Organization, ON and NSERC for the financial support and to graduate students, A. Shirazi, A. Mahyari, M. Najari, A. Letendre, B. Hekimi and A. Głowacki of the Environmental Geomechanics Group for their contributions.

## References

- Mahyari AT, Selvadurai APS 1998. Enhanced consolidation in brittle geomaterials susceptible to damage, *Mechanics of Cohesive Frictional Materials*, **3**, 291-303.
- Pellet F and Selvadurai APS 2016. Rock Damage Mechanics, Chapter 3 in *Rock Mechanics and Engineering* (X.-T. Feng, Ed.), CRC Press, Boca Raton, FL, pp. 65-107.
- Selvadurai APS, 2004. Stationary damage modelling of poroelastic contact, *International Journal of Solids and Structures*, **41**, 2043-2064.
- Selvadurai, APS, Głowacki A 2017. Stress-induced permeability alterations in an argillaceous limestone, *Rock Mechanics and Rock Engineering*, DOI 10.1007/s00603-016-1153-3
- Selvadurai APS, Najari M 2016 Isothermal permeability of the argillaceous Cobourg Limestone, *Oil and Gas Science and Technology, Special Issue on Low Permeability Geomaterials*, **71**: 53-69.
- Selvadurai APS, Shirazi A, 2004. Mandel-Cryer effects in fluid inclusions in damage-susceptible poroelastic geologic media, *Computers and Geotechnics*, **37**, 285-300.
- Selvadurai APS, Letendre A, Hekimi B, 2011. Axial flow hydraulic pulse testing of an argillaceous limestone, *Environmental Earth Sciences*, DOI 10.1007/s12665-011-1027-7.



**Fig 1.** The heterogeneous Cobourg Limestone

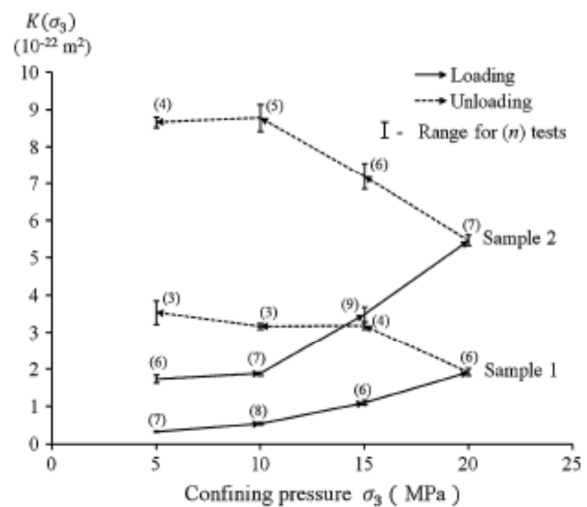


**Fig 2.** Permeability variation with isotropic compression (100 mm diameter samples)

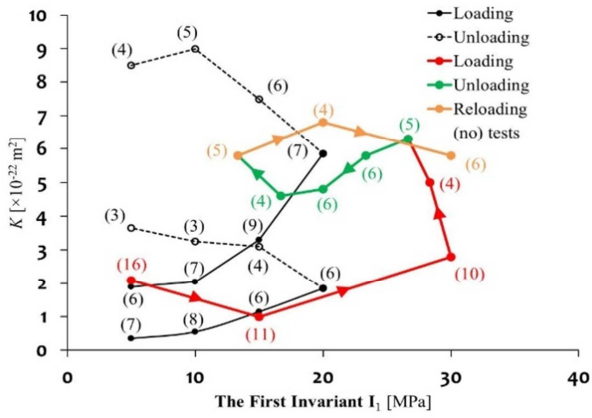


**Fig 3.** Permeability variation with isotropic (85 mm diameter samples)

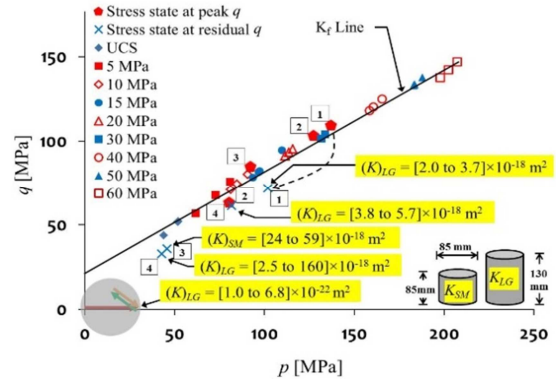
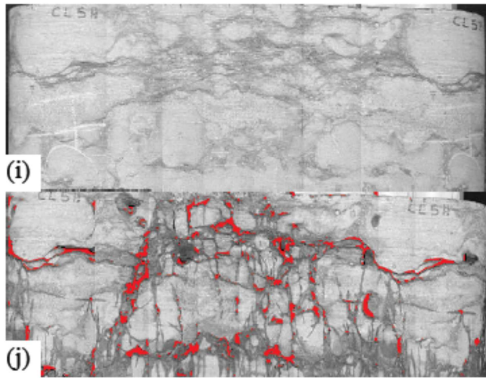
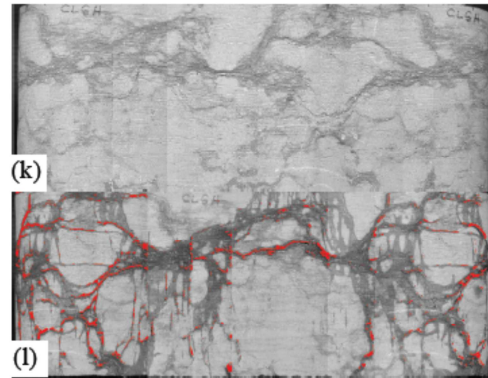


**Fig 4.** Post-failure permeability compression evolution



CL5H:  $K_{cc} = 2.5E-18m^2$  ; D=85.6 mm H=132 mm



CL6H:  $K_{cc} = 2.0E-17m^2$  ; D=85.3 mm H=121.4

**Fig 5.** Post-failure localization of damage and in the argillaceous regions of the Cobourg Limestone

# Failure processes and damage evolution in transversely isotropic rocks by DEM

Ö. Dinç<sup>1,2\*</sup> and L. Scholtès<sup>1</sup>

<sup>1</sup>*\*University of Lorraine, CNRS, GREGU, Georessources Lab., 54000 Nancy, France*

<sup>2</sup>*Çanakkale Onsekiz Mart University, Applied Geology Division, 17020 Çanakkale, Turkey*  
*e-mail: osgedc@gmail.com, luc.scholtes@univ-lorraine.fr*

The aim of this research is to investigate failure processes and damage evolution in transversely isotropic rocks through micro mechanical analyses. In particular, we use an enhanced discrete element method (DEM) implemented in the open source code, Yade open DEM, and propose a multi-scale approach to clarify damage development and strain localisation in argillaceous rocks. Because it has been shown that its inherent anisotropy plays a critical role in the development of damage around the drifts of the Meuse-Haute-Marne Underground Laboratory (MHM URL), the Callovo Oxfordian (COx) claystone was chosen as the reference material in our study. Transverse isotropy is introduced in the model at the interparticle scale in the form of weakness planes with specific micromechanical properties and a predefined orientation related to the microstructure of the considered rock. The methodology is an offspring of the approach first proposed by Duan et al. [4]. A number of compression tests under plain strain and triaxial conditions were performed under different confining stresses and the predictions of the model systematically compared to experimental results [1]. Among other characteristic properties, we found that the post peak response of the COx claystone was only reproducible when the anisotropic DEM was used (Fig 1).

Progressive failure mechanisms were investigated through the analysis of both the damage developing at low strain and the shear bands appearing at high strain in combination with strain softening. For low confining stresses (2 and 5 MPa), the predicted shear bands present similar orientations to the ones observed experimentally [2, 3] (Fig 2). On the other hand, a slight discrepancy can be observed for higher confining stresses (10 and 20 MPa). A systematic description of the local mechanisms leading to the appearance of the shear bands is proposed. In particular, we show that strain localisation is always related to the development of shear enhanced micro cracks inside the model, the latter presenting characteristic orientation distributions with respect to the shear band orientation. In addition, a specific emphasis is put on studying the influence of the numerical parameters on the model's predictions. We show that the predicted shear band's thickness is not particle size dependent but rather structure size dependent as it appears to be directly influenced by the geometry of the model.

Finally, in an attempt to apply this newly developed DEM model at the engineering scale, we simulated excavation processes representative of the stress conditions encountered in the MHM URL. Our results show that, although laboratory scale observations and discrete simulations in terms of the failure envelope and stress-strain relations agree fairly well, additional developments are still needed in order to reproduce the deformation and failure processes observed in-situ. Among the numerous aspects needed for a better description of the material behaviour, the introduction of hydromechanical coupling appears to be the most important [5] and is currently underway.

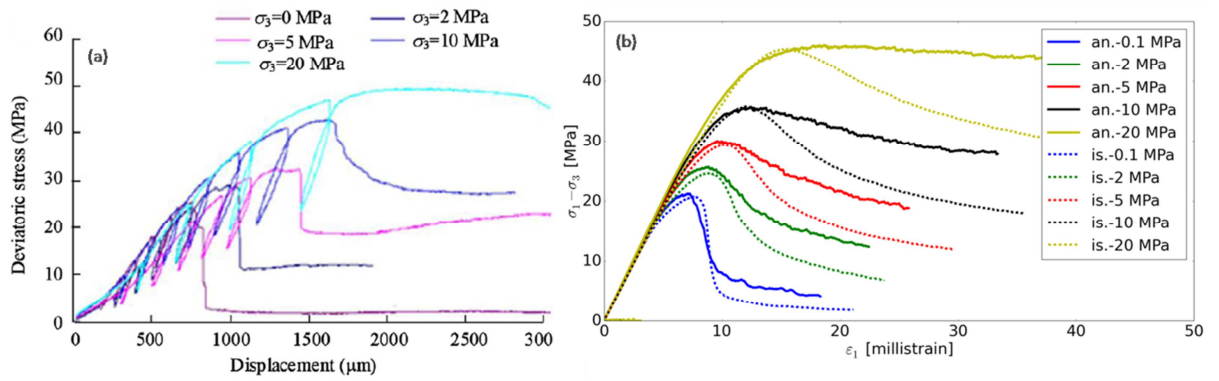


Fig 1. Triaxial compressive test results under various confining stresses a) Stress-strain curves recorded experimentally [1] b) Stress-strain curves obtained from both isotropic (is) and anisotropic (an) DEM modelling

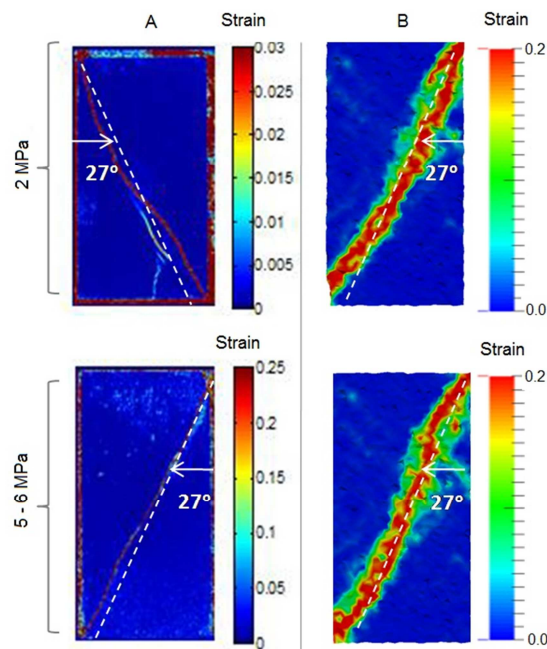


Fig 2. Shear bands under plain strain loading conditions A) Experimental results [2, 3] B) DEM predictions

## References

- [1] Armand G., Leveau F., Nussbaum C., de La Vaissiere R., Noiret A., Jaeggi D., Landrein P., Righini C., Geometry and Properties of the Excavation-Induced Fractures at the Meuse/Haute-Marne URL Drifts, *Rock Mech Rock Eng* (2014) 47:21–41.
- [2] Bésuelle P. and Hall S.A., Characterization of the Strain Localization in a Porous Rock in Plane Strain Condition Using a New True-Triaxial Apparatus, *Advances in Bifurcation and Degradation in Geomaterials*, (11), 345-352 (2011).

- [3] Bésuelle P., Lanatà P., Desrues J. and Salager S., Analyse de la rupture et de l'anisotropie de l'argilite-développements récents, *Andra Internal Report* (2016).
- [4] Duan K., Kwok C.Y. and Pierce M., Discrete element method modeling of inherently anisotropic rocks under uniaxial compression loading, *Int. J. Numer. Anal. Meth. Geomech.*, DOI: 10.1002/nag.2476 (2015).
- [5] Seyedi D. M., Armand G., Noiret A., “Transverse Action” – A model benchmark exercise for numerical analysis of the Callovo-Oxfordian claystone hydromechanical response to excavation operations, *Computers and Geotechnics*, doi : 10.1016/j.compgeo.2016.08.008 (2016).

# The effect of chemical solutions upon the hydromechanical properties and the structure of two clays

H. Souli

*Ecole Nationale d'Ingénieurs de Saint Etienne*  
*Laboratoire de tribologie et dynamique des systèmes*  
*CNRS UMR 5513*  
*E-mail : hanene.souli@enise.fr*

## Introduction

When clays are subjected to chemical solutions, it is often difficult to perceive the evolution of their mechanical and physico-chemical properties. The aim of this article is to demonstrate via two examples the effect of the presence of heavy metal pollutants upon the hydromechanical and structural properties of two clays. The first case consists of studying the evolution of the properties of a smectite that is likely to be used as a barrier in an industrial waste deposit installation. The focus is put upon the evolution of the permeability and the porosity in the presence of zinc. The second case explores the effect of electro kinetic treatment upon the structure of a kaolinite mixed with water and lead. Within the framework of using clays in a waste deposit installation, the studies done by Shakelford et al. (2000), Julien et al. (2002), and Souli et al. (2008) have shown that the permeability of clays, notably smectites, increased with the increase of the concentration of heavy metals. Souli et al. (2008) demonstrated that the presence of lead led to variation of porosity, particle size and particle orientation. From an electrokinetic standpoint, this method has already been the subject of previous studies whose aim was to study the effect of electrical parameters such as the current intensity, the value of the applied electric potential difference upon the efficiency of the method (Acar et al. 1990, Reddy et al. 2002...). Certain studies have been interested by studying the evolution of the structure of natural clay samples after treatment (Steger et al. 2005, Ben Hassine et al. 2016).

## Evolution of hydromechanical and physico-chemical properties of a smectite

The permeability measurements carried out in the presence of zinc at concentrations from 0.01 and 1M have shown a decrease of the permeability with an increase of zinc concentration. The analyses of porosity by mercury porosimetry (Fig.1) have shown that for a small concentration of zinc (0.01M), the distribution of the pore sizes is comparable to that obtained for a sample mixed with water. However, a significant re-organisation of the porosity is observable in the presence of zinc at a concentration level of 1M. Indeed, as shown by the results in Figure 1, an enlargement of the inter-aggregate pore sizes can be observed. The X-ray diffraction (Fig.2) showed that the rise in the concentration of zinc leads to a diminution of the (001) reflexion intensity compared to the same reflexion intensity proper to the sample mixed with water. This shows a variation in the organisation of the particles in the presence of zinc (Guillot et al. 2002). In the presence of zinc at a concentration of 1M, the full width at half the maximum of the (001) reflexion decreases, which means that the number of clay layers in a particle increases. The increase of zinc concentration leads to a decrease of the thickness of the double layer and to the decrease of repulsion forces. The consequence is an increase of the size of the particles with an increase in the number of clay layers per particle (DRX). On the other hand, the X-ray diffraction shows an evolution in the organisation of the structure in the presence of zinc. The association of these parameters leads to a variation of the pore sizes which is responsible for the permeability increase in the presence of zinc.

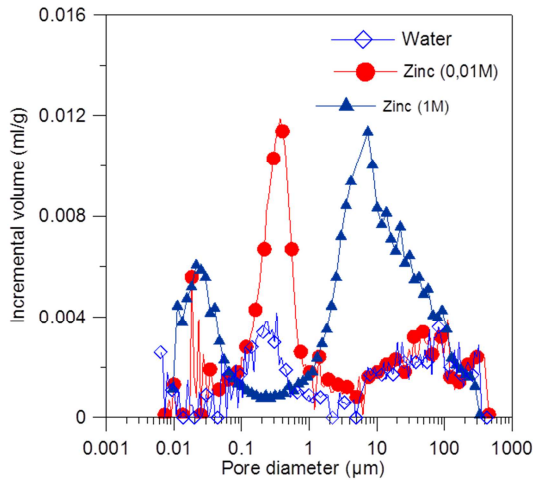


Figure 1 Evolution of pore sizes in smectite mixed with water and zinc (0,01 et 1 M) measured by mercury porosimetry

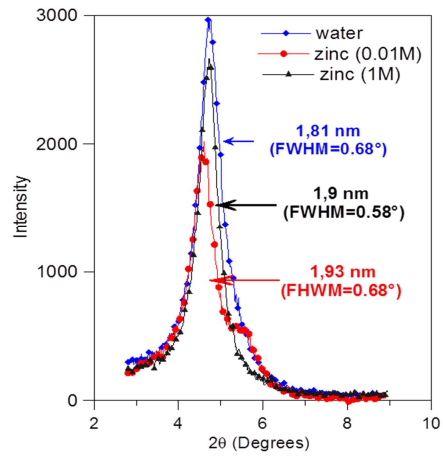


Figure 2 Evolution of (001) reflexion intensity in smectite mixed with water and zinc (0,01 et 1 M)

### Evolution of the structure of a kaolinite mixed with lead after an electro kinetic treatment

The benefit of this study comes from the evolution of the structure of the kaolinite mixed with water and lead. The samples with initial water content equal to the liquid limit are consolidated under a small stress before being subjected to an electro kinetic treatment. During the test, different parameters such as the pH, the current intensity, the electric potential difference are measured as a function of time. After the test, the samples are cut into small pieces so that the structure can be studied by X-ray diffraction. The results show that for the kaolinite water mixture, there is an increase of the electrical conductivity, this being due to the diffusion of the cations  $H^+$  in the structure. However, in the presence of zinc, a decrease of the electrical conductivity has been obtained (Fig.3). This decrease is due to the displacement of the lead and its replacement by the cations  $H^+$ . The measures of pH show that the samples acidify as a consequence of the diffusion of ions  $H^+$  within the structure (Reddy et al. 2002).

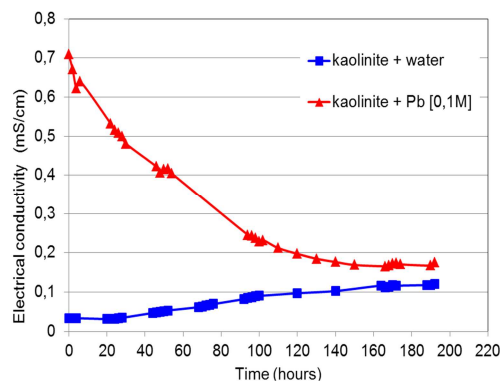


Figure 3 Evolution of the electrical conductivity in kaolinite mixed with water and lead

As far as the study of the structure is concerned, the comparison of the (001) reflexion intensities, shows that in the presence of water, we observe a decrease in the intensity of the (001) reflexion compared to the intensity of the (001) reflexion of the sample before the test (Fig.4a). This shows that the treatment in this case leads to an increase in the level of the

disorder of the structure (isotropy). The elimination of lead, on the contrary, leads to the development of a more ordered structure, in comparison also with the sample before the electro kinetic treatment (Fig.4b). In both cases, the full width at half the maximum increased, compared to the initial state, which means that the size of the particles increased. The evolution of the structure in this case is due to the pH variation of the structure following the diffusion of the  $H^+$  cations in the structure. Indeed, when the pH decreases, the repulsion forces decrease which leads to particle formation of a higher number of clay layers. This is at the origin of the particle size increase as shown by the X-ray diffraction.

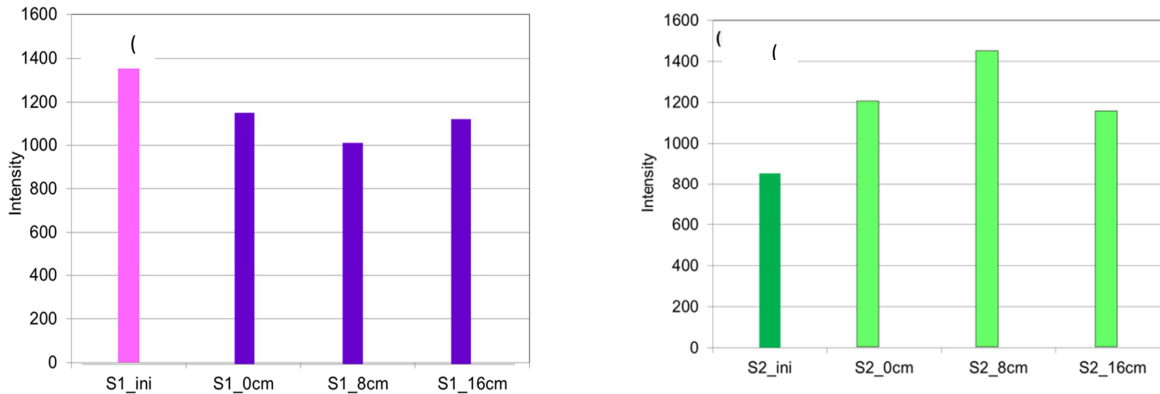


Figure 4 Evolution of (001) reflexion intensity in kaolinite mixed with water (a) and with lead (b) before and after the electro kinetic test

### 3 Conclusion and perspectives

The two examples presented in this study have shown that the presence of chemical solutions, especially heavy metals, leads to an evolution of the structure of the specified clays. Evolution in particle sizes, in particle orientation, and in pore sizes have been observed. These variations have an effect on the mechanical properties as shown in the first case. However, this study has only shown the short-term effects. Longer tests and modelling will allow us to study the long-term behaviour of these materials.

### References

- Acar YB, Gale RJ, Putnam G (1990) Electrochemical processing of soils: theory of pH gradient development by diffusion and linear convection. *Journal of Environmental Science and Health. Environmental Science and Engineering* 26687-714.
- Ben Hassine A, Souli H, Dubujet Ph, Ayari F, Trabelsi-Ayadi M (2016) Kaolinite carbonate mixture fabric evolution after electrokinetic tests. *Géotechnique Letters* 6, 45–49.
- Jullien A, Proust Ch, Le Forestier L, Baillif P (2002) Hydro-chemio-mechanical coupling effects on permeability and swelling behaviour of a Ca smectite soaked by Cu solutions. *Applied Clay Science* 21, 143–153.
- Guillot X, Bergaya F, Fleureau J-M, Al-Mukhtar M (2002) Influence of stresses and suction on volume change behavior and microscopic properties of a Ca smectite in: *Proceedings of the International Symposium on Suction, Swelling, Permeability and Structure of Clays*. Shizuoka, 69-77.
- Reddy KR, Saichek RE, Maturi K, Prasanth A, (2002) Effects of Soil Moisture and Heavy Metal Concentrations on Electrokinetic Remediation. *Indian Geotechnical Journal* 32, 258-288
- Shackelford CD, Craig H, Benson CH, Hatsumi T, Edil TB, Lin L, 2000. Evaluating the hydraulic conductivity of GCLs permeated with non-standard liquids. *Geotextiles and Geomembranes* 18, 133–161.
- Souli H, Fleureau J-M, Trabelsi Ayadi M, Besnard M (2008). Physicochemical analysis of permeability changes in the presence of zinc. *Geoderma* 145, pp. 1–7.

Steger H., Zorn R., Gregolec G., Czurda K., Borst M. (2005). Soil Structure Changing caused by electrokinetic processes, *5ème Symposium on Electrokinetic Remediation, Fundamental and Industrial Aspects*, 22 -25 May, Ferrera (Italy).

# Mechanical stability of granular materials subjected to suffusion

A. Wautier<sup>1,2,3</sup>, S. Bonelli<sup>2</sup>, F. Nicot<sup>3</sup>

<sup>1</sup> *AgroParisTech-ENGREF, France.*

<sup>2</sup> *Irstea UR RECOVER, Aix-en-Provence, France.*

<sup>3</sup> *Université Grenoble Alpes, Irstea, UR ETGR, St-Martin-d'Hères, France  
Antoine.wautier@irstea.fr*

## Abstract

Among the four types of internal erosion identified today, suffusion is the only one which affects the internal fabric of granular materials. This selective erosion process has a noticeable impact on the microstructure of soils which may lead, in some cases, to serious consequences on the mechanical stability of the overall grain assembly. Thanks to the DEM (Discrete Element Method) approach, the link between the microstructure and the overall mechanical stability can be investigated through the force chains concept and the directional analysis within the theoretical framework of the second order work. The internal fluid impact on stress transmission can be calculated with a PFV (Pore-scale Finite Volume) fluid/grain coupling scheme. With respect to the onset of mechanical instabilities, the particular role of mobile particles can be highlighted.

## Introduction

Many hydraulic structures such as dams or dikes are made of granular materials which, for most of them, are permeable. Consequently, they are often subjected to internal flows which may modify their microstructure and their overall hydraulic and mechanical properties. Within the geomechanics community, this process is referred to as internal erosion, a phenomenon which might affect the hydraulic structure through four processes, namely backward erosion, contact erosion, piping erosion and suffusion (Bonelli, 2013). Among these four types of internal erosion, suffusion is the only one affecting directly the internal fabric of granular materials which impacts the constitutive behaviour of the material of the hydraulic structure body. At the microscale, this process consists of a rearrangement of particles driven by three elementary mechanisms, namely the detachment of grains from the granular skeleton, their transport through the pore network and possibly their re-attachment to the granular skeleton farther away.

Since the end of the 20<sup>th</sup> century, many criteria have been proposed for assessing the internal stability of a particular soil with respect to suffusion (Kézdi, 2013), (Kenney & Lau, 1985), (Li & Fannin, 2008), (To, Scheuermann, & Galindo-Torres, 2015). These criteria based either on the particle size distribution (PSD) or on the constriction size distribution (CSD) have in common the fact that they aim to identify soils in which the fabric modifications induced by the fluid are negligible due to the impossibility to detach or transport grains. However, very few studies go so far as to consider the evolution of the mechanical properties of soils subjected to suffusion, which is still an open issue today.

Recently, with the capacity of discrete element methods (DEMs) (Cundall & Strack, 1979) to consider a substantial number of particles, as well as the recent development of efficient fluid/grains coupling schemes, it is now possible to model the complete coupled problem of suffusion at the material scale and to explore the onset of mechanical instabilities resulting from the coupling between microstructure, stress state and hydraulic loading. With regard to this problem, this paper investigates the ability of a coupled DEM-PFV approach (Chareyre, Cortis, Catalano, & Barthélemy, 2012) to model the effect of an internal flow on cohesionless soils modelled as a poly-dispersed assembly of spheres. Thanks to the use of micromechanical

tools based on the identification of chained particles (Peters, Muthuswamy, Wibowo, & Tordesillas, 2005), the impact of an internal flow on stress transmission is presented in the first section. In the second section of the paper, the specific influence of the microstructure on the mechanical stability of granular assemblies is estimated within the theoretical framework of the second order work (Nicot & Darve, 2007).

### Numerical assessment of the grain detachment phenomenon

With the YADE software, a cubic assembly of 50,000 spherical particles is generated following a gap-graded particle size distribution (PSD) characterized by a large aspect ratio between the largest and smallest particles ( $r_{\max}/r_{\min} = 25$ ) and by a fine fraction of 25 %. Based on Shire *et al.* (2014), a significant fraction of the fine particles is expected to be incorporated in the primary fabric of the corresponding granular material. At the microscale, the interactions between grains can be modelled with a classical elasto-frictional contact law with parameters given in Table below (Cundall & Strack, 1979).

Parameters	Value
Density	3,000 kg.m <sup>-3</sup>
Young Modulus (E)	356 MPa
Stiffness ratio ( $\nu$ )	0.42
Inter-particle friction angle ( $\phi$ )	35°
Particle-wall friction angle	0°
Number of particles	50,000

A relatively loose sample (shown in Figure 1 (a)) with a void ratio of 0.4 has been prepared following the radius expansion technique until an isotropic confining pressure of 20 kPa is reached. Under this mechanical stress state, a hydraulic loading is then applied in the form of a horizontal hydraulic gradient  $I = 1$ . The modelling of the fluid/grain interactions is achieved numerically through the use of the DEM/PFV scheme implemented in YADE. Pressure type boundary conditions are used in the direction of the fluid while zero flux boundary conditions are imposed on the other sides of our cubic sample. The PFV scheme is based on a tessellation of the pore space on which the Stokes equations are solved in the form of a piecewise constant pressure field. A detailed description of the numerical scheme can be found in (Chareyre, Cortis, Catalano, & Barthélemy, 2012). For the interaction between the particles and the bounding walls, a frictionless contact law is used and no particles are allowed to leave the sample (the eroded particles are retained on the downstream side of the sample).

The impact of the fluid flow on the stress transmission in our sample is assessed with the micromechanical concept of force chains. An enriched definition is used as in (Peters, Muthuswamy, Wibowo, & Tordesillas, 2005) (Wautier, Bonelli, & Nicot, 2017):

- The particles belonging to a force chain have a higher principal stress than the mean particle principal stress;
- The principal stress direction of chained particles is aligned with the geometrical contact direction (less than 45° deviation);
- A force chain contains at least three contacting particles.

Based on this definition, the population of particles transmitting large stresses within the sample is identified and tracked while applying a fluid flow. In Figure 1, the sample used in this section is shown with all the particles (a) and only the chained particles (b).

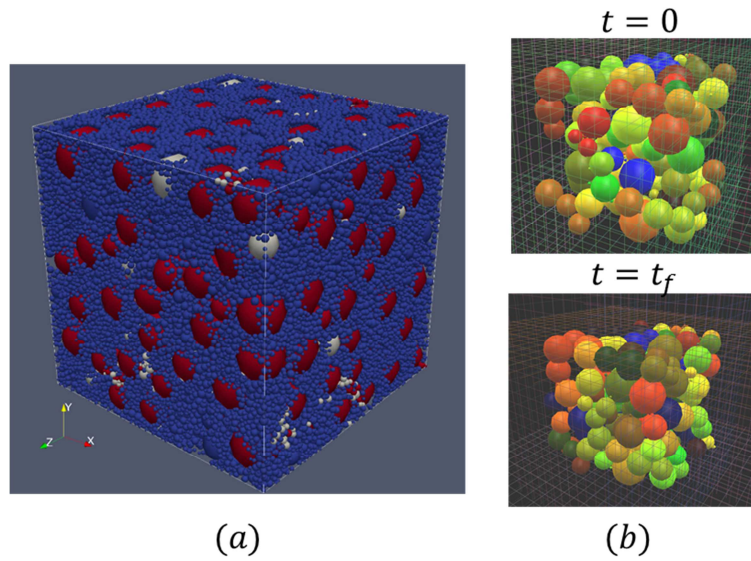


Figure 1. Sample visualisation (a) and force chains visualisation before and after applying a fluid flow (b).

The probability density functions (pdfs) which indicate that a particle of a given radius belongs to the whole sample or to the chained particles are plotted in Figure 2. Generally, the force chains are mainly composed of large particles (positive bias compared to the pdf for the whole sample) but a non-negligible fraction of fine particles is also part of these force chains. The impact of the fluid is visible through the evolution of the chained particles' pdfs before and after the action of the fluid. The number of chained particles increases with time, and more and more fine particles are incorporated into the force chains. As a result, for the considered sample and under the particular stress state and hydraulic loading, the fluid seems to have rather a stabilising effect through an increase in the chained particles' population able to transmit stresses through the medium.

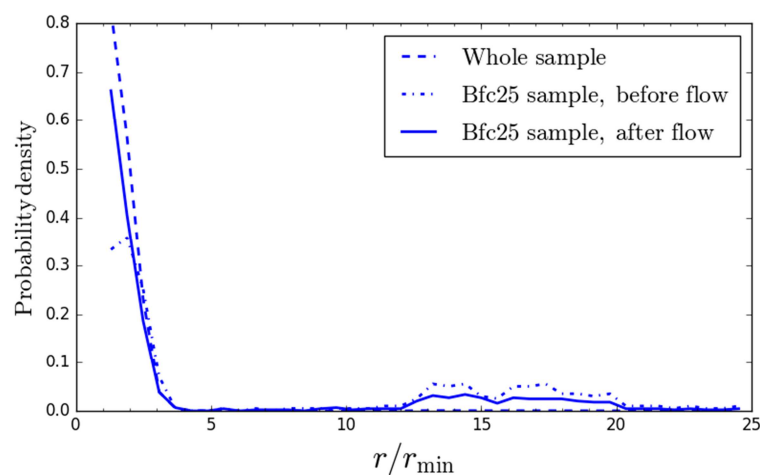


Figure 2. Pdfs corresponding to the whole sample (dashed line), the chained particles before (dot-dashed line) and after (solid line) applying a fluid flow.

## Microstructure influence on the mechanical stability of the specimen

At the material scale, the mechanical stability of a given material can be assessed within the framework of the second order work theory (Nicot & Darve, 2007). Given two infinitely close equilibrium states characterised by the two stress tensors  $\boldsymbol{\sigma}$  and  $\boldsymbol{\sigma} + \delta\boldsymbol{\sigma}$  and the two strain tensors  $\boldsymbol{\varepsilon}$  and  $\boldsymbol{\varepsilon} + \delta\boldsymbol{\varepsilon}$ , the second order work reads

$$W_2 = \delta\boldsymbol{\sigma} : \delta\boldsymbol{\varepsilon}$$

where ":" stands for the double contraction product.

The onset of a mechanical instability is detected provided a direction of an incremental loading leading to the vanishing of the second order work exists ( $W_2 < 0$ ). As shown in (Nicot, Sibille, & Darve, 2009), under some particular loading conditions, the second order work is equal to the opposite of the variation of the kinetic energy per unit volume. As a result, for the considered loading program, a negative  $W_2$  corresponds to a transition from a quasi-static to a dynamic regime.

In this paper, the set of accessible stress states has been reduced to the Rendulic's plane (axisymmetric loadings), and the existence of a loading direction corresponding to  $W_2 < 0$ , is performed thanks to a stress controlled directional analysis within the Rendulic's plane with stress probes of 5 kPa (Nicot, Sibille, & Darve, 2009).

Compared with the first section of the paper, a sample of 10,000 particles with a restricted range of radius values is used ( $r_{\max}/r_{\min} = 3.5$ ) while keeping the same material parameters and the same sample preparation procedure. As shown in Figure 3(b), the existence of instability is found for a triaxial state corresponding to a confining pressure of  $\sigma_0 = 100$  kPa and a stress ratio  $\eta = q/p = 0.45$  where  $q$  is the deviatoric stress and  $p$  the mean pressure.

In order to investigate the role played by the free particles (unaffected by the mechanical loading but highly sensitive to the hydraulic loading) with respect to the mechanical stability of the whole specimen, directional analyses are performed on artificially eroded samples in which all free particles are removed. In Figure 3, for the same confining pressure  $\sigma_0$ , two mechanical stress ratio  $\eta \in \{0.35; 0.45\}$  are considered. For  $\eta = 0.35$  the removal of free particles produces an instability. For  $\eta = 0.45$ , the removal of free particles increases the width of the instability cone.

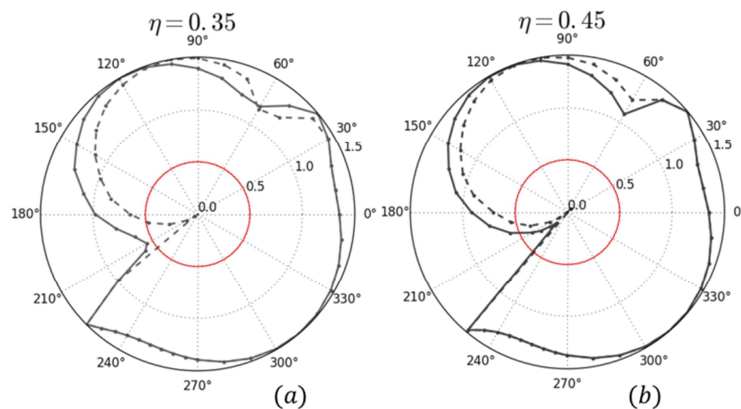


Figure 3. Polar normalised second order work envelopes for two stress ratio ( $\eta = 0.35$  ((a) and  $\eta = 0.45$  (b)). The solid envelopes are computed with all particles while the dashed ones correspond to the "no-rattlers" case. The solid circle corresponds to  $W_2 = 0$  the polar angle to the stress probe direction within the Rendulic's plane.

## Conclusion

In this paper, the impact of a fluid on the mechanical stability of a granular assembly has been explored given the definition of force chains. Surprisingly, the fluid seems to have a rather stabilizing impact for the considered situation as the number of chained particles increases. This might result from the clogging of transported particles (the third step of suffusion). This hypothesis is consistent with the macroscale stability analysis of samples deprived of their movable particles in which the vanishing of the second order work is observed for more stress loading directions within the Rendulic's plane.

## References

- Bonelli, S. (2013). *Erosion in Geomechanics Applied to Dams and Levees*. John Wiley & Sons.
- Chareyre, B., Cortis, A., Catalano, E., & Barthélemy, E. (2012). Pore-scale modeling of viscous flow and induced forces in dense sphere packings. *Transport in Porous Media*, 94(2):595–615.
- Cundall, P. A., & Strack, O. D. (1979). A discrete numerical model. *Geotechnique*, 29(1):47–65.
- Kanit, T., Forest, S., Galliet, I., Mounoury, V., & Jeulin, D. (2003). Determination of the size of the representative. *International Journal of Solids and Structures*, 40(13):3647–3679.
- Kenney, T., & Lau, D. (1985). Internal stability of granular filters. *Canadian Geotechnical Journal*, 22(2):215–225.
- Kézdi, Á. (2013). *Soil Physics: Selected Topics*. Elsevier.
- Li, M., & Fannin, R. J. (2008). Comparison of two criteria for internal stability of granular soil. *Canadian Geotechnical Journal*, 45(9):1303–1309.
- Nicot, F., & Darve, F. (2007). A micro-mechanical investigation of bifurcation in granular materials. *International Journal of Solids and Structures*, 44(20):6630–6652.
- Nicot, F., Sibille, L., & Darve, F. (2009). Bifurcation in granular materials: An attempt for a unified framework. *International Journal of Solids and Structures*, 46(22):3938–3947.
- Peters, J., Muthuswamy, M., Wibowo, J., & Tordesillas, A. (2005). Characterization of force chains in granular materials. *Physical Review E*, 72(4):041307.
- Shire, T., O'Sullivan, C., Hanley, K., & Fannin, R. (2014). Fabric and effective stress distribution in internally unstable soils. *Journal of Geotechnical and Geoenvironmental Engineering*, 140(12):04014072.
- To, H. D., Scheuermann, A., & Galindo-Torres, S. A. (2015). Probability of transportation of loose particles in suffusion assessment by self-filtration criteria. *Journal of Geotechnical and Geoenvironmental Engineering*, 04015078.
- Wautier, A., Bonelli, S., & Nicot, F. (2017). Scale separation between grain detachment and grain transport in granular media subjected to an internal flow. *Granular Matter*, 19(2):22.

# Numerical modelling of sinkhole formation by means of a coupled LBM-DEM model

L.H. Luu<sup>1</sup>, P. Philippe<sup>1</sup>, G. Noury<sup>2</sup>, J. Perrin<sup>3</sup> and O. Brivois<sup>2</sup>

*IIRSTEA, UR RECOVER, 3275 route de Cézanne, 13182 Aix-en-Provence, France.*  
*2BRGM, DRP (Direction Risques et Prévention), 3 Av. Claude Guillemin, BP 36009, 45060 Orléans Cedex 2*  
*3BRGM, D3E (Direction Eau, Environnement, Ecotechnologies), 3 Av. Claude Guillemin, BP 36009, 45060 Orléans Cedex 2*

In this study, we have attempted to reproduce the erosion of a cohesive soil above an underground cavity from numerical hydro-geomechanical modelling. Two scenarios deduced from observations on the site have been taken into consideration: the clogged conduit washout and the dropout sinkhole. The proposed approach is to explore the elementary mechanisms at the scale of the interaction between the fluid and the grains that constitute the soil by using a numerical method which combines the Lattice Boltzmann Method (LBM) for describing the fluid phase and the Discrete Elements Method (DEM) for the solid phase. This coupling is more and more in use for treating complex geomechanical problems such as the phenomenon of erosion [1-5].

## Numerical Method

On the one hand, we have adopted the Lattice Boltzmann schema corresponding to a 2D network in which a fluid particle is constrained to propagate in 9 directions, including the one where it remains immobilised on the same node. The classical resolution of the Boltzmann equation is based on the model developed by Bhatnager-Gross-Krook which uses one single relaxation time. For these studies, we have chosen to implement a more stable model which introduces a collision operator with various relaxation times, called the Multiple Relaxation Time (MRT) (8). On the other hand, the erodible soil has been modelled by a 2D assemblage of rigid disks *via* the discrete elements method which calculates their trajectories by a simple integration of Newtonian movement equations [9]. In order to reproduce a weakly cemented soil, we have implemented a cohesion model which introduces solid bridges between the particles in such a way that a bond is broken when the interaction force exceeds a threshold in traction and in shearing [1, 3, 10]. Finally, a fluid-particle coupling is given by a generalised *bounce-back* relation developed by Bouzidi *et al.* (2001). The hydrodynamic forces exerted by the fluid upon the particles are thus determined from the variation of momentum at the level of the fluid-particle interface.

## Scenario 1: Clogged conduit washout

We have begun by reproducing the process of collapse in a clogged conduit when the ground was liquefied under high hydraulic gradients. Figure 1a shows the implemented numerical schema into which we imposed a preferential draining path within the modelled soil by applying a stark contrast in cohesion between the external layers and the internal conduit (the upper part of the underground conduit). In varying the cohesion, the size of the conduit, and the input pressure, we observed three systems of erosion: the formation of a stable cavity, the regressive collapsing of the granular column within the internal conduit (Fig.1b) and of its entire collapse. A parametric study that can trace the phase diagrams corresponding to these different systems is presently under study.

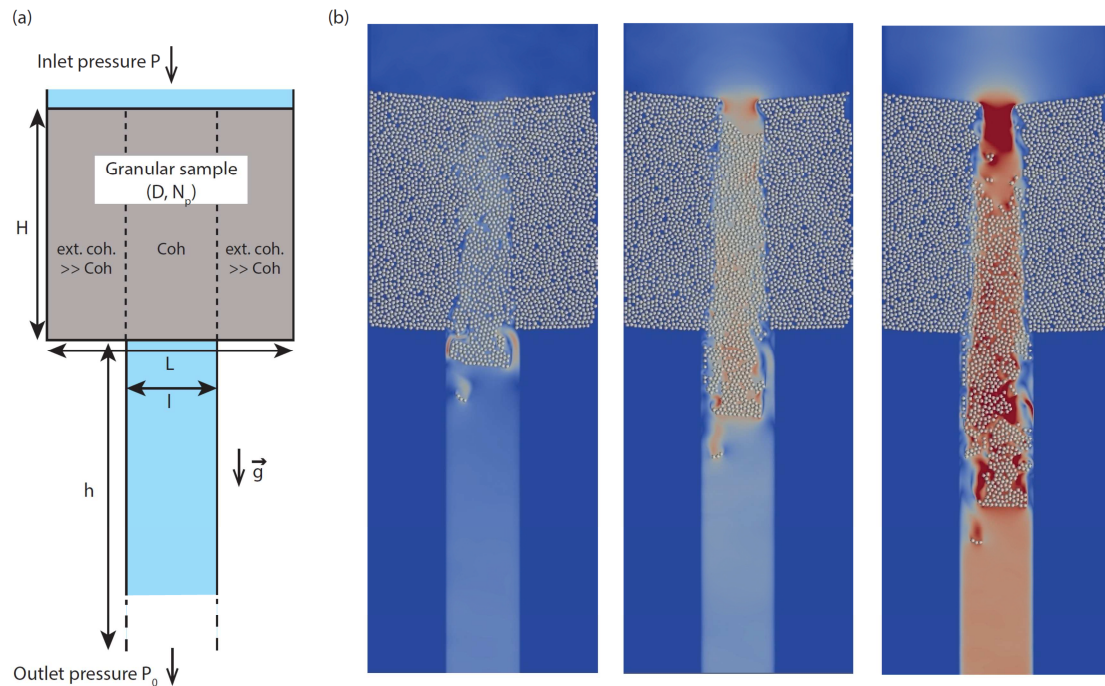


Figure 1 : (a) Numerical schema : diameter and number of particles  $D=6$  mm and  $N_p=3042$ , input pressure  $P=10$  Pa, cohesive force  $C=20$  N, width and height of conduit  $l=11$  cm and  $h=60$  cm, width and height of granular sample  $L=40$  cm and  $H=42$  cm.

## Scenario 2: Dropout sinkhole

The second configuration evoked is almost the same as the preceding one, albeit without the presence of the internal conduit. At first, we observed a progressive evacuation of the particles through the conduit, without any surface movement. Then the top of the soil layer begins to sag. To better understand the structural evolution of the granular sample while it is collapsing, we have examined the process from a micromechanical point of view, at the scale of the inter-particle bonds. Figure 2 focuses on the structure of the granular medium during erosion, in the zone close to the exit towards the conduit. Subjected to the pressure gradient, the granular media auto-organises itself in the form of networks of force chains under compression, more or less perpendicular to the hydraulic flow. The front of the regressive erosion appears to advance in a series of vault-to-vault movements. This structuring clearly reveals an evolving destabilisation of the soil in the shape of a bell, as it has often been observed on the terrain. It is moreover interesting to study the tensile bonds, since this corresponds to one of the failure mechanisms in our cohesion model. Figure 2 shows the lines of highest intensity which are indeed normal to the destabilisation lines in the shape of a bell. To confirm these tendencies in a more quantitative fashion, we represent the distribution of the polar angles of inter-particle bonds in relationship to the centre of the conduit at the level of the exit shown in Figure 3. In considering only the normal forces superior to 30 N in the case of compression, we have found the vault effect by a distribution excepting the angles of  $0^\circ$  and  $180^\circ$ . In traction, by only considering the normal forces inferior to -10 N, we obtained a distribution focused around the excluded angles by compression, that is  $0^\circ$  and  $180^\circ$ . The process of erosion, therefore, takes place through the progressive breaking of force chains, subjected to a mechanism of traction. The next step will be to examine in fine detail the evolution of the hydrodynamic parameters (velocity field, pore pressure, hydrodynamic

force) and to carry out a systematic study of these parameters in order to better understand the physical origin of this regressive process.

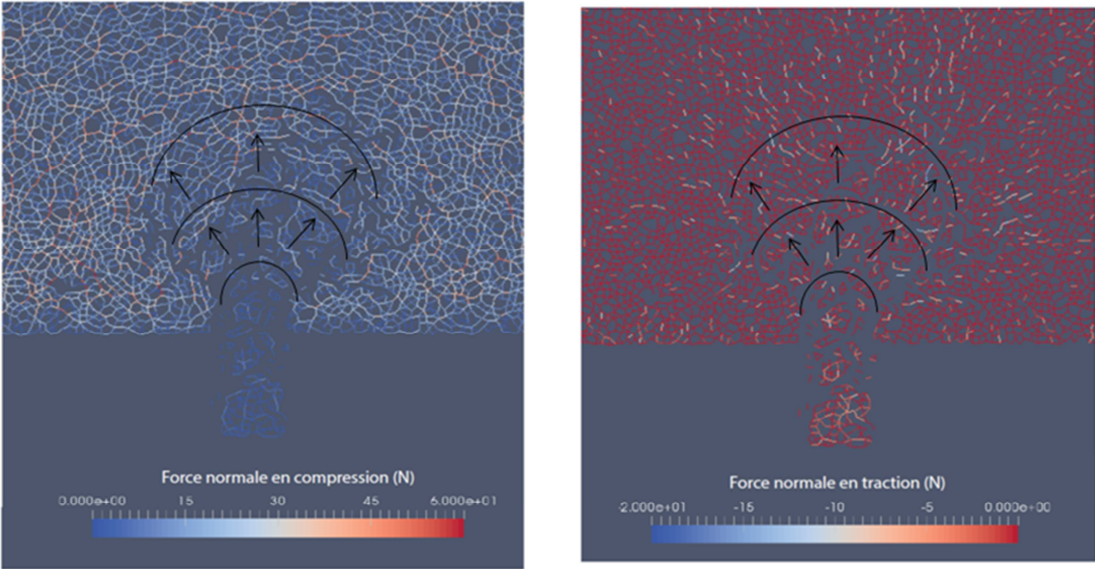


Figure 2 : Network of compressive (left) and tensile (right) normal forces for a simulation with the following parameters: diameter and number of particles  $D=5$  mm and  $N_p=8150$ , input pressure  $P=100$  Pa, cohesive force  $C=20$  N, width and height of conduit  $l=6$  cm and  $h=60$  cm, width and height of granular sample  $L=40$  cm and  $H=40$  cm.

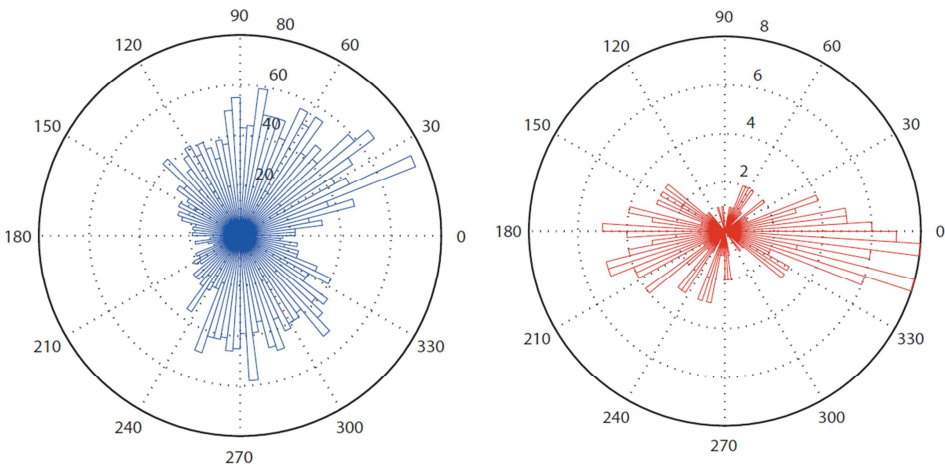


Figure 3 : Angular distribution of bonds between the grains, in compression (left) and traction (right) condition.

**References**

- [1] J.-Y. Delenne *et al.*, *Int. J. Numer. Anal. Meth. Geomech*, 28 1577–1594 (2004)
- [2] L. Sibille *et al.*, *Hydrol. Process.* 29(9) 2149-2163 (2015)
- [3] P. Cuéllar *et al.*, *Proc. 4th Int. Conf. on Particle-based Methods*, PARTICLES (2015)
- [4] P. Cuéllar *et al.*, *Proc. 8th Int. Conf. on Scour and Erosion*, ICSE (2016)
- [5] D.K. Tran *et al.*, *European J. Environ. Civil Eng.* 1-28 (2016)
- [6] S. Succi, *the Lattice-Boltzmann Equation for fluid dynamics and beyond*. Oxford University Press (2001)
- [7] P. Lallemand, L.-S. Luo, *J. Comp. Phys.* 184 406-421(2003)
- [8] R. Du *et al.*, *Physics Letters A*, 359(6), 564-572 (2006)
- [9] P. A. Cundall & O. D. Strack, *Geotechnique*, 29(1), 47-65 (1979)
- [10] M. Jiang *et al.*, *Granular Matter*. 15(1) 65-84 (2013)
- [11] M. Bouzidi *et al.*, *Phys. Fluids* 13 1111-1134 (2007)

# Soil erosion by suffusion: various attempts at describing different mechanisms

L. Sibille<sup>1</sup>, F. Lominé<sup>2</sup>, I. G. Tejada<sup>3</sup>, B. Chareyre<sup>1</sup> and D. Marot<sup>4</sup>

<sup>1</sup> Univ. Grenoble Alpes, CNRS, Grenoble INP, 3SR, Grenoble, France

*Luc.sibille@3sr-grenoble.fr*

<sup>2</sup> INSA Rennes, LGCGM, Rennes, France

<sup>3</sup> Universidad Politécnica de Madrid, ETSI de Caminos, Madrid, Spain

<sup>4</sup> Université de Nantes, CNRS, Institut GeM, Saint-Nazaire, France

Internal erosion in granular soils may involve different steps: the detachment of solid particles from the granular skeleton under the action of water seepage; the transport of the detached particles carried with the water seepage inside the pore space; and eventually, for certain erosion processes, such as suffusion, the possible reattachment of some transported particles to the solid skeleton of the soil, acting as a filter.

The first part of this report will describe and interpret the first step of particle detachment. The analysis is mainly based on direct numerical simulations performed with a fully coupled discrete element–lattice Boltzmann method (DEM-LBM) [3]. The dynamics of the solid granular phase is represented thanks to the DEM in which each solid particle is explicitly described, whereas the dynamics of the interstitial water flow is solved with the LBM. Interactions between the solid phase and the fluid phase are computed at the particle scale, without introducing into the model any phenomenological expression of the fluid-solid interactions (for instance, permeability or drag forces are presumptively not introduced, but constitute a result from the numerical model).

Numerical modellings of piping erosion (Fig. 1) can be interpreted similarly to laboratory hole erosion tests where the erosion rate is linearly related to the hydraulic shear stress (Fig. 2) [3, 5]. Further investigations from the numerical results suggest that the erosion rate for hole erosion in granular matter at low Reynolds number, can also be interpreted as a function of the water stream power (Fig. 1) according to a power law (Fig. 2) [5].

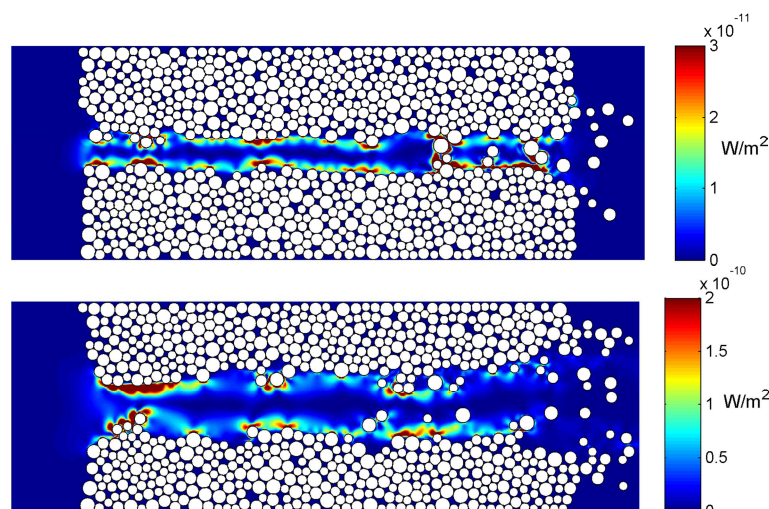


Figure 1. Numerical modelling with the DEM-LBM of a pipe erosion at low Reynolds number. Due to the applied pressure drop, water flows in the preexisting hole from the left to the right. The colour scale represents the field of density of the power dissipated in the fluid by viscosity [5].

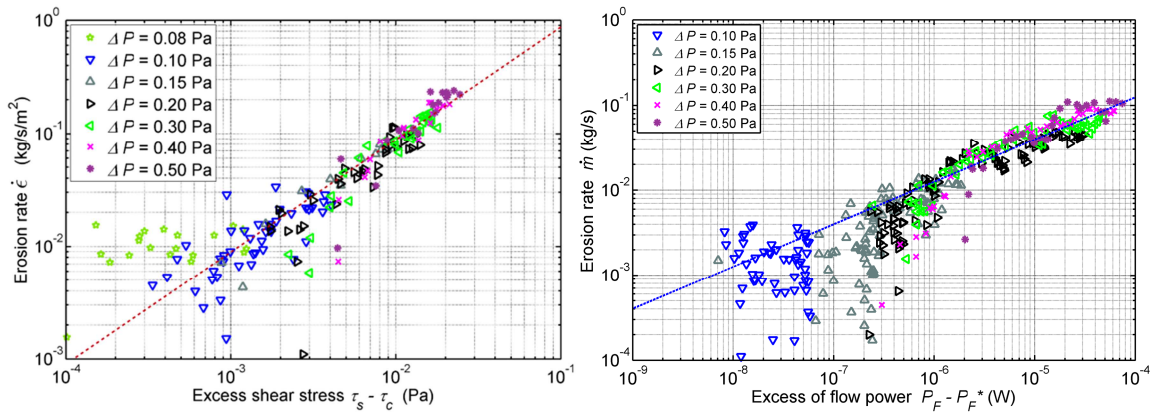


Figure 2. Simulated erosion rate represented, on the left, in terms of excess hydraulic shear stress and, on the right, in terms of excess stream (or flow) power [5].

In the second part of this report, the latter interpretation is applied to experimental data from suffusion tests on a cohesionless soil and glass bead mixtures [4, 6]. Here again, if the change of the erosion rate due to filtration is discarded, the erosion rate is correctly described by the water seepage power according to a power law. Thus, a simple phenomenological model is suggested to describe the whole suffusion process [6], based on the previous results describing the particle detachment, and completed to take also into account the transport and filtration phases. Predictions of this model are compared with experimental results from suffusion tests on glass bead mixtures (Fig. 3).

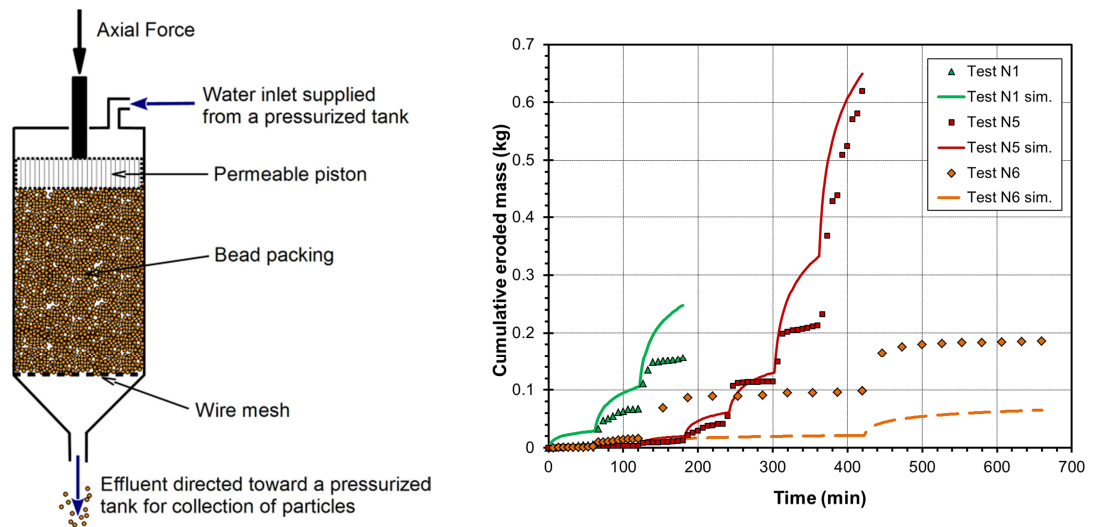


Figure 3. Sketch, on the left, of the oedo-permeameter used to perform suffusion tests on glass bead assemblies. On the right is presented the cumulative eroded mass produced from these suffusion tests, symbols represent experimental data whereas continuous lines represent a model prediction [6].

Finally, as the model proposed suffers from a rather over-simplified, and very phenomenological, description of the transport and filtration of the detached particles, the particle migration in soils has been investigated at a low scale thanks to a new numerical model designed for this purpose. The model is based on the coupling between the DEM and the PFV combining the distinct element method, used for the solid particles, with a pore-scale finite volumes method that solves the fluid flow equations [1, 2]. PFV is developed for Stokes flows of incompressible and Newtonian fluids. After numerical experiments, particle tracking

allows us to obtain, for different cases, the parameters to include in a general advection-dispersion equation (ADE), the advective velocity and the dispersion coefficients. However, in some circumstances, we discovered that particle transport becomes anomalous, which means that the ADE fails to describe the process [7]. Indeed, some conditions may lead to the formation of blockages in the constrictions of the granular assembly (Fig. 4). Blockages constantly appear and disappear, trapping and releasing particles (Fig. 4), and changing the local fluid flows. Such events are the cause of anomalous transport. Under these circumstances we reproduce the evolution of the concentration of particles by using a system of ADEs that are stochastically either time integrated or frozen [7]. Random choices are made according to the PDFs of traveling and blockage life times measured from the numerical experiments.

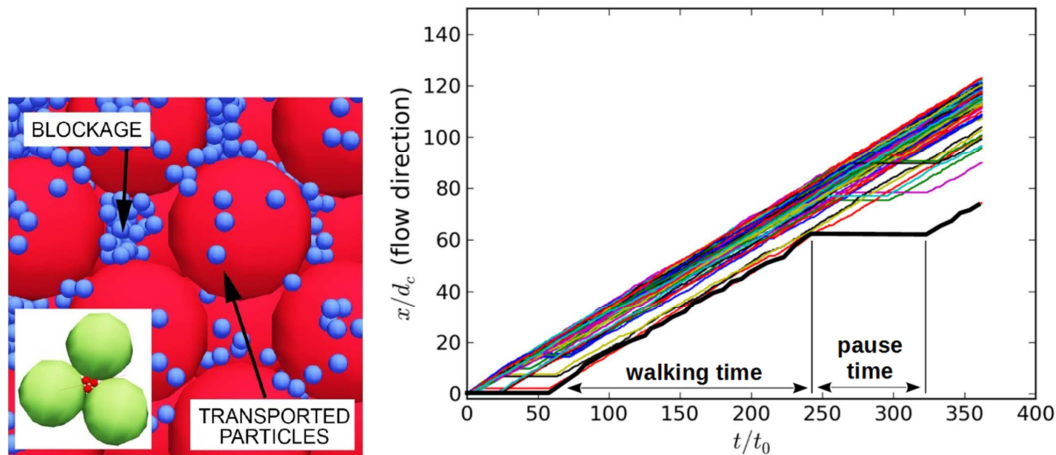


Figure 4. Numerical experiments of particle transport based on the DEM-PFV. On the left: intermittent formation of blockages in the constrictions (the inset represents the arch formed by three fine frictionless particles that originates a blockage). On the right: sample of time series of particle positions in the main flow direction. Horizontal intervals represent periods in which particles were trapped.

## References

- [1] Catalano, E., B. Chareyre, & E. Barthlmy (2014). Pore-scale modeling of fluid-particles interaction and emerging poromechanical effects. *International Journal for Numerical and Analytical Methods in Geomechanics*, 38(1): 51-71.
- [2] Chareyre, B., A. Cortis, E. Catalano, & E. Barthlemy (2012). Pore-scale modeling of viscous flow and induced forces in dense sphere packings. *Transport in Porous Media*, 92(2): 473-493.
- [3] Lominé, F., L. Scholtès, L. Sibille, & P. Poullain (2013). Modelling of fluid-solid interaction in granular media with coupled lb/de methods: application to piping erosion. *International Journal for Numerical and Analytical Methods in Geomechanics*, 37(6): 577-596.
- [4] Sail, Y., D. Marot, L. Sibille, & A. Alexis (2011). Suffusion tests on cohesionless granular matter. *European Journal of Environmental and Civil Engineering*, 15(5): 799-817.
- [5] Sibille, L., F. Lominé, P. Poullain, Y. Sail, & D. Marot (2015). Internal erosion in granular media: direct numerical simulations and energy interpretation. *Hydrological Processes*, 29(9): 2149-2163.
- [6] Sibille, L., D. Marot, & Y. Sail (2015). A description of internal erosion by suffusion and induced settlements on cohesionless granular matter. *Acta Geotechnica*, 10(6): 735-748.
- [7] Tejada I.G., Sibille L., Chareyre B. (2016). Role of blockages in particle transport through homogeneous granular assemblies. *Europhysics Letters (EPL)*, 115(5): 54005.

# Numerical modelling of the hydro-mechanical internal erosion process

J. Yang <sup>a,b</sup>, Z.Y. Yin <sup>a\*</sup>, P.Y. Hicher <sup>a</sup> and F. Laouafa <sup>b</sup>

<sup>a</sup>*Ecole Centrale de Nantes, GeM UMR CNRS 6183, Nantes, France*

<sup>b</sup>*INERIS, Verneuil en Halatte, France*

*Email: jie.yang@ec-nantes.fr*

**Keywords:** internal erosion; hydro-mechanical coupling; finite element method; sand-silt mixture

The phenomenon of internal erosion occurs when fine particles are washed away by seepage forces and transported throughout the matrix of soil particles. The loss of fine particles affects the mechanical behavior of soil. Conversely, the change of porosity influences the soil permeability as, therefore, the hydraulic behaviour. Internal erosion may cause significant damage to geo-engineering works, such as earth dams, dikes and tunnels. To address this problem, the present work proposes a numerical model of the hydro-mechanical internal erosion process by a continuous approach.

At first, a four-phase continuum model of internal erosion was reviewed: in a fluid-saturated granular medium, two constituents, water and fluidized particles, were introduced to describe the fluid suspension hydraulic behavior. The soil skeleton itself consists of a mixture of coarse grains and fine particles, and only the fine particles are erodible. The flow rate in a porous medium was governed by Darcy's law, and a Carman-Kozeny equation was adopted to consider the influence of porosity on the physical permeability. The boundary value problem (BVP) was then completed by a formulation for the volume exchange termed by  $\hat{n}$ . The mechanical behaviour of the solid skeleton is reproduced by an elastoplastic constitutive model for sand-silt mixture (Yin et al. 2016), so that the influence of the change of void ratio and fines content on the mechanical behaviour of the eroded soil could be taken into account. For each soil mixture, the expression of the critical state line

$$e_c = e_{cr0} - \lambda \left( \frac{p'}{p_{at}} \right)^\zeta \quad (1)$$

has been adopted, where  $e_{cr0}$  is the critical void ratio at a given confining pressure,  $\zeta$  and  $\lambda$  are material constants,  $p'$  is the mean effective stress, and  $p_{at} = 101.325$  kPa represents the atmospheric pressure. Only the initial critical state void ratio  $e_{cr0}$  changes with the fines content. The evolution of  $e_{cr0}$  can be determined as proposed by Yin et al. (2016):

$$e_{cr0} = \left[ e_{hc,cr0} (1 - f_c) + \alpha f_c \right] \frac{1 - \tanh \left[ \xi (f_c - f_{th}) \right]}{2} + e_{hf,cr0} \left( f_c + \frac{1 - f_c}{(R_d)^m} \right) \frac{1 + \tanh \left[ \xi (f_c - f_{th}) \right]}{2} \quad (2)$$

where  $e_{hc,cr0}$  and  $e_{hf,cr0}$  are the initial critical void ratios for the coarse and fine grains, respectively.  $\alpha$ ,  $\xi$ ,  $R_d$ ,  $m$  and  $f_{th}$  are material constants. Therefore, the location of the critical state line can be obtained by combining Eqs. (1) and (2) for sand-silt mixture.

The mathematical problem, consisting of a stress equilibrium equation, a mixture flow equation and a mass balance equation, is solved numerically by a discretization procedure through the Galerkin finite element method in space and the finite differences in time.

It was then applied to a 2D computational example shown in Figure 1. An erosion process takes place leading to a decrease of fines in the soil skeleton near the crack. The alteration of porosity and fines was observed. Comparisons of simulations based on different initial fines contents were made, which indicate that the mechanical behaviour of sand–silt mixtures is highly dependent on the proportions of the fines content.

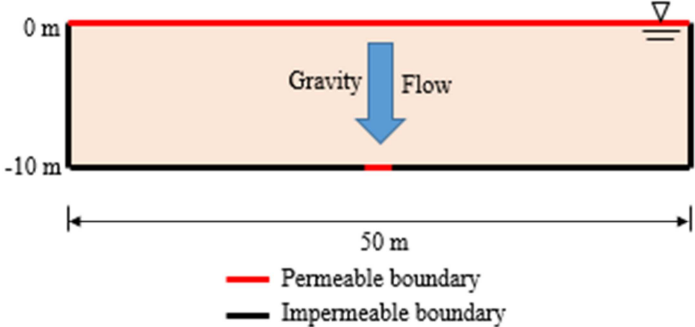


Figure 1. 2D computational example of internal erosion

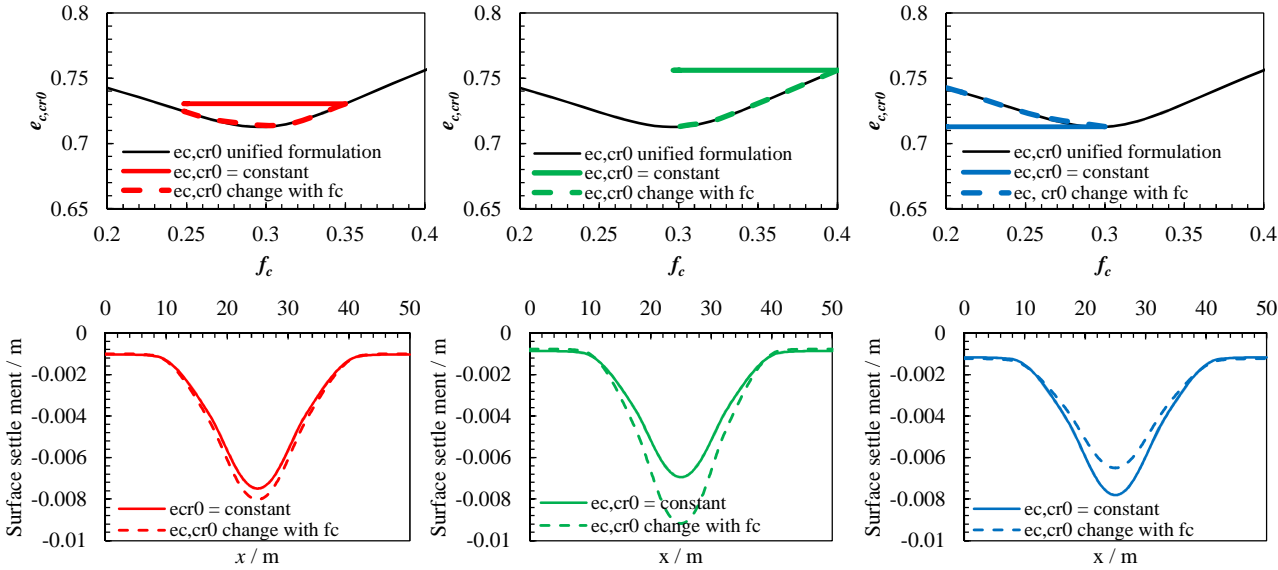


Figure 2. Spatial profiles of surface settlement under different conditions of initial fines content

**References**

Schaufler A, Becker C, Steeb H. (2013) Infiltration processes in cohesionless soils. *ZAMM - Journal of Applied Mathematics and Mechanics*, 93(2), 138-146.

Stavropoulou M, Papanastasiou P, and Vardoulakis I. (1998). Coupled wellbore erosion and stability analysis. *International Journal for Numerical and Analytical Methods in Geomechanics*, 22(9), 749-769.

Vardoulakis I, Stavropoulou M, Papanastasiou P. (1996) Hydro-mechanical aspects of the sand production problem. *Transport in Porous Media* 22: 225-244.

Yin ZY, Huang HW, Hicher PY. (2016) Elastoplastic modeling of sand-silt mixtures. *Soils and Foundations*, 56(3): 520-532.

# Micromechanical aspects of partially saturated granular media with reference to capillary and effective stresses

R. Wan and J. Duriez

*Department of Civil Engineering, Schulich School of Engineering,  
University of Calgary, Canada  
wan@ucalgary.ca*

Geomaterials are usually under unsaturated, i.e. partially saturated, conditions above the water table, thus revealing a three-phase system that consists of a solid phase (the granular skeleton), a liquid phase (water, or any other wetting fluid phase), and a gaseous phase (air, or any non-wetting fluid phase). For engineering purposes, it is important to properly describe their mechanical properties which turn out to be vastly different from those under dry or saturated conditions. Unfortunately, the mathematical analysis of such three-phase system presents some difficulties due to the occurrence of a variety of internal forces and microstructural interconnects. It is found that distinct water and air pressures lead to a non-zero suction,  $s = u_a - u_w$ , which greatly affects the behaviour, in addition to air-water interfaces and corresponding surface tension forces which are basically absent in the dry or saturated conditions. As such, these intricate features have much delayed the generalization of Terzaghi's effective stress concept from saturated to unsaturated conditions, since the early Bishop's attempts (e.g. Bishop & Blight, 1963). At any rate, a fundamental drawback in Bishop's equation is that the corresponding effective stress is expressed from the total stress and an average fluid pressure that is proportional to the suction through a scalar coefficient  $\chi$ . However, it is well-known that the spatial distribution of particle contact normals is most often anisotropic in nature, while the water menisci are also intrinsically linked to contact distribution. Thus, an anisotropic distribution of local suctions is expected in partially saturated media, which requires the suction to be described by a non-spherical tensor rather than a scalar as in Bishop's equation.

Quite recently, the necessity for such a tensorial nature attributed to the coefficient  $\chi$  has been recognised in micro-mechanical analyses of partially saturated granular materials that adopt a resultant force description of the internal forces at hand (Hicher & Chang, 2007, Scholtès et al., 2009). This issue is here revisited through a different micro-mechanical approach where the distributed nature of fluid pressures (within fluid volumes and along wetted surfaces) and surface tension (within air-water interfaces and along three phase contact lines) is explicitly taken into account, instead of reducing these internal forces into a resultant force. From the analytical equations derived in Section I, such an approach also reveals an anisotropic nature that is absent in Bishop's equation. The combination of this analytical approach with a DEM model presented in Section II enables one to actually quantify this anisotropy and to address the effective stress discussion in Section III.

## 1. Homogenisation of stresses in partially saturated granular media

In order to revisit Bishop's equation from micromechanics, the macroscopic i.e. total stress of partially saturated media is homogenised from all the microscopic internal forces at hand. Among these microscopic internal forces, it is important to distinguish:

- the solid phase stress within the solid volume  $V_s$ , caused by various tractions along solid particles such as fluid pressures, surface tension and contact forces,
- the distinct air and water pressures within the corresponding volumes  $V_a$  and  $V_w$ ,
- and also the surface stress  $\pi_{ij} = \gamma(n_i n_j - \delta_{ij})$  for the air-water interface, with  $\gamma$  the air-water surface tension coefficient,  $n_i$  the interface normal, and  $\delta_{ij}$  the identity tensor.

Such a surface stress properly describes the surface tension internal forces existing within the air-water interface (Gurtin & Murdoch, 1975; Chateau & Dormieux, 1995).

The total stress  $\Sigma_{ij}$  is thus expressed as per Eq. (1):

$$\Sigma_{ij} = \langle \sigma_{ij} \rangle = \frac{1}{V} \left[ \int_{V_s} \sigma_{ij} dV + \int_{V_w} u_w \delta_{ij} dV + \int_{V_a} u_a \delta_{ij} dV + \int_{S_{aw}} \pi_{ij} dS \right] \quad (1)$$

which eventually leads to the following expression (Chateau & Dormieux, 1995; Duriez & Wan, 2016; Duriez et al., 2017)

$$\Sigma_{ij} - u_a \delta_{ij} = \frac{1}{V} \left[ \Sigma_{cont.} f_i l_j - s \left( V_w \delta_{ij} + \int_{S_w} n_i x_j dS \right) - \gamma \left( \int_{\Gamma} \nu_i x_j dl + \int_{S_{aw}} (\delta_{ij} - n_i n_j) dS \right) \right] \quad (2)$$

with  $x_i$  the position from the grains centroids of any point along the grains surfaces,  $\nu_i$  the tangent to the interface surface  $S_{aw}$  being orthogonal to the contact lines contours  $\Gamma$  where the three phases meet, and  $n_i$  the outwards normal to the wetted surfaces  $S_w$  or the interface surface  $S_{aw}$ .

Eq. (2) reveals a partitioning of the total stress between a contact stress  $\sigma_{ij}^{cont}$  arising from the contact forces  $f_i$ , i.e.

$$\sigma_{ij}^{cont} = \frac{1}{V} \Sigma_{cont.} f_i l_j \quad (3)$$

and the so-called capillary stresses  $\sigma_{ij}^{cap}$  due to the air-water mixture:

$$\sigma_{ij}^{cap} = \Sigma_{ij} - u_a \delta_{ij} - \sigma_{ij}^{cont} = -\frac{1}{V} \left[ s \left( V_w \delta_{ij} + \int_{S_w} n_i x_j dS \right) + \gamma \left( \int_{\Gamma} \nu_i x_j dl + \int_{S_{aw}} (\delta_{ij} - n_i n_j) dS \right) \right] \quad (4)$$

It is clear from Eq. (4) that the capillary stress does not correspond to an average fluid pressure in the general case, with a non-spherical tensorial expression that is at fundamental variance with Bishop's equation.

## 2. Numerical DEM modelling of wet granular media

In order for Eqs. (2)-(4) to be evaluated and the associated contact and capillary stresses thoroughly investigated, a comprehensive description of the microstructure is necessary, in terms for instance of wetted solid surfaces  $S_w$  or air-water interface surfaces  $S_{aw}$ . To do so, the DEM model recently proposed by Duriez & Wan (2017a) is now considered. The DEM model applies to low water saturation conditions and spherical solid particles, where water distributes into distinct liquid bridges between particles pairs (Fig. 1).

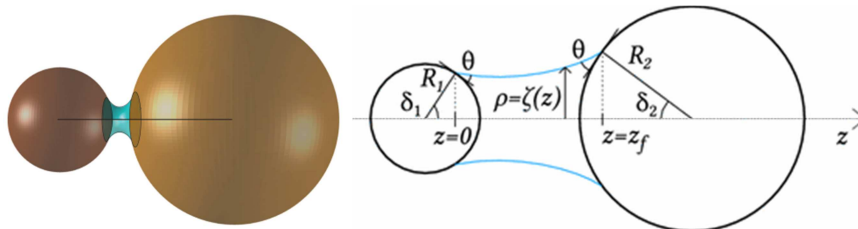


Fig. 1: An axisymmetric liquid bridge between spherical particles

Extending the DEM model by Scholtès et al. (2009), liquid bridges are introduced solving the Laplace-Young equation under uniform suction conditions, for any contact angle  $\theta$  (Fig. 1). Due to the knowledge of the liquid bridge profile (the function  $\zeta(z)$  in Fig. 1), all menisci properties are determined, including the air-water interface  $S_{aw}$ . The DEM model then

provides a direct access to the microstructure of all phases, and a description of strains and stresses in unsaturated conditions through the classical DEM computation cycle. It is to be noted that the resultant force-based stress description of the DEM model is completely equivalent to the above analytically homogenised Eq. (2) (Chateau & Dormieux, 1995; Duriez & Wan, 2017b), provided that the air pressure is taken as reference.

### 3. Multiscale unsaturated soil mechanics

The anisotropic nature of the capillary stresses is now demonstrated via DEM simulations of triaxial compression of an unsaturated granular material. Upon loading, the solid phase microstructure obviously orients itself towards the major principal direction, which reflects on the distribution of wetted solid surfaces for instance, and eventually the capillary stresses (Fig. 2).

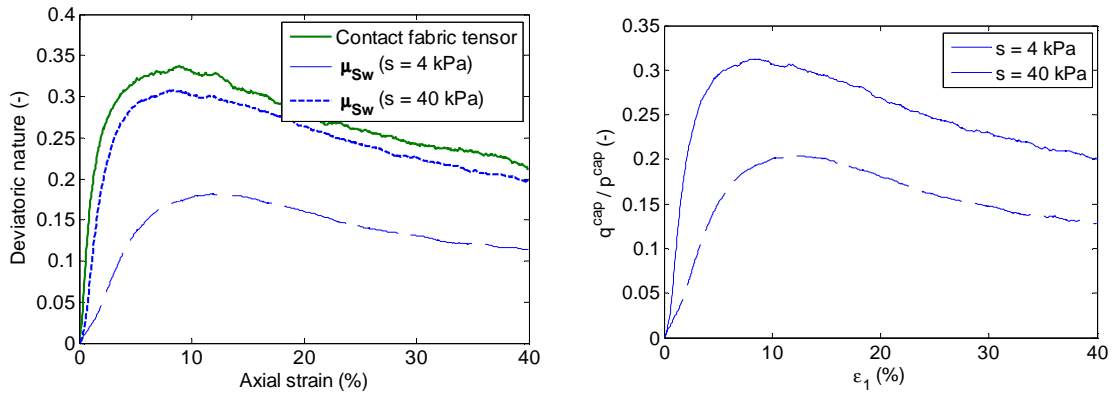


Fig. 2: Deviatoric nature of the contact network, the wetted solid surfaces microstructure  $(\mu_{Sw})_{ij} = \int_{S_w} n_i x_j dS$  and the capillary stress themselves during two triaxial compression tests

From the knowledge of the capillary stresses, the contact stress can also be accessed, and it is shown that the contact stress is an adequate effective stress variable that describes the strength of wet and dry granular media with a unique cohesionless failure criterion (Fig. 3).

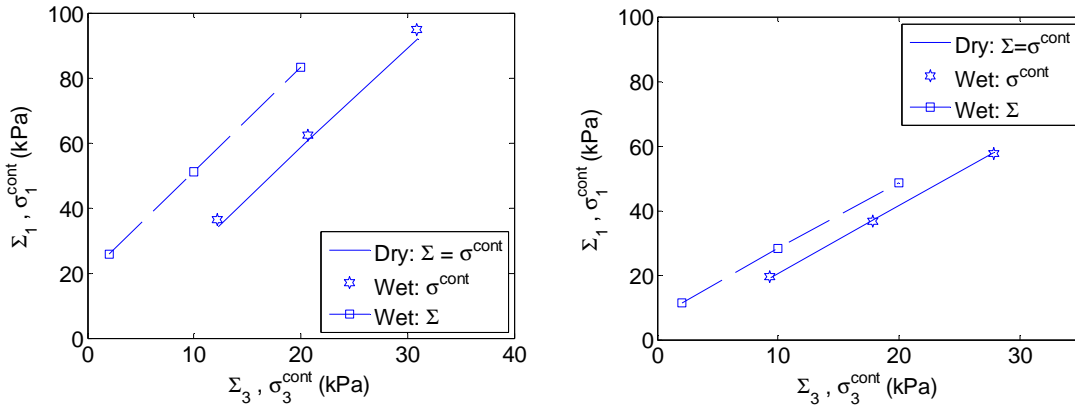


Fig. 3: Stress-strength effective nature of the contact stress for dense (left) or loose (right) granular soils

The complete stress-strength-strain effective nature of the contact stress is currently under investigation, with preliminary results suggesting that the same constitutive relations apply to the quasi-elastic regime of dry and wet granular media using the contact stress defined herein as the effective stress variable.

## References

- A. W. Bishop, G. E. Blight (1963) Some Aspects of Effective Stress in Saturated and Partly Saturated Soils, *Géotechnique* 13:3, 177-197
- X. Chateau, L. Dormieux (1995) Homogenization of a non-saturated porous medium: Hill's lemma and applications, *Comptes Rendus de l'Académie des Sciences*, 320:II, 627–634
- J. Duriez, R. Wan (2016), Stress in wet granular media with interfaces via homogenization and discrete element approaches, *Journal of Engineering Mechanics*, 142:12, 04016099-1–9
- J. Duriez, M. Eghbalian, R. Wan, F. Darve (2017) The micromechanical nature of stresses in triphasic granular media with interfaces, *Journal of the Mechanics and Physics of Solids* 99, 495—511
- J. Duriez, R. Wan (2017a) Contact angle mechanical influence in wet granular soils, *Acta Geotechnica*, 12(1), 67—83
- J. Duriez, R. Wan (2017b) Subtleties in Discrete Element Modelling of wet granular soils, *Géotechnique* 67(4), 365–370,
- M. E. Gurtin, A. I. Murdoch (1975) A continuum theory of elastic material surfaces, *Archive for Rational Mechanics and Analysis* 57:4, 291-323
- P.-Y. Hicher, C.S. Chang (2007), A microstructural elastoplastic model for unsaturated granular materials, *International Journal of Solids and Structures* 44:7-8, 2304 - 2323
- L. Scholtès, P.-Y. Hicher, F. Nicot, B. Chareyre and F. Darve (2009) On the capillary stress tensor in wet granular materials, *International Journal for Numerical and Analytical Methods in Geomechanics* 33:10, 1289-1313

# Modelling gravity-driven segregation in porous media by a phase field approach to unsaturated poromechanics

G. Sciarra<sup>1</sup> F. Casini<sup>2</sup> and J. Vaunat<sup>3</sup>

<sup>1</sup>*Institut de Recherche en Génie Civil et Mécanique  
Ecole Centrale de Nantes, France  
e-mail: [giulio.sciarra@ec-nantes.fr](mailto:giulio.sciarra@ec-nantes.fr)*

<sup>2</sup>*Dipartimento di Ingegneria Civile e Informatica  
Università di Roma TorVergata, Italy*

<sup>3</sup>*Department of Geotechnical Engineering and Geo-Sciences  
Universitat Politècnica de Catalunya, Spain*

**Abstract.** The phase field model of unsaturated poromechanics introduced by one of the authors is numerically implemented within CODE\_BRIGTH, focusing attention only on the behaviour of the air-water mixture saturating the pore space. Within the framework of gradient poromechanics, the problem of gravity driven segregation, in counter-current flow, is addressed naturally reproducing the formation and the propagation of a bulge in the vertical saturation.

## 1 The governing equations

The partially saturated porous medium is described as the superposition of a porous skeleton and a binary mixture of a liquid and a gaseous phase, in particular liquid water and wet air. The partial saturation of the pore space is accounted for conceptualising the fluid mixture as a non-uniform fluid in the sense of Cahn-Hilliard [1], i.e. a fluid possibly having a spatial variation in one of its intensive scalar properties (phase-field). We limit our attention to the case of a non-deformable solid skeleton; thus, only the behaviour of the air-water mixture saturating the pore space is discussed; the (Eulerian or Lagrangean) porosity therefore remains constant and is characterised by its reference value  $n$ .

Following the approach to partial saturation introduced by one of the authors, see [3], the biphasic nature of the fluid is characterised regarding the degree of saturation  $S_r$  as the above mentioned Cahn-Hilliard-like phase-field, where  $S_r=0$  and  $S_r=1$  indicate the gaseous and the liquid phase, respectively. To do this, the liquid phase of the mixture (water) is assumed incompressible and the density of the gaseous phase (wet air) is neglected with respect to that of the liquid; the balance of the fluid mass can therefore be stated as follows:

$$\frac{d(nS_r)}{dt} + (nS_r w_k)_{,k} = 0 \quad (1)$$

where  $w_k$  is the seepage velocity. The governing equations of the problem can be deduced from eq. (1) and from the generalised Darcy law, which takes into account the non local properties of the Cahn-Hilliard fluid describing the saturating mixture, see [3], by means of the following system of partial differential equations

$$\begin{cases} \frac{d(nS_r)}{dt} = \left[ K_{\text{sat}} k(S_r) \left( \mu_{,j}^{\text{eff}} - \frac{b_j^f}{nS_r} \right) \right]_{,j} , \\ \mu^{\text{eff}} = \frac{\partial(\Psi_f + U)}{\partial S_r} - C_{\kappa}(nS_r)_{,kk} . \end{cases} \quad (2)$$

## 2 Modelling counter current flow

Using the results of the laboratory experimental campaign conducted by [2] as a benchmark, a two stage process culminating in gravity-driven counter-current flow through a porous formation is simulated starting from a reference homogeneous configuration, with respect to the saturation degree, passing through an intermediate segregated stage and finally considering the evolution which stems from a  $180^\circ$  rotation of this last one. The formation of a bulge of the wetting and heavier phase can be observed when reproducing the two above mentioned stages of the laboratory test. The numerical simulation is developed assuming the retention characteristics and the permeability of the sand, prescribed by a Van Genuchten model, to be homogeneous over the domain.

*Stage 1* The main goal of this stage is to establish initial conditions which can trigger counter-current, gravity-driven flow in the sample starting from a homogeneous distribution of the phases. The sample initially characterised by a uniform value of the saturation degree,  $S_r = S_r^0 = 0.37$ , is shut into a box, so that water and wet air are allowed to exchange places one with the other in the sample, driven by their density difference, without allowing in-coming or out-coming flow. The result of the simulation is reported in Figure 1.

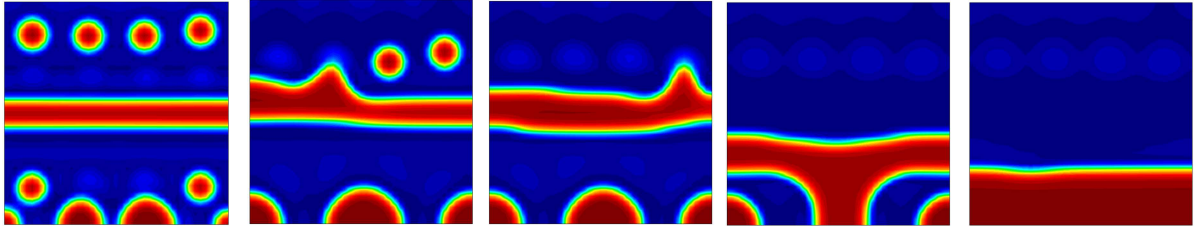


Figure 1. Stage 1- gravity segregation for time  $t=13$  min,  $t=36$  min  $t=45$  min,  $t=76$  min,  $t=81$  min

*Stage 2* The counter-current gravity-driven flow is now obtained, considering a  $180^\circ$  rotation of the sample once equilibrium conditions have been achieved at the end of stage 1. It is reasonable to consider an initial state which is perturbed with respect to this ideal state in the sense that the interface between the coexisting phases is translated by a given length  $l$  along the vertical axis, and the profile is consequently deformed in such a way that the amount of water initially shut into the box remains unchanged. A critical value of  $l$  exists so that, keeping fixed the natural boundary conditions assumed for the stage 1, different evolutions of the perturbed rotated initial state are admissible. In particular, if  $l < l_c$  the equilibrium solution describes a condition of suspended water: no counter-current flow occurs and consequently no gravity-segregation: after the rotation the water remains trapped at the top of the box. On the other hand if  $l > l_c$  the bulge appears at the top of the box and starts to move towards the bottom. In Figure 2, the formation and the propagation of the bulge are depicted at the mean section of the sample along the  $x$  axis.

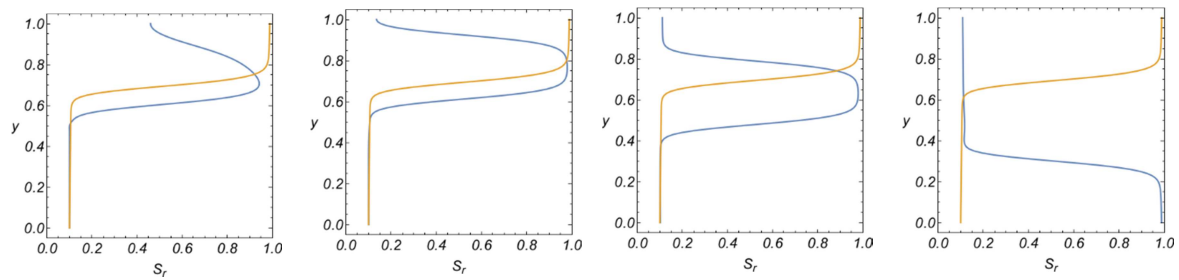


Figure 2: Stage 2 - Gravity segregation for time  $t=0$  min,  $t=1$  min,  $t=8$  min,  $t=33$  min

## References

- [1] Cahn J.W., J.E. Hilliard, 1958. Free energy of a nonuniform system. I. Interfacial free energy. *The Journal of Chemical Physics*, 28 No 2, pp: 258-267
- [2] Karpyn Z.T., Li G., Grader A.S. and Halleck P.M. 2006. Experimental Conditions Favoring the Formation of Fluid Banks During Counter-Current Flow in Porous Media. *Transport in Porous Media*, 62: 109-124
- [3] Sciarra G., 2016. Phase field modeling of partially saturated porous media. *Journal of the Mechanics and Physics of Solids*, 94: 230-256

# First results from a new tomographic survey of early localisation in triaxial tests on sand

J. Desrues

*Univ. Grenoble Alpes, CNRS, Grenoble INP1, 3SR, F-38000 Grenoble, France  
Jacque.desrues@3sr-grenoble.fr*

Strain localisation in soils and rocks has been extensively studied for the last 40 years. On the experimental side, a large number of these studies has been devoted to the experimental observation of localised deformation in laboratory element tests such as biaxial (plane strain) and triaxial tests. 2D and 3D imaging techniques and image analysis methods have been used to characterise the onset and subsequent development of strain localisation. In recent years, these techniques and methods have improved significantly, leading to far more accurate measurement of displacement and strain field in the laboratory specimens. With these new improved lenses, it is time to re-examine some decade-old results in order to assess what can be confirmed and what should be reconsidered.

## 1 Introduction

Strain localisation in soils and rocks has been studied extensively in Laboratoire 3SR, Grenoble, for around the last 40 years (3; 5; 6). It has been shown, using strain field measurement methods, e.g. stereophotogrammetry, that shear banding can take place in both contractive and dilative specimens, under either drained or undrained conditions. Complex localisation patterns have been revealed in axisymmetric triaxial tests using medical X-ray scanners to perform tomographic studies, allowing for the first time to look inside the specimens rather than simply at their outer surface (4; 1). These studies, using imaging techniques that were new at one time, already opened new vistas on the early mechanisms of strain localisation in laboratory specimens: it became clear that the initiation of strain localisation in specimens undergoing a loading process was not properly characterised by the naked eye observation of the specimen during the test, because it could only capture the final gross patterns that can be rather different from the early ones.

In recent years, imaging techniques and image analysis methods have been improved significantly, allowing the displacement and strain fields in the laboratory specimens to be much more accurately measured. High resolution computed tomography (CT), associated with 3D volume digital image correlation (DIC), are the new improved lenses that have changed our observation capabilities. Nowadays, performing *in-situ* (i.e. inside a tomograph) triaxial tests on 70 mm specimens of Hostun sand with a voxel size as small as 50  $\mu\text{m}$  is possible. With such a resolution, one single grain among the 14 million contained in the 538  $\text{cm}^3$  volume of the specimen contains on average  $63 = 216$  voxels. Even though this is not enough to perform an exhaustive survey of the kinematics of the individual grains, as successfully made on 10 mm diameter triaxial specimens of the same sand using our CT scanner (discrete analysis, Andò et al. (2)), it is enough to perform high resolution DIC in terms of continuum kinematics, allowing for a completely new insight of the pre-peak deformation of granular media in axisymmetric triaxial tests, as will be shown in this paper. The present study has been performed on standard scale laboratory specimens, subjected to classical axisymmetric triaxial tests under various test conditions in terms of initial void ratio, end lubrication, slenderness ratio. The results can be compared directly with our 25 year-old tomographic results published in 1996 (4). The goal is to check whether early localisation events can be detected under classical test conditions, and, if yes, to try to characterise these events in detail.

## 2 Materials and methods

Hostun NH31 sand produced by SIBELCO-France has been used in this study. HN31 is the present denomination of Hostun RF sand that was used in the past by our laboratory. The characteristics of the two sands are the same:

(info: [http://www.sibelco.fr/item\\_img/medias/images/ft14\\_hn31.pdf](http://www.sibelco.fr/item_img/medias/images/ft14_hn31.pdf)).

The micro-tomograph used in the study was designed and built by RX-Solution, Annecy, France. The DIC code Tomowarp2 used is an in-house code developed by Tudisco et al. (7).

The triaxial device was designed specifically for this study. The pressure cell is made of PVC, it can sustain up to 600 kPa (limited pressure in order to avoid cell walls too thick that would absorb too much of the X-ray flux). The loading frame allows platen displacement speed in the range of 1-25  $\mu\text{m}$  per second. The nominal specimen diameter and length are, respectively, 70 mm and 140 mm (or 70 mm for short specimens).

Figure 1 shows the triaxial device ready for operation inside the CT scan. From left to right, one can see the X-ray source, the rotation table on which the triaxial cell is fixed, and the detector. The cell is placed close to the detector because the field to be imaged is large (specimen in its possible laterally expanded configuration).

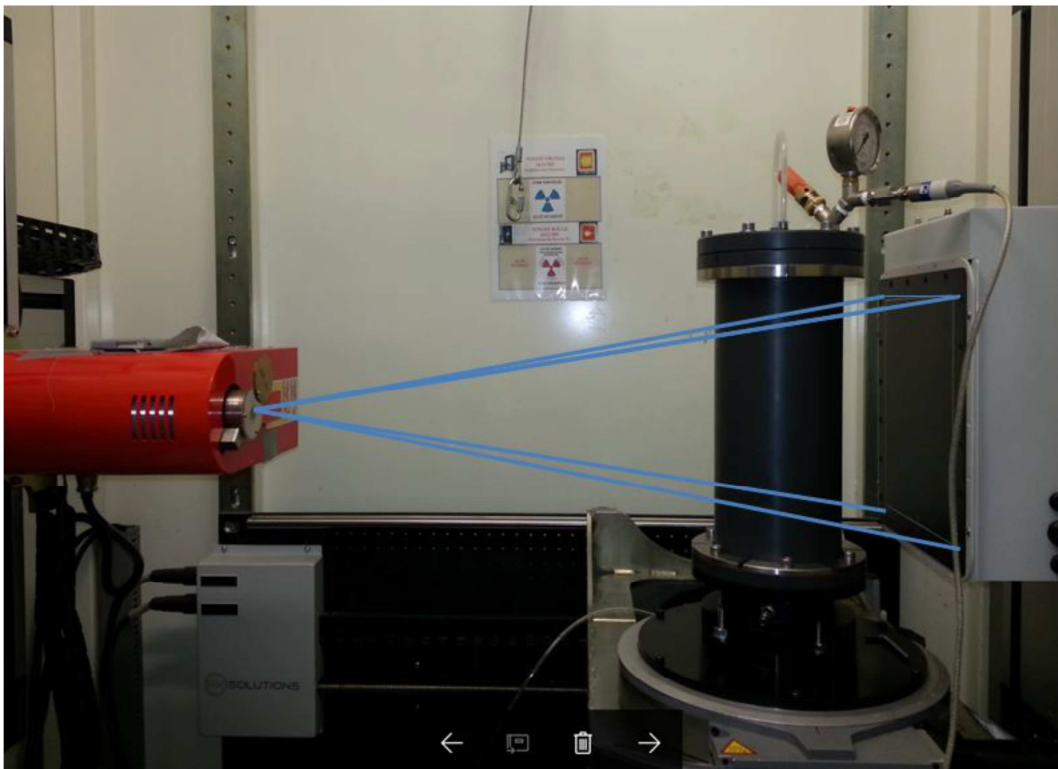


Figure 1: "Tomotriax \_70" setup in the X-ray scanner at 3SR.

## 3 Results and analysis

Although the test campaign is still running, and despite the very time-consuming data processing steps (tomographic image acquisition and reconstruction, digital image correlation, strain field computation, resulting 3D images exploration and rendering) to perform on 3D images as big as 20 Gbytes each, the image that has already emerged is the following: early localisation events are present almost from the beginning of the loading in all the tests, including those performed on loose specimens. These events are numerous, and for each of

them, the geometrical extension (length of the band) is significant with respect to the size of the specimen: typically from one third to one half of the specimen's length, often more. Some of these events tend to grow in intensity as the global deformation of the specimen progresses, some tend to decay. At 20% global axial strain, a few shear bands can be clearly identified, concentrating all of the deformation process, and visible on the surface of the specimen, visible to the naked eye. Still, the direct observation at the stress peak (about 6% to 8% axial strain) did not reveal any visible localisation.

Illustrating these results as 2D images can be challenging, because the very subtle and numerous early localised events become confused when projected onto a plane to produce a 2D picture; 3D dynamic rendering is necessary to separate the events, and to understand their spatial organisation. However, a few images are proposed in this paper to evidence the above statements. They illustrate the test TT70-HN31-001 performed on a dense specimen, slenderness ratio 2, non-lubricated ends, tested under 100 kPa confining pressure.

Figure 2 shows the sequence of incremental deviatoric strain fields presented as 3D volumes with transparency in order to reveal the inner organisation of the deformation events. Each image corresponds to a 2% increment of global axial strain. As indicated by the lookup table, dark blue is for zero and intense red for 10% deviatoric strain. Although difficult to observe clearly on such 2D projections, early events can already be detected in the first increment.

In other tests, not presented in this paper, it was observed that such pre-peak structuration of the deformation process occurs in all the tests performed so far, including tests on dense and loose specimens, long and short, end-lubricated or not.

#### 4 Conclusions

Diffusely distributed strain localisation events have been observed from the early stages of triaxial tests on sand, using X-ray micro tomography and Digital Image Correlation. These findings seem to be rather general: dense and loose specimens, long and short, end-lubricated or not. These events have all the characteristics of shear bands. Should they be considered as precursors of strain localisation, or as already achieved localised events? The theoretical interpretation of these findings presents a number of interesting questions to be studied in future work.

#### Acknowledgments

The research leading to these results has received funding from the European Research Council under the European Union's Seventh Framework Program FP7-ERC-IDEAS Advanced Grant Agreement No 290963 (SOMEF).

The laboratory 3SR is part of the LabEx Tec 21 (Investissements d'Avenir - grant agreement No ANR-11-LABX-0030).

#### References

- [1] Alshibli, K., Sture, S., Costes, N., Frank, M., Lankton, M., Batiste, S., and Swanson, R., "Assessment of Localized Deformations in Sand Using X-Ray Computed Tomography," *Geotechnical Testing Journal*, Vol. 23, No. 3, 2000, pp. 274-299
- [2] E. Andò, S. A. Hall, G. Viggiani, J. Desrues, and P. Bésuelle. Grain-scale experimental investigation of localised deformation in sand: a discrete particle tracking approach. *Acta Geotechnica*, 7(1):1–13, 2012.
- [3] J. Desrues. La localisation de la déformation dans les matériaux granulaires, 1984. *Thèse de Doctorat es Sciences*.
- [4] J. Desrues, R. Chambon, M. Mokni, and F. Mazerolle. Void ratio evolution inside shear bands in triaxial sand specimens studied by computed tomography. *Géotechnique*, 46(3):529–546, 1996.

[5] J. Desrues, J. Lanier, and P. Stutz. Localization of the deformation in tests on sand sample. *Engineering Fracture Mechanics*, 21:909–921, 1985.

[6] J. Desrues and G. Viggiani. Strain localization in sand: an overview of the experimental results obtained in Grenoble using stereophotogrammetry. *International Journal for Numerical and Analytical Methods in Geomechanics*, 28(4):279–321, 2004.

[7] E. Tudisco, E. Andò, R. Cailleteau, and S. A. Hall. Tomowarp2 : a local digital volume correlation code. submitted to *Software XC*, 2017.

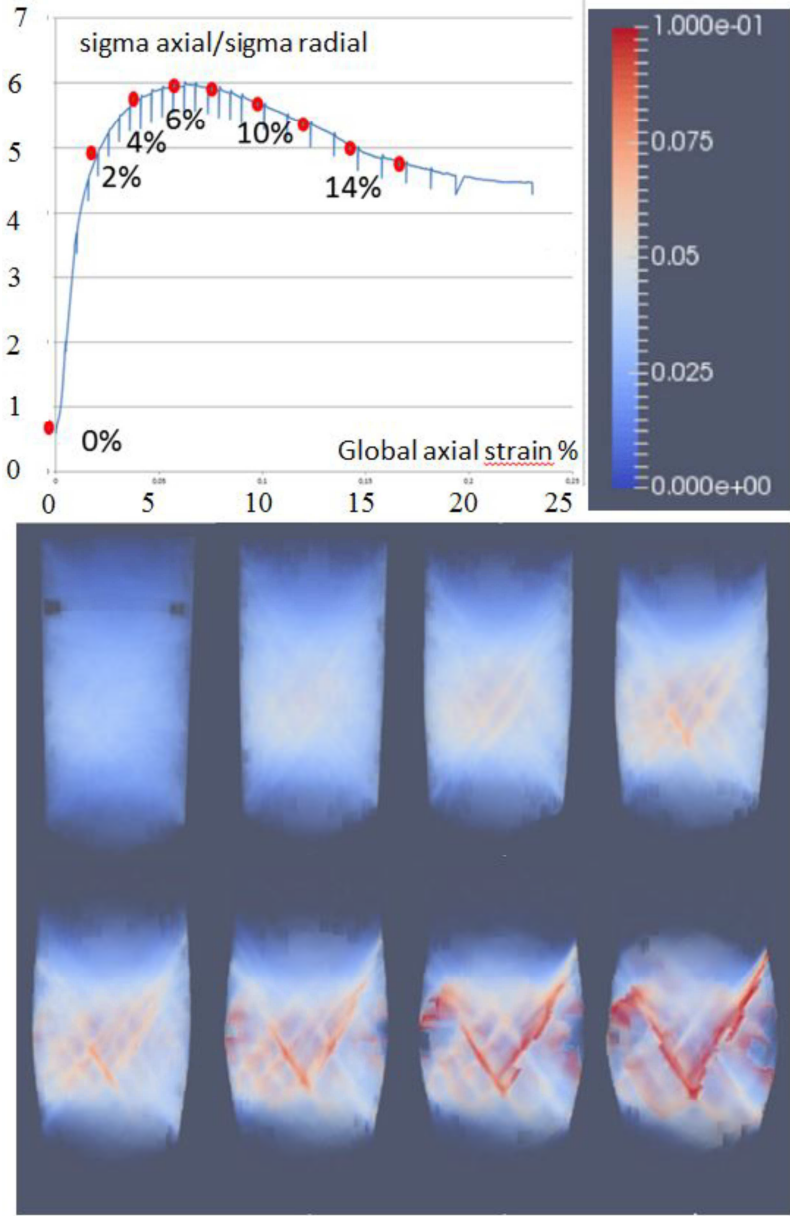


Figure 2: Incremental deviatoric strain fields in axisymmetric triaxial test on Hostun HN31 sand observed using micro-tomography and continuum DIC.

# **Influence of microstructural evolutions on macroscopic mechanical behaviour: contributions of mean-field homogenisation**

**J. Sanahuja and S. Huang**

*Edf lab Les Renardières  
julien.sanahuja@edf.fr*

EDF manages the long term operation of an extensive set of nuclear, thermal and hydraulic power plants. Civil engineering facilities are, as any concrete structure, subject to ageing phenomena in association with environmental conditions, operating conditions and potential internal pathologies. Structure analysis and computations require relevant material constitutive models, which can integrate the influence of degradation, damage and ageing mechanisms. Such mechanisms often occur in pore space, or more generally at a much lower scale than the structure scale. This paper examines the mechanisms associated to chemical processes. Through dissolution and precipitation, the latter induce progressive evolutions of the microstructure. In turn, this microstructural evolution yields variations of the mechanical behaviour. The changes in the microstructure are thus the key linking the chemical processes occurring at lower scales to the mechanical behaviour at the scale of engineering or structure. To bridge the scales, micromechanics represent an appealing tool. This paper proposes applications of cement paste, investigating both improvement (hydration) and degradation (portlandite leaching) mechanisms, and also elastic and creep behaviours. As far as upscaling is concerned, mean-field homogenisation has been used to benefit from its efficient computations.

## **1. Influence of hydration on elasticity of cement paste**

Cement paste and concrete mechanical properties increase during the first months (and even years, albeit in a slower manner) due to the hydration of cement grains. When cement is mixed with water, two progressive time dependent processes start: the anhydrous phases dissolve and the hydrated phases precipitate. Precipitated materials occupy a larger volume than dissolved materials, so that porosity decreases. When the amount of precipitated hydrates is enough to establish percolation between the cement grains, the material transitions from liquid to solid (setting). In short, during hydration, the microstructure evolves to a great extent, and thus mechanical properties also evolve.

To predict the evolution of these properties, a morphological model of cement paste has been built (Figure 1 left). The phases volume fractions are estimated with the Powers model [1] as functions of the  $w/c$  (water to cement mass ratio) which characterises the mix design parameter, and of the hydration degree  $\alpha$  (amount of hydrated anhydrous over initial amount of anhydrous). Then, for each set of these parameters, the paste stiffness can be estimated using homogenisation schemes, from the elastic characteristics of elementary phases measured by nano-indentation. Predictions of the Young's modulus of cement paste are consistent with experimental data at both early and late ages, see Figure 1 right [2].

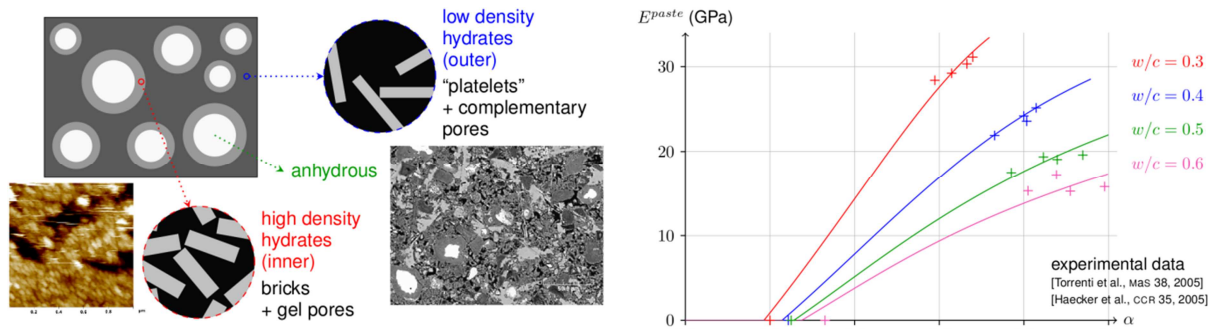


Figure 1 – Left: morphological model of cement paste, with AFM image of hydrates precipitated over an anhydrous grain [Garrault-Gauffinet, PhD, 1998], and a SEM image of paste. Right: Comparison of estimated cement paste Young’s modulus evolution to experimental results

## 2. Influence of portlandite leaching on elasticity of cement paste

From the starting point of a mature and sound cement paste, the influence of portlandite leaching (progressive dissolution due to a continuous renewal of aggressive,  $\text{pH} < 13$ , surrounding water) on cement paste stiffness can be investigated [3]. The first step is to explicitly introduce portlandite in the morphological model, separating it from other hydrates. Even if portlandite can also precipitate, as small crystals are intermixed with C-S-H, only the large and flat hexagonal crystals are considered here. The in-plane size of the latter ( $> 10 \mu\text{m}$ ) suggests to introduce them at the same scale as the anhydrous grains (diameter  $\sim 50 \mu\text{m}$ ), see Figure 2 left. The simplified leaching mechanism adopted here considers that each portlandite crystal can be either sound or completely dissolved, thus replaced by a pore. Then, for each percentage of dissolved portlandite (which could be estimated from a coupled chemistry-transport model, as a function of time, position in structure and external conditions), the loss of Young’s modulus due to degradation can be estimated (Figure 2 right).

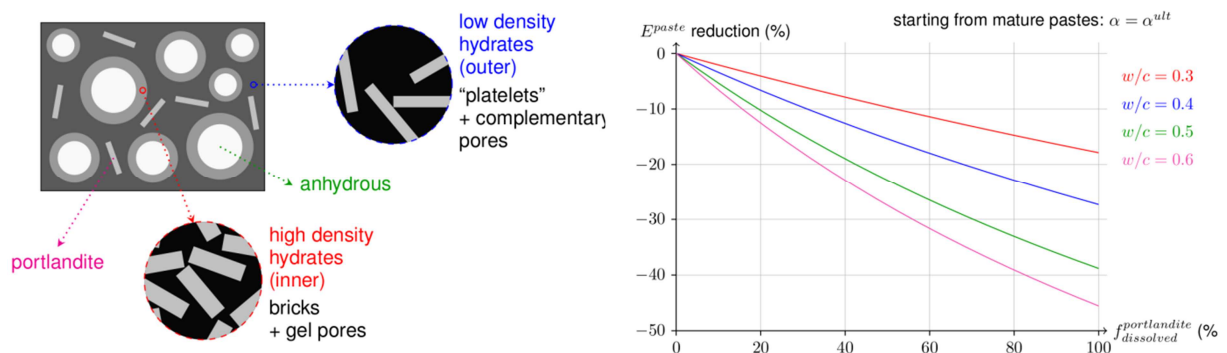


Figure 2 – Left: morphological model of cement paste, separating portlandite from other hydrates. Right: estimation of Young’s modulus loss due to portlandite leaching

## 3. Influence of hydration on ageing basic creep of cement paste

The previous examples considered the elastic behaviour, which does not involve time, thus allowing upscaling to be performed on a time by time basis, working on a “snapshot” of the microstructure. When the investigated behaviour involves time, such as creep, it should be done carefully, as time now appears in both morphological evolutions and the elementary phases behaviour.

Upscaling viscoelasticity has been possible for decades, when the microstructure is constant and phases are non ageing linear viscoelastic, thanks to the correspondence principle [4] which allows the problem to be converted into a series of elastic upscaling problems. However, when phases are ageing or when microstructure evolves, only specific cases could

be considered. Bažant’s solidification theory [5] is applicable to one of these cases: from an evolving microstructure, an ageing viscoelastic behaviour is built. Ageing comes directly from the evolving nature of the microstructure. Unfortunately, this evolution is limited to the precipitation of layers in a parallel arrangement.

Inspired by these pioneering works, a micromechanical extension has recently been made possible, thanks to a new approach of upscaling ageing linear viscoelastic behaviours [6]. In short, the idea is to replace an evolving microstructure by an equivalent composite, whose microstructure is constant but made up of many fictitious ageing phases [7]. The ageing behaviour of each one of these fictitious phases is established to be the equivalent of the behaviour of a domain experiencing phase transformations such as dissolution or precipitation. Then, the macroscopic behaviour of this equivalent composite is estimated by considering an ageing linear viscoelastic mean-field homogenisation [6].

This method is illustrated on cement paste. As the approach is still under development, the adopted morphological model is not as detailed as are the previous ones. Cement paste is considered as a polycrystalline assemblage of anhydrous, hydrates and pores. Initially, only anhydrous particles and pores (full of water, which is not considered here: the drained behaviour is sought) are present. Then, as time proceeds, some anhydrous particles are replaced by hydrates (dissolution followed by precipitation) and some pore particles are replaced by hydrates (precipitation), see Figure 3. Both mechanisms coexist, as, globally, precipitated hydrates occupy a larger volume than do the dissolved anhydrous.

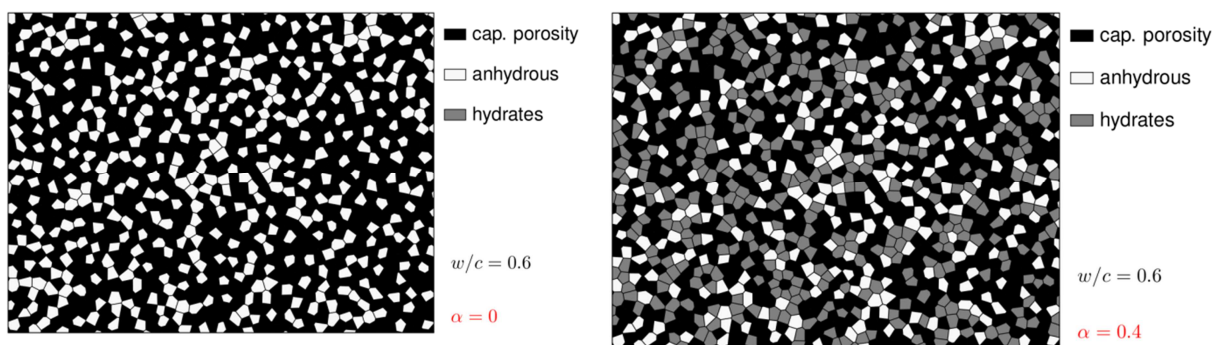


Figure 3 – Simplified evolving morphological model of cement paste, at hydration degrees 0 and 0.4

The paste ageing compliance functions can then be estimated [7]. The classical approach (blue lines on Figure 4 left) assumes microstructure to be “frozen” once mechanically loaded, thus allowing work on a “snapshot” of the microstructure. The new approach (red lines) considers the whole microstructure evolution during mechanical loading, thus working on a “movie” of the microstructure. The inverse of the elastic Young’s modulus (green line), estimated as described in previous sections, is consistent with the initial elastic strain. The “frozen microstructure” assumption induces important differences in the macroscopic behaviour, as long as the microstructure evolves significantly during mechanical loading.

As the upscaling process directly outputs the complete macroscopic ageing linear viscoelastic behaviour, that is the bulk and shear relaxation functions of times  $t$ ,  $t'$  (albeit discretized), to simulate the material response in any mechanical loading path is only a matter of post-processing. For example, creep recovery can be investigated, and is found to be qualitatively consistent with experimental results on cement paste (Figure 4 right).

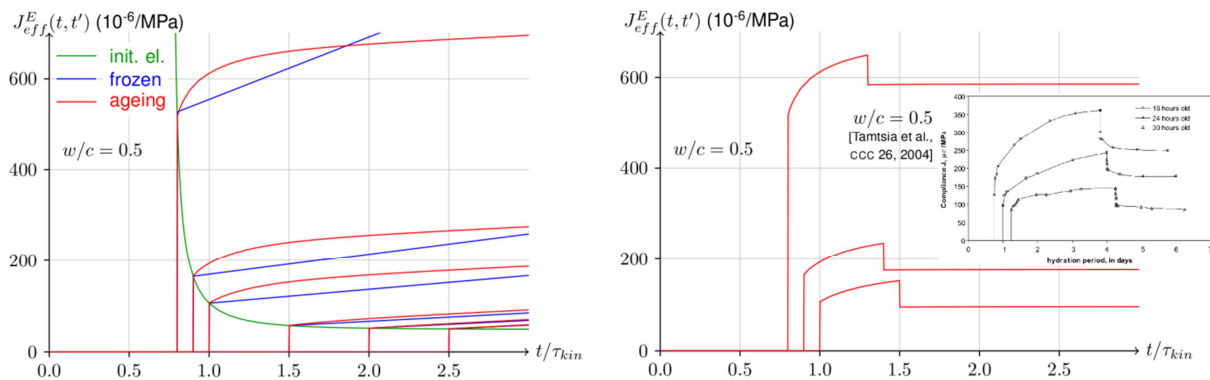


Figure 4 – Estimation of uniaxial ageing basic creep of cement paste. Left: comparison of approximate model considering microstructure as frozen once stress loaded, and model considering microstructure evolution. Right: simulation of creep recovery and qualitative comparison to experimental results

#### 4. Conclusion

Degradation or reinforcement chemical processes affect the mechanical behaviour of materials, often through microstructural evolutions. The microstructure is thus the key for linking chemical processes (such as dissolution or precipitation) occurring at smaller scales to the mechanical behaviour at the structure or engineering scale. Once the mechanisms driving microstructure evolution have been identified, upscaling, from either full-field [8] or mean-field (as illustrated here) homogenisation, allows the macroscopic behaviour to be estimated. Whereas this method can estimate elastic properties in a straightforward manner, estimating the ageing creep would require more advanced homogenisation approaches.

#### References

- [1] T. C. Powers and T. L. Brownyard, "Studies of the physical properties of hardened Portland cement paste (nine parts)," *Journal of the American Concrete Institute*, no. 43, oct. 1946 to april 1947.
- [2] J. Sanahuja, L. Dormieux and G. Chanvillard, "Modelling elasticity of a hydrating cement paste," *Cement and Concrete Research*, vol. 37, no. 10, pp. 1427-1439, 2007.
- [3] S. Garrault-Gauffinet, "Étude expérimentale et par simulation numérique de la cinétique de croissance et de la structure des hydrosilicates de calcium, produits d'hydratation des silicates tricalcique et dicalcique," PhD thesis from Université de Bourgogne, Dijon, France, 1998.
- [4] J. Mandel, "Sur les corps viscoélastiques à comportement linéaire," *Comptes rendus hebdomadaires des séances de l'Académie des Sciences*, vol. 241, no. 25, pp. 1910-1912, 1955.
- [5] Z. P. Bažant and S. Prasanna, "Solidification theory of concrete creep. I: Formulation," *Journal of Engineering Mechanics*, vol. 115, no. 8, pp. 1691-1703, 1989.
- [6] J. Sanahuja, "Effective behaviour of ageing linear viscoelastic composites: homogenization approach," *International Journal of Solids and Structures*, vol. 50, pp. 2846-2856, 2013.
- [7] J. Sanahuja and S. Huang, "Mean-field homogenization of time-evolving microstructures with viscoelastic phases: application to a simplified micromechanical model of hydrating cement paste," *Journal of Nanomechanics and Micromechanics*, vol. 7, no. 1, 2017.
- [8] X. Li, Z. C. Grasley, E. J. Garboczi and J. W. Bullard, "Modeling the apparent and intrinsic viscoelastic relaxation of hydrating cement paste," *Cement and Concrete Composites*, vol. 55, pp. 322-330, 2015.

# The advantages of using a geochemical transport model to simulate the durability of concretes exposed to seawater and sulphates

V.Q. Tran<sup>a</sup> and A. Soive<sup>a,b</sup>

<sup>a</sup>*Cerema, Centre d'études et d'expertise sur les risques, l'environnement, la Mobilité et l'Aménagement,, 9 rue René Viviani, 44262 Nantes, France*

<sup>b</sup>*LUNAM Université, Institut de Recherche en Génie Civil et Mécanique (GeM), UMR-CNRS 6183, Ecole Centrale de Nantes, 1 rue de la Noë, 44321 Nantes, France  
anthony.soive@ec-nantes.fr*

Physically and chemically coupled models contribute to a better understanding of the processes at work during sulfate or chloride reactive ingress into cementitious materials. Several reactive transport models for concrete have been used for durability of cementitious materials in chloride [1] or sulfate environments [2]–[7]. The authors have considered that the current chemical equilibrium state has been obtained locally. Assuming thermodynamic equilibrium implies that the chemical reaction is instantaneous, so that the mineral species are transformed abruptly. However, this behaviour has not been observed experimentally [3], [7]. The mineral dissolution/precipitation of the cement hydrates under coupled thermodynamic equilibrium and kinetic may have a significant influence [8]–[10]. The modelling of this phenomenon seems therefore necessary. In addition, Elakneswaran and al. [11] propose to model the absorption of chloride ions by a surface complexation model. This model describes the binding of the ions on the mineral surface such as C–S–H. It would be interesting to apply this principle to sulfates. Such a physico-chemical description permits overcoming the use of empirical chloride binding isotherms that can be difficult to assess, especially for concretes with supplementary cementitious materials.

In this study, a new physically and chemically coupled model taking into account multiionic diffusion, precipitation/dissolution kinetics and surface complexation has been proposed to predict the reactive transport of ions into saturated cementitious materials. The results are compared to experimental data and numerical profiles that were previously obtained in the literature.

The results show good agreements between experimental and numerical results and better numerical results than those proposed in the literature for sulfate ingress. They also show that the surface complexation has to be taken into account in order to reproduce the sulfate amount peak experimentally observed during sulfate ingress. In addition, dissolution and precipitation kinetics are indispensable for retrieving the sulfate amount amplitude and, even, the slow decay of the sulfate amount after the peak. Finally, the model may explain the supersaturation of the sulfate concentration with respect to ettringite because of the monosulfoaluminate dissolution and the ettringite (see Figure 1).

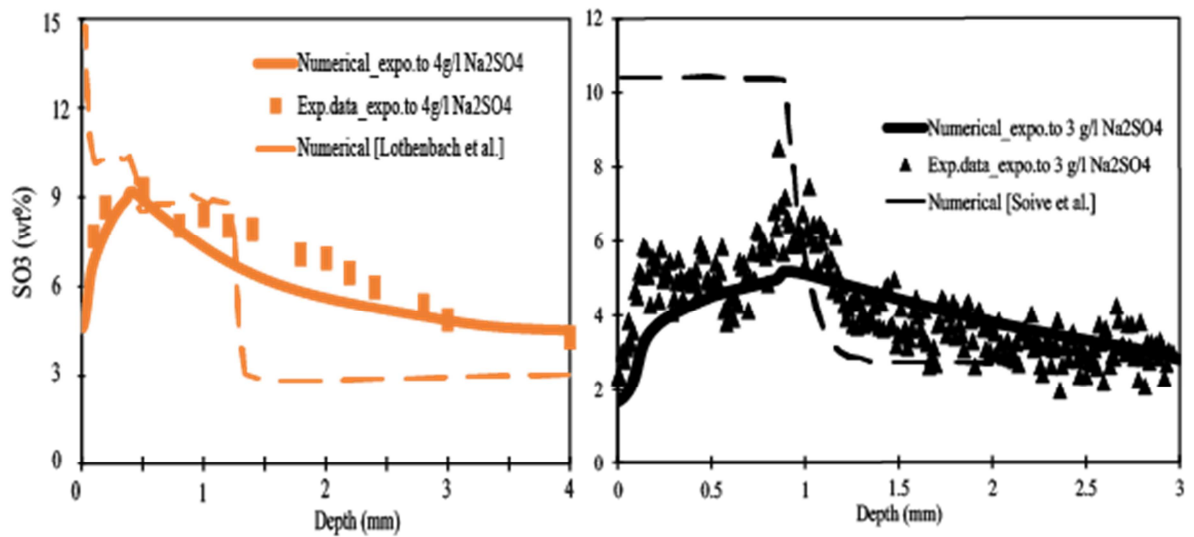


Figure 1. Comparison between experimental and numerical SO<sub>3</sub> profile for two CEM I mortars after 56 days of exposure to 4 g/l of Na<sub>2</sub>SO<sub>4</sub> (left) and for 160 days of exposure to 3 g/l of Na<sub>2</sub>SO<sub>4</sub> at 20°C (right)

Concerning the chloride ingress, Figure 2 shows comparisons between experimental and numerical results of the chloride binding capability of concretes exposed to NaCl, KCl, MgCl<sub>2</sub> and CaCl<sub>2</sub> solutions. This is distinct evidence that the numerical model can be used as a reliable tool to predict the chloride binding capability.

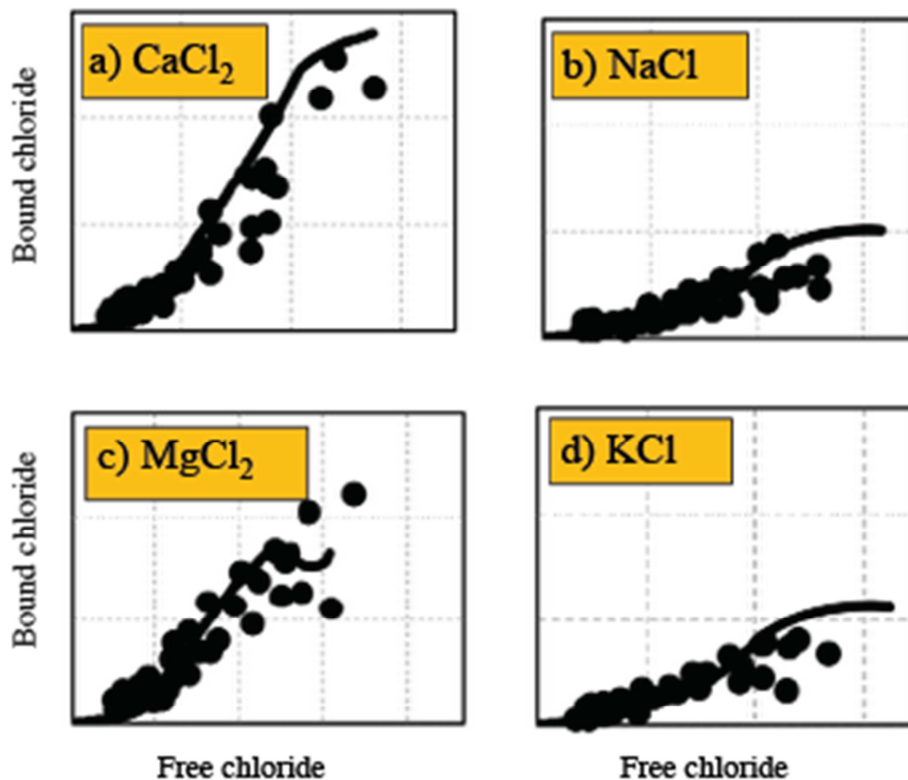


Figure 2. Chloride binding isotherm for an OPC exposed to different solutions (CaCl<sub>2</sub>, NaCl, MgCl<sub>2</sub>, KCl)

## References

- [1] E. Samson and J. Marchand, "Modeling the effect of temperature on ionic transport in cementitious materials," *Cem. Concr. Res.*, vol. 37, pp. 455–468, 2007.
- [2] Y. Maltais, E. Samson, and J. Marchand, "Predicting the durability of Portland cement systems in aggressive environments—Laboratory validation," *Cem. Concr. Res.*, vol. 34, no. 9, pp. 1579–1589, Sep. 2004.
- [3] B. Lothenbach, B. Bary, P. Le Bescop, T. Schmidt, and N. Leterrier, "Sulfate ingress in Portland cement," *Cem. Concr. Res.*, vol. 40, no. 8, pp. 1211–1225, 2010.
- [4] Y. Hosokawa, K. Yamada, B. Johannesson, and L.-O. Nilsson, "Development of a multi-species mass transport model for concrete with account to thermodynamic phase equilibriums," *Mater. Struct.*, vol. 44, no. 9, pp. 1577–1592, 2011.
- [5] B. Bary, N. Leterrier, E. Deville, and P. Le Bescop, "Coupled chemo-transport-mechanical modelling and numerical simulation of external sulfate attack in mortar," *Cem. Concr. Compos.*, vol. 49, pp. 70–83, 2014.
- [6] M. M. Jensen, K. De Weerd, B. Johannesson, and M. R. Geiker, "Use of a multi-species reactive transport model to simulate chloride ingress in mortar exposed to NaCl solution or sea-water," *Comput. Mater. Sci.*, vol. 105, pp. 75–82, 2015.
- [7] A. Soive, E. Rozière, and A. Loukili, "Parametrical study of the cementitious materials degradation under external sulfate attack through numerical modeling," *Constr. Build. Mater.*, vol. 112, pp. 267–275, 2016.
- [8] N. C. M. Marty, C. Tournassat, E. Giffaut, E. C. Gaucher, R. J. Monnet, and F.- Cha, "Influence of reaction kinetics and mesh refinement on the numerical modelling of concrete / clay interactions," *J. Hydrol.*, vol. 364, no. 1–2, pp. 58–72, 2009.
- [9] T. J. Tambach, M. Koenen, L. J. Wasch, and F. Van Bergen, "Geochemical evaluation of CO<sub>2</sub> injection and containment in a depleted gas field," *Int. J. Greenh. Gas Control*, vol. 32, pp. 61–80, 2015.
- [10] N. C. M. Marty, O. Bildstein, P. Blanc, F. Claret, B. Cochevin, E. C. Gaucher, D. Jacques, J.-E. Lartigue, S. Liu, K. U. Mayer, J. C. L. Meeussen, I. Munier, I. Pointeau, D. Su, and C. I. Steefel, "Benchmarks for multicomponent reactive transport across a cement/clay interface," *Comput. Geosci.*, vol. 19, no. 3, pp. 635–653, 2015.
- [11] Y. Elakneswaran, A. Iwasa, T. Nawa, T. Sato, and K. Kurumisawa, "Ion-cement hydrate interactions govern multi-ionic transport model for cementitious materials," *Cem. Concr. Res.*, vol. 40, no. 12, pp. 1756–1765, 2010.

# Modelling the coupling of chloride and carbonation in concrete

M. Achour<sup>1,2</sup>, O. Amiri<sup>2</sup>, F. Bignonnet<sup>2</sup> and E. Rozière<sup>1</sup>

<sup>1</sup> Ecole centrale de Nantes, GeM, Institut de recherche en Génie Civil et Mécanique,  
1 Rue de la Noë, 44321 Nantes, France

[mohamad.achour@eleves.ec-nantes.fr](mailto:mohamad.achour@eleves.ec-nantes.fr) – [emmanuel.roziere@ec-nantes.fr](mailto:emmanuel.roziere@ec-nantes.fr)

<sup>2</sup> Université de Nantes, GeM, Institut de recherche en Génie Civil et Mécanique,  
1 Quai de Tourville, 44035 Nantes, France

[ouali.amiri@univ-nantes.fr](mailto:ouali.amiri@univ-nantes.fr) – [francois.bignonnet@univ-nantes.fr](mailto:francois.bignonnet@univ-nantes.fr)

**Abstract.** Chloride attack and carbonation are the predominant degradation mechanisms governing the service-life of reinforced concrete structures. In order to evaluate the service-life of these structures against the penetration of carbon dioxide, chloride ions and moisture, a physico-chemical model is proposed. The model has been developed by taking into account multi-species transfer of aggressive ions, including diffusion, migration, chemical activity of ions, interaction between chloride ions and cement paste of concrete and convection due to the exposure conditions. The microstructure evolution due to the precipitation and the dissolution reactions during the carbonation process is taken into account by following the evolution of the porosity. Several applications of the numerical model are developed by predicting the service-life of a porous concrete specimen exposed to an aggressive environment containing chloride, carbon dioxide and moisture. Finally, the effects of carbonation and convection on the estimation of the concrete cover are emphasised and analysed.

**Keywords:** Degradation mechanisms, Carbonation, Multi-species transfer, Moisture, Service-life

## 1. Introduction

The service life of reinforced concrete structures depends on many variables among them environmental ones, such as chloride, moisture and carbon dioxide penetration. The aim of this work is to develop an original model able to describe the combined transport of chloride ions and carbon dioxide under various cycles of wetting and drying conditions.

Many research works have studied only the effect of chloride transport [PHU 2016], while others only the transport of carbon dioxide [VIL 2006]. Recently, a few studies have shown that for concrete subjected to both chloride ions ingress and carbonation, carbonation influences the transport of chloride ions significantly [MAI 2013]. In this work, a 1D multi-species model has been developed to study the transport of ions in porous concrete considering the effect of electrostatically interactions and chemical activity between ions [HUC 1923], convection and interaction between chloride ions and cement paste of concrete.

## 2 Numerical modelling

### 2.1 Ionic transport

The transport of ions in pore solution is described using the Nernst Planck equation:

$$J_i = -D_i \left[ \text{grad}C_i + \frac{z_i F}{RT} C_i \text{grad}\Psi + C_i \text{grad}(\ln Y_i) \right] + C_i V \quad (1)$$

where  $D_i$ ,  $C_i$ ,  $z_i$  and  $\gamma_i$  are respectively the effective coefficient of diffusion, the concentration, the valence and the coefficient of activity of the ion  $i$ .  $F$  the Faraday constant,  $R$  the ideal gas constant,  $T$  the temperature,  $\psi$  the electrostatic potential and  $v$  the velocity of water.

## 2.2 Carbon dioxide transport

The transport of carbon dioxide is resumed with the physico-chemical equilibrium which exists between solid components and the pore solution in the concrete [THI 2005]. During the coupling of carbonation-chloride ions, the porosity changes. This table presents the equilibrium corresponding to the two aspects of the carbonation process: dissolution of  $CO_2$  and carbonation reaction, in addition to the evolution of the porosity.

**Table 1.** Chemical kinetics, thermodynamical equilibrium of  $CO_2$  transport in concrete and law of evolution of the porosity.

Chemical kinetics	Evolution of the porosity	Thermodynamical equilibrium
$\delta_{CSH}^0 = \frac{\partial S_{CSH}}{\partial t}$ $\delta_{CSH}^0 = \frac{1}{3} \frac{\partial S_{CaCO_3-CSH}}{\partial t}$ $\delta_{CSH}^0 = 3 \frac{\partial S_{SH(gel\ de\ silice)}}{\partial t}$ $\delta_{CaOH_2}^0 = \frac{\partial S_{Ca(OH)_2}}{\partial t} = -X_P^0 \frac{1}{1 + \frac{h}{D} \frac{R_p(\gamma)}{R_c(\gamma)} (R_c(\gamma) - R_p(\gamma))}$ <p><math>S_{Ca(OH)_2}</math> is the amount of portlandite, <math>R_p(\gamma)</math>, <math>R_c(\gamma)</math>, <math>X_P^0</math>, <math>h</math> and <math>D</math> are the parameters which depend on the portlandite.</p>	$\Delta \varepsilon = \bar{\gamma}_{NaCl} C_{NaCl} + \bar{\gamma}_{CaCO_3} S_{CaCO_3} - \bar{\gamma}_{CaOH_2} (S_{CaOH_2}^0 - S_{CaOH_2}) + \Delta \bar{\gamma}_{CSH} (S_{CSH}^0 - S_{CSH})$	$[H_2CO_3] = K_H [CO_2]$ $[HCO_3^-] = K_1 [OH^-] [H_2CO_3]$ $[CO_3^{2-}] = K_2 [OH^-] [HCO_3^-]$ $K_p = [Ca^{2+}] [OH^-]^2$ $K_c = [Ca^{2+}] [CO_3^{2-}]$ $K_e = [OH^-] [H^+]$

$K_H$ ,  $K_1$ ,  $K_2$ ,  $K_E$ ,  $K_P$ , and  $K_C$  are the equilibrium constants of the carbonation process,  $\bar{\gamma}_{NaCl}$ ,  $C_{NaCl}$ ,  $S_{CSH}^0$ ,  $S_{CSH}$  and  $\Delta \bar{\gamma}_{CSH}$  are, respectively, the molar volume and the concentration of NaCl, the initial and instantaneous amount of CSH and the variation of the volume due to the carbonation of 1 mole of CSH.

## 2.3 Humidity transport

The model adopted for the moisture transport takes into account the water released by the carbonation process. This equation can be derived as follows:

$$\frac{\partial S_e}{\partial t} = - \frac{K_e K_{re}}{\varepsilon \mu_e} \frac{\partial P_c}{\partial S_e} grad S_e + \frac{R_a D_{va}}{\rho_e} \frac{\partial \rho_v}{\partial S_e} grad S_e - \frac{M_{H_2O}}{\rho_e} \frac{\partial S_{CaOH_2}}{\partial t} \quad (2)$$

$K_e$ ,  $K_{re}$ ,  $R_a$ ,  $D_{va}$ ,  $P_c$ ,  $\mu_e$ ,  $M_{H_2O}$  and  $\rho_e$  are, respectively, the intrinsic and relative water permeability, the resistance into the air, the coefficient of diffusion of water vapor, capillary pressure, the viscosity, the density and the molar mass of water.

## 3 Results and discussion

The concrete mixture used in this study has been designed and characterised by [KHO 2010]. It has the following composition :

**Table 2.** Composition of the concrete specimen

Materials used (Kg/m <sup>3</sup> )	Eco-concrete
Cement CEM I 52.5N	103
Gravel	1037
Sand 0/4	816
Blast furnace slag	310
Ratio E/C	1.65

The initial porosity  $\varepsilon_0$  was measured and found equal to 15 % and the intrinsic water permeability in initial state was estimated around  $2 \times 10^{-20} \text{m}^2$ . Chloride binding isotherms are modelled with a Langmuir isotherm. The concrete specimen was exposed to combined carbonation (2%) and chloride attack (0.5 M) over 1 year of 6h/6h of wetting and drying cycles. The coefficient of diffusion of ions and  $\text{CO}_2$  are calculated as a function of saturation degree and porosity [BUC 2000], [THI 2005]. The model allows predicting the final contents of all solid phases in the concrete according to time.

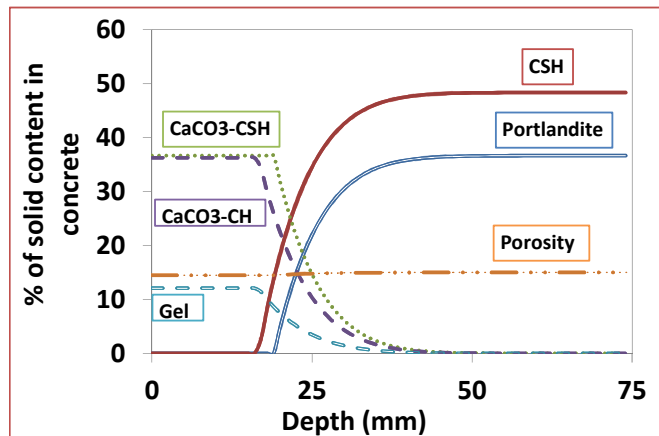


Figure 1. Amount of solid components after 1 year of test period

The originality of the model lies in the coupling of carbonation and chloride ions penetration. The penetration depth of chloride ions is greater when we consider the combined transport. These figures show that for a specific concentration of chloride ions (sea water for example) the concrete cover is underestimated when we neglect the effect of carbonation.

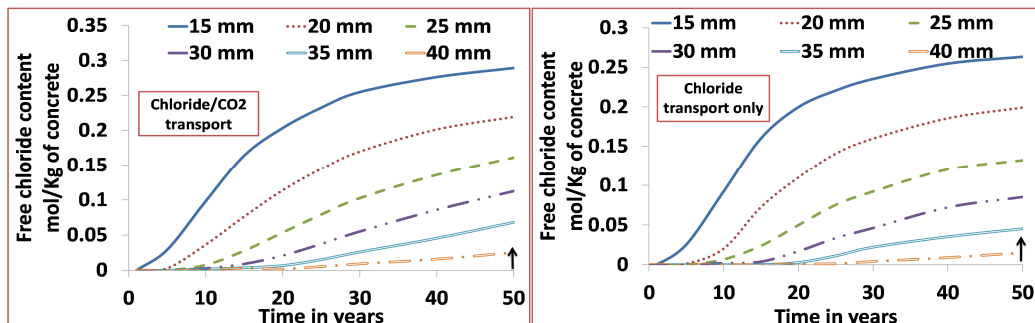


Figure 2. Comparison of the penetration depth of chloride ions in the 2 cases

## 4 Conclusions

- The model is able to describe ions, carbon dioxide and humidity transport into concrete.
- Porosity decreases due to the precipitation of calcite and silica gel and to the dissolution of portlandite and CSH. The model is able to predict the amount of solid components in the concrete.
- The model predicts the service life of concrete. The results show that if the carbonation is neglected, the service life of concrete is overestimated.

## References

- [BUC 2000] Buchwald A., ““Determination of the Ion Diffusion Coefficient in Moisture and Salt Loaded Masonry Materials by Impedance Spectroscopy.” in *3rd International Symposium Vienna*, 2000, pp. 475–482.
- [HUC 1923] Huckel P., *Zur Theorie der Elektrolyte*. Springer Berlin Heidelberg, 1923.
- [KHO 2010] Khokhar M., Rozière E., Turcry P., Grondin F., Loukili A., “Mix design of concrete with high content of mineral additions: Optimisation to improve early age strength,” *Cem. Concr. Compos.*, vol. 32, no. 5, pp. 377–385, 2010.
- [MAI 2013] Mai-Nhu J., “Corrosion des armatures du béton: Couplage carbonatation/chlorures en présence des cycles hydriques,” *PhD thesis at l’université de Toulouse*, 2013.
- [PHU 2016] Nguyen P., Amiri O., “Study of the chloride transport in unsaturated concrete: Highlighting of electrical double layer, temperature and hysteresis effects,” *Constr. Build. Mater.*, vol. 122, pp. 284–293, 2016.
- [THI 2005] Thiery M., “Modélisation de la carbonatation atmosphérique des matériaux cimentaires : Prise en compte des effets cinétiques et des modifications microstructurales et hydriques,” *PhD thesis at l’Ecole Nationale des Ponts et Chaussées*, 2005.
- [VIL 2006] VILLAIN G., THIERY M., “Gammadensimetry: A method to determine drying and carbonation profiles in concrete,” *NDT E Int.*, vol. 39, no. 4, pp. 328–337, 2006.

# Transition from energy dissipative processes to displacement discontinuities during concrete failure

S.Y. Alam and A. Loukili

*L'UNAM Université, Institut de Recherche en Génie Civil et Mécanique (GeM), UMR-CNRS 6183, Ecole Centrale de Nantes, Nantes, France  
e-mail: [syed-yasir.alam@ec-nantes.fr](mailto:syed-yasir.alam@ec-nantes.fr)*

## 1 Introduction

The description of a failure process is one of the key factors to improve the durability and life time. Failure of concrete is usually assessed by the loss of stiffness and material strength due to damage growth associated with microcracks. The mechanisms observed at the macroscopic scale result from the local fracture process occurring at the material level. Hillerborg et al. [1] presented a cohesive crack model where the mechanical behaviour can be modelled by the local fracture behaviour, as described by a characteristic post-peak stress-crack opening softening curve. Their model, however, neglects fracture energy dissipation before the peak load. Many experimental studies have described efforts made to identify the fracture mechanisms [2] and characteristic size-independent material fracture parameters, such as the fracture energy [3] or the relative crack length [4]. Attention is mostly paid to understanding the size and shape of the fracture process zone (FPZ) ahead of the propagating crack tip and the boundary effects on FPZ [5]. Few experimental studies have focused their analysis upon energy dissipation or fracture energy during the fracture process [6,7].

In most of the experimental studies cited above, fracture or damage has been considered either as the source of energy dissipation mechanisms or as the development of displacement discontinuities. Such analysis produce results in which only one type of damage mechanism is monitored, i.e. damage as a source of energy dissipation or fracture on the basis of discrete crack openings. None of these experimental studies considered that damage in quasi-brittle materials such as concrete is governed by two processes: (1) high energy dissipation mechanisms during which crack openings may or may not be important and (2) the displacement discontinuous phase where energy dissipations may or may not be important. Such analysis can only be performed if two techniques can be simultaneously applied; one characterising the energy dissipation and the other monitoring the displacement discontinuities.

In this paper, acoustic emission (AE) and digital image correlation (DIC) are applied simultaneously on bending tests of notched specimens. AE parameters, such as events and acoustic energy, are analysed to determine the energy release rate and the fracture growth due to energy dissipation mechanisms. Full-field displacements are obtained by DIC, where crack openings are measured on the surface of the specimen [4]. The transition from the energy dissipation phase to the displacement discontinuity phase is discussed. A new approach is then presented to model the local fracture process based on the transient and steady state response of a local damage parameter. The transient phase indicates the energy dissipation and the steady phase indicates the crack opening phase.

## 2 Experimental procedure

Two sizes of concrete beams (designated hereafter as D1 and D2) with geometrically similar dimensions (length  $l$  and depth  $D$ ) and one constant dimension (width  $B$ ) were tested. The cross sectional depths  $D$  were 100, and 200 mm, respectively, with constant width  $B$  equal to 100 mm and the span to depth ratio ( $l/D$ ) equal to 3:1. The beams were notched at mid-span with a notch length ( $a$ ) varying proportionally to the size of the beam ( $a/D$  kept equal to 0.2). The design of the beam followed the RILEM recommendation [8].

The DIC method was applied and images were continuously obtained during the whole loading branch. Displacement fields were calculated and crack opening were derived. The AE system comprised of a general-purpose interface bus ( $2 \times$  PCI-DISP4 having 4 channels each). A 3D analysis is performed for the localisation of AE events using 8 piezoelectric transducers. The details of DIC and AE setup can be found in [9].

### 3 Experimental results and analysis

The average mechanical curves are presented in Figure 1 which shows the characteristic quasi-brittle response of a concrete material. The behaviour is typical and explains the overall load carrying capacity of the concrete beams. Different stages of the failure process of the beams cannot be assessed by this macroscopic response.

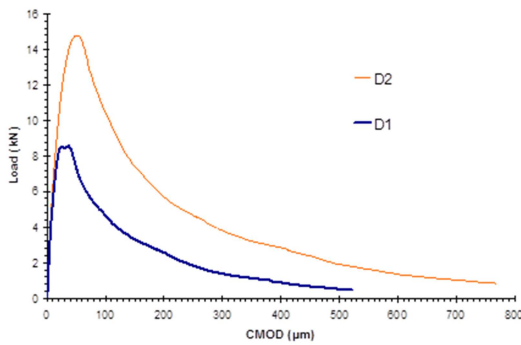


Figure 1: Macroscopic mechanical behaviour of beams

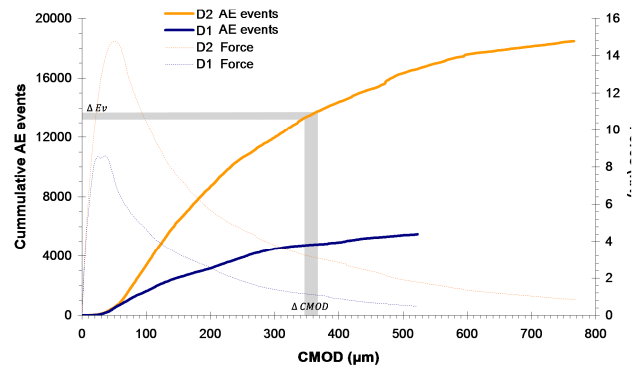


Figure 2: Increase of cumulative AE events during load tests

As loading increases, the number of AE events ( $Ev$ ) increases (Figure 2). The curves show no or low activity in the initial part, during which loadings are elastic. Afterwards, a smooth increase in  $Ev$  can be observed due to a progressive increase in the damage. In order to observe the development of damage and to relate the development of AE events with the failure process, the AE event rate ( $Ev'$ ) is plotted in Figure 3. It is computed by measuring the increase in the event number in AE events  $\Delta Ev$  over a very small interval of CMOD ( $\Delta CMOD \approx 1 \mu m$ ) as shown in Figure 3.

$$Ev' = \Delta Ev / \Delta t \quad (1)$$

where  $\Delta t$  is the corresponding time interval.

Thus, Figure 3 represents the AE event rate or simply the rate of development of new microcracks during the fracture process of concrete beams. During the initial loadings,  $Ev'$  is very low. Due to progressive microcracking in concrete,  $Ev'$  increases due to the increasing rate of microcrack formation. It has been confirmed by several studies that microcracks are formed in the fracture process zone and the size of FPZ increases as the load approaches the peak load [9]. It should be noted that  $Ev'$  continues to increase even after peak loading and immediate subsequent decreasing. The decreasing segment of  $Ev'$ -CMOD curve for each beam shows the same trend, as shown by the post-peak segment of Force-CMOD curve for the corresponding beam.

The failure process of concrete involves mechanisms with various energy dissipation levels. The stress waves resulting from these energy dissipative processes are detected by the piezoelectric sensors which convert them into transient electric signals. The AE energy  $En$  is plotted in Figure 4. In the pre-peak loadings,  $En$  is very low and increases smoothly when the load increases. The dissipation process is progressive, unlike brittle materials which fail due to a sudden release of potential energy.

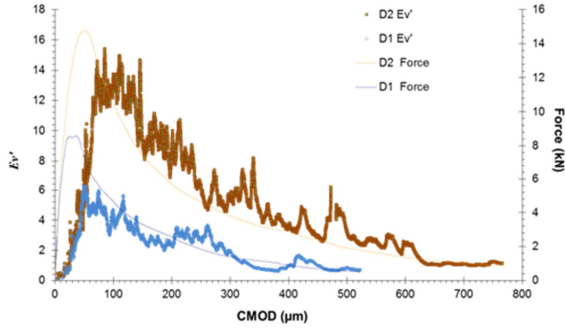


Figure 3: Evolution of AE event rate

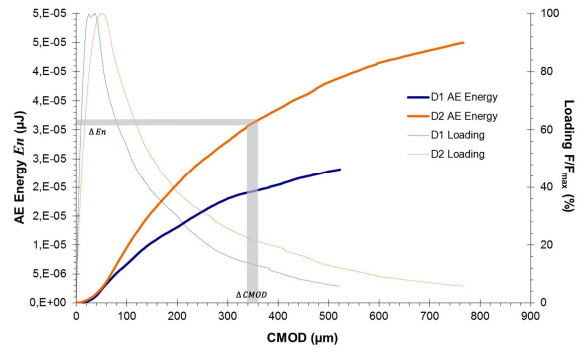


Figure 4: Increase of cumulative AE energy

The cumulated AE energy can be related to the fracture energy [7]. Therefore, one can relate the AE energy release rate to the fracture energy release rate or the so-called specific fracture energy. Thus, the rate of AE Energy ( $En'$ ) is computed by measuring the increase in the AE energy ( $\Delta En$ ) over a very small interval of CMOD ( $\Delta CMOD < 1 \mu m$ ), as shown in Figure 4.

$$En' = \Delta En / \Delta t \quad (2)$$

where  $\Delta t$  is the corresponding time interval.

Three distinct stages of development of  $En'$  can be noticed in Figure 5. During the first stage, the AE Energy release rate  $En'$  increases under the pre-peak loadings. At peak load,  $En'$  increases suddenly and it further increases during the initial post-peak loadings.  $En'$  becomes maximum at about 85% post-peak loadings. The energy dissipation mechanisms thus become very active near the peak load. These mechanisms are usually centered in the fracture process zone. It should be noticed that the energy release rate  $En'$  is not maximum at peak load, rather the peak load is defined by a very sudden increase in the energy release rate. The maximum value of  $En'$  is achieved at about 85% peak loading.

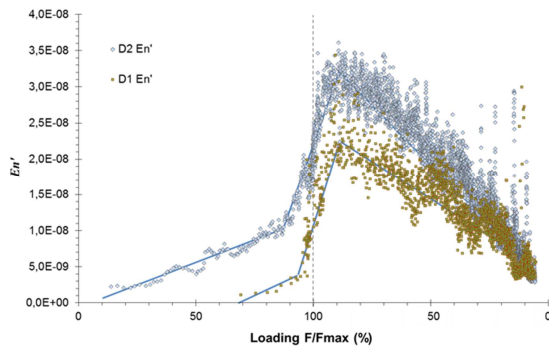


Figure 5: Evolution of AE energy rate with loading steps

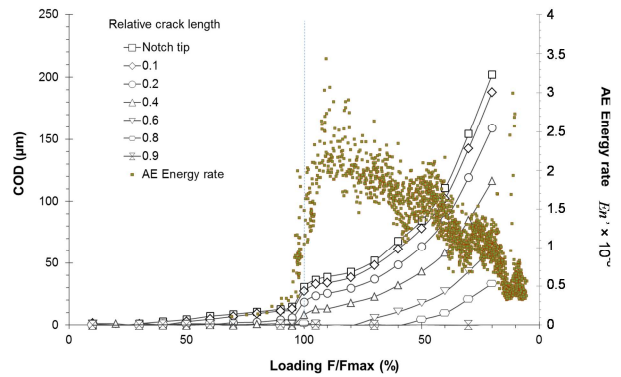


Figure 6: Increase of crack openings with loading steps

The evolution of crack openings with loading intervals is presented in Figure 6. It can be observed that during pre-peak loadings, there are no crack openings. Thus, displacement discontinuities are very small and may be in the form of distributed microcracks near the notch tip. Crack opening increases almost linearly with the loadings during the pre-peak loadings. The behaviour changes near the peak load and an increase in the crack openings is observed in the post-peak loadings.

## 4 Conclusions

The paper describes the transition between the energy dissipation phase and the discontinuum phase during the fracture process in concrete. Three point bending tests were conducted; AE and DIC techniques were applied simultaneously to analyse the energy dissipation process and the crack openings, respectively. The AE energy release rate indicates three phases of energy dissipation. During the first and second phases, energy release rate increases. The first phase ends just before the peak load; however, the second phase, when the energy release rate reaches the maximum, ends just after the peak load. During these two phases, the rate of microcracks, as detected by the AE technique (i.e. only the microcracks releasing AE energy), show a similar behaviour. Also, during these two phases, crack openings are very small, as measured by the DIC technique. In the third (or the crack opening) phase, the energy release rate begins to decrease with a corresponding increase in crack openings.

## References

- [1] Hillerborg A., Modéer M. and Petersson P.E. 1976. Analysis of crack formation and crack growth in concrete by means of fracture mechanics and finite elements. *Cement and Concrete Research* 6(6):773-781.
- [2] Landis E. N. and Bolander J. E. 2009. Explicit representation of physical processes in concrete fracture. *Journal of Physics D: Applied Physics* 42(21):1-17.
- [3] RILEM 50-FMC Recommendation. 1985. Determination of fracture energy of mortar and concrete by means of three-point bend test on notched beams. *Materials and Structures* 18:285-290.
- [4] Alam S. Y., Loukili A. and Grondin F. 2012. Monitoring size effect on crack opening in concrete by digital image correlation. *European Journal of Environmental and Civil Engineering* 16(7):818-836.
- [5] Cedolin L., Dei Poli S. and Iori I. 1983. Experimental determination of the fracture process zone in concrete. *Cement and Concrete Research* 13(4):557-567.
- [6] Grégoire D., Verdon L., Lefort V., Grassl P., Saliba J., Regoin J.-P., Loukili A. and Pijaudier-Cabot G. 2015. Mesoscale analysis of failure in quasi-brittle materials: comparison between lattice model and acoustic emission data. *Int. J. Numer. Anal. Meth. Geomech.* 39:1639-1664.
- [7] Landis E. and Baillon L. 2002. Experiments to relate acoustic emission energy to fracture energy of concrete. *Journal of Engineering Mechanics* 128(6):698-702.
- [8] RILEM Recommendation. 1990. Size-effect method for determining fracture energy and process zone size of concrete. *Materials and Structures* 23:461-465.
- [9] Alam S. Y., Saliba J. and Loukili A. 2014. Fracture examination in concrete through combined digital image correlation and acoustic emission techniques. *Construction and Building Materials* 69:232-242.

# Multi-scale modelling of healing mechanism in cementitious materials

**B. Hilloulin<sup>a</sup>, D. Hilloulin<sup>b</sup>, A. Soive<sup>a,c</sup>, M. Matallah<sup>d</sup>, F. Grondin<sup>a</sup> and A. Loukili<sup>a</sup>**

*a. LUNAM Université, Institut de Recherche en Génie Civil et Mécanique (GeM), UMR-CNRS 6183, Ecole Centrale de Nantes, 1 rue de la Noë, 44321 Nantes, France. E-mails : benoit.hilloulin@ec-nantes.fr, frederic.grondin@ec-nantes.fr,*

*anthony.soive@ec-nantes.fr, ahmed.loukili@ec-nantes.fr*

*b. Oracle Labs, Zurich, Switzerland*

*c. Centre d'Etudes et d'Expertise sur les Risques, l'Environnement, la Mobilité et l'Aménagement (Cerema), 9 rue René Viviani - BP 46223, 44262 - Nantes Cedex 2, France*

*d. RISAM, Tlemcen Université, Tlemcen, Algeria*

## Abstract

Characterising mechanical regains that can be obtained due to self-healing of cementitious materials is difficult and developing models considering this phenomenon seems to be a real challenge because of the coupled phenomena involved. Several types of models have recently been developed to numerically reproduce self-healing or its effects in terms of impermeability or mechanical regain. A general discussion about self-healing modelling is provided after a quick review of novel experimental characterisation techniques and their advantages regarding self-healing analysis. A comparison of mesoscopic and microscopic models highlights some paths that might be followed to achieve realistic multi-scale modelling of the self-healing phenomenon.

**Keywords:** Self-healing; Modelling, Mechanical properties, Reactive transport modelling; Cementitious materials; Environmental conditions, Calcium-Silicate-Hydrate (C-S-H), 3D microscope.

## Introduction

Cracks in concrete generate important inspection and repairing costs, especially for public services and governments. Some of them can seriously affect the durability and the stability of the structures because entering harmful substances can cause corrosion or leakage. Thus, using self-healing concrete could permit considerable savings in the costs incurred by monitoring, restoring or repairing, as well as the indirect costs inherent to repair works, such as traffic jams [1, 2]. Moreover, self-healing solutions could help the design of structures with long term durability properties for future nuclear waste disposal, for example.

Self-healing can occur naturally, without any particular additive, under favourable conditions with the continuous or alternate presence of water by local restart of hydration [3-5] or formation of healing products by reaction with the environment (mainly calcium carbonate from calcium in the concrete and carbonate ions contained in water) [6, 7]. Some studies have reported the predominance of the precipitation phenomenon in common concrete with a water-to-cement (w/c) ratio around 0.4 - 0.5. Natural healing, called 'autogenic' healing, has been observed to be limited to cracks with a maximal width of around 100 – 200  $\mu\text{m}$  [6-9]. Due to this limitation, novel engineered techniques have been developed to maximise healing, such as embedded capsules/vascular system [10-14], or calcium carbonate precipitating bacteria [15, 16].

Autogenic healing by further hydration has been studied by several researchers because of expected mechanical regains due to the creation of new calcium silicate hydrates (CSH) [3, 17-19]. A complete recovery of stiffness can be achieved by further hydration but mechanical

regain seems very limited when calcite is formed into the crack [20]. However, the kinetics and the limits of the phenomenon are not totally understood. More experimental tests are needed to determine the intrinsic characteristics of the healing products, with the purpose to propose predictive models. Self-healing observation and monitoring, usually performed by optical microscope on the crack surface, needs to be supplemented by tomography [21] or non-destructive techniques [22, 23], in order to describe and quantify the filling of cracks inside the specimens.

Up to now, only a few models have been developed to describe the self-healing of concrete. Some models have been proposed to determine the needed amount of unhydrated cement particles in concrete specimens considering w/c ratio and cement fineness, which underlies the self-healing potential, or to calculate the amount of healing product caused by further hydration, considering two crack modes [24, 25]. Recently, one hydration-based model has been built to perform micro-mechanical tensile tests after several healing periods and has shown promising results [26]. A model simulating further hydration by water release by a capsule in a crack using water transport theory, ion diffusion theory and thermodynamics theory has recently been developed [27, 28], while the characterisation of the healing products of relatively low mechanical properties have been assessed at a mesoscopic scale [29]. However, these models do not reveal which parameters mainly influence the creation of the second type of healing products: calcite at the concrete – water interface, whereas it is the most observed phenomenon. Some recent attempts have been made using reactive transport modelling at a mesoscale [30, 31].

In this study, a general discussion on self-healing modelling is provided after a quick review of novel experimental characterisation techniques and their advantages regarding self-healing analysis. A comparison of mesoscopic and microscopic models highlights some possible paths that might be followed to achieve realistic multi-scale modelling of the self-healing phenomenon.

### **Insights from the use of novel experimental characterisation techniques**

From a general point of view, self-healing speed has initially been monitored with the local crack width measurement [20]. In the past, volumetric information could be extracted by using X-ray computed tomography [21, 32, 33] and post-processing algorithms to calculate the crack volume aside from the pore volume, and its evolution over time due to healing. Tomography results could be introduced in the near future into transport models to assess the potential damage due to the ingress of aggressive substances. In a complementary manner, information over large cracked area can be obtained using a 3D microscope [32] without focus preoccupations unlike the classic 2D microscope (Fig. 1). After the 3D image reconstruction, several outputs can be used to objectively assess the healing performance over zones larger than several dozens of squared centimeters. Moreover, using apparent volume calculation or Abbott-Firestone curves analysis, the self-healing phenomenon can be accurately monitored with minimal human intervention, which will open the way to future *in situ* applications. Besides, investigations have been done recently at a microscale to analyse in greater detail the basic self-healing phenomena. SEM image analyses of artificially created micro cracks can help understand the development of healing products which can be compared to modelling outputs. However, even if it is possible to identify the healing products, we cannot be sure of their mechanical properties and their bond with the initial matrix, especially in characterising the mechanical regain.

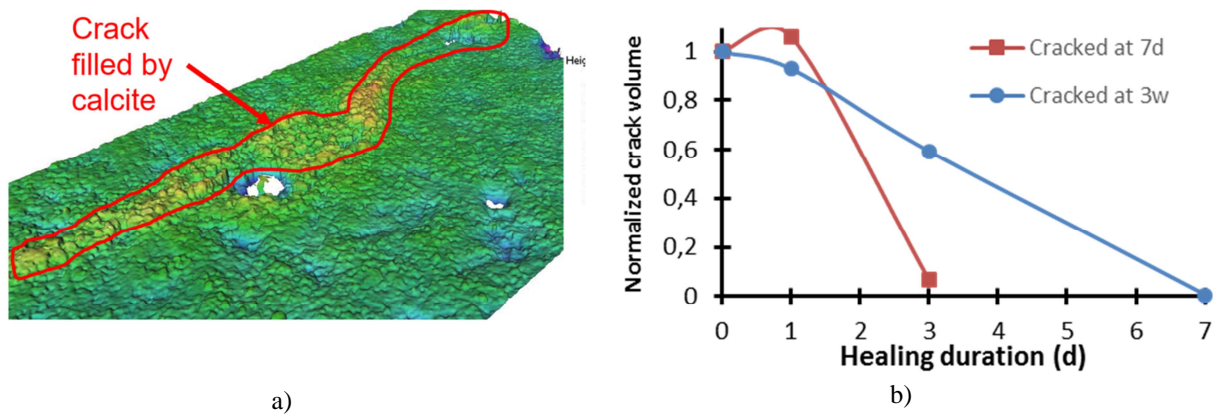


Fig 1: 3D microscope crack filling observation: (a) picture of some squared centimeters large zone after healing and, (b) evolution over time of apparent crack volume due to healing for two series of mortar specimens.

Imaging techniques can be supplemented by non-destructive acoustic techniques. Ultrasonic techniques are effective methods to monitor healing and several developments are ongoing. Ultrasonic pulse velocity [34] has been found to be a rather good technique to monitor healing due to crack filling to some extent although it may sometimes be imprecise for long term healing cases. More recently, nonlinear ultrasonic techniques have been developed and their ability to deliver crack geometric information (even for very small cracks) has been investigated [23] (Fig. 2). A recent review paper resumes all the ultrasonic methods in use and highlights their possibilities regarding self-healing [35]. One of the major findings of this review paper is the lack of techniques devoted to a mechanical regain evaluation. Besides acoustic emissions for self-healing considerations [3, 20], a partially or totally destructive method, as the specimens need to be reloaded to create acoustic emissions, no other method has so far been proposed to characterise self-healing mechanical regain.

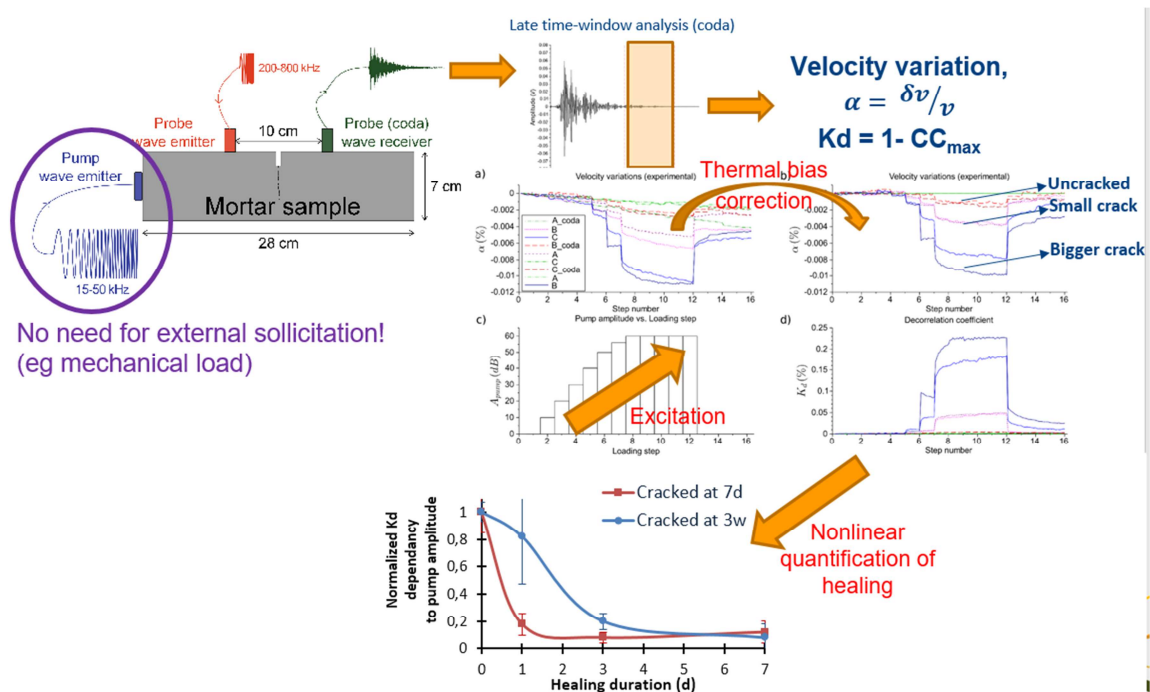


Fig 2: Nonlinear coda wave interferometry for crack geometrical characterisation

### Self-healing modelling using hydration models

Several tools have been developed over the last decades to model the microstructural evolution of concrete / mortar / cement paste over time from hydration to degradation.

Modelling codes such as CEMHYD3D simulating concrete hydration can lead to good estimations of mechanical properties [36, 37]. A few models have been developed to describe the self-healing of concrete. Some models have been proposed to determine the amount of unhydrated cement particles in concrete specimens considering w/c ratio and cement fineness which underlies the self-healing potential [18, 38, 39], or to calculate the amount of healing product due to further hydration considering two crack modes [24, 25]. Recently, a model simulating further hydration using the water transport theory, the ion diffusion theory and thermodynamics theory has been developed to determine the evolution of the filling fraction of cracks [27]. However, these models do not provide any information about the mechanical effects of self-healing. The same observation applies to more macroscopic models based on hydration[40].

A first micro-mechanical model for self-healing in cementitious materials has been introduced by the authors [26]. Healing by further hydration is simulated using our modified version of CEMHYD3D called CemPP to understand the kinetics and the potential of the healing phenomenon for different crack widths, age at cracking and healing period duration. The microstructure of healed specimens then served as input to the finite element code Cast3M [41] to monitor the mechanical regains and provide explanations for some experimental observations. This coupling has been made possible by extending the CEMHYD3D code to run different independent modules, each one providing part of the information necessary to the coupling with Cast3M, or directly operating on the microstructure. This model provides very satisfactory results for the development of secondary hydration products of CEM I based cement paste. The localisation of the healing products is realistically reproduced as illustrated in Fig. 3. Numerical micromechanical tests were then performed on subvolumes of the healed samples. The evolution of the Young's modulus exhibits very similar trends as observed experimentally for strength and stiffness regain: it quickly increases after some dozens of hours of immersion and reaches a maximum value which can be called the 'healing potential'.

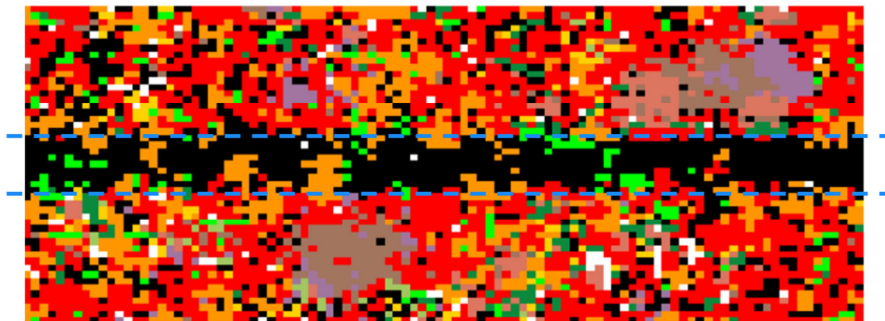


Fig 3: Hydration-based model (CEMHYD3D) healing simulation of an initially 10  $\mu\text{m}$ -wide crack (delimited by blue dashed lines) created at 3 days and healed within 4 weeks. Filling is due to the precipitation of portlandite (orange), CSH (red), aluminum precipitates (hydrogarnet in green). Clinkers are colored in brown.

These hydration-based models deserve further development because of their ability to describe the ongoing hydration taking place in some of the recent low water-to-cement ratio concretes. However, some points need to be investigated. For example, the creation of calcite, which is not a primary hydration product, while it may contribute to the mechanical regains. Secondly, the influence of the crack width may be studied as the dispersion of reactants should be greater when the crack width increases, decreasing the precipitation probability. Finally, even though this type of models describes the self-healing phenomenon realistically at the microscale, a subsequent homogenisation work should be made to obtain mesoscopic mechanical or transport properties.

## Mesoscopic models: mechanical considerations versus impermeability preoccupations

Regains due to healing can be quantified at a mesoscale with the use of appropriate models. Finite element models have been introduced to obtain information about the localisation and the global mechanical properties of healing products using backward analysis from experimental bending tests (loading -unloading for pre-cracking and then reloading after healing)[29, 42]. Interestingly, due to the initial stiffness regain development coming before strength regain in bending (and a two-slopes behaviour illustrated in Fig. 4), these models suggest that healing may primarily develop near the external surfaces of a specimen. These predictions are supported by recent experimental observations or similar numerical models [40]. Although these numerical and experimental observations were developed in the scope of tiny microcracks of some microns, it is worth noting that they tend to circumvent logical assertions stating that the smaller the crack, the faster the healing.

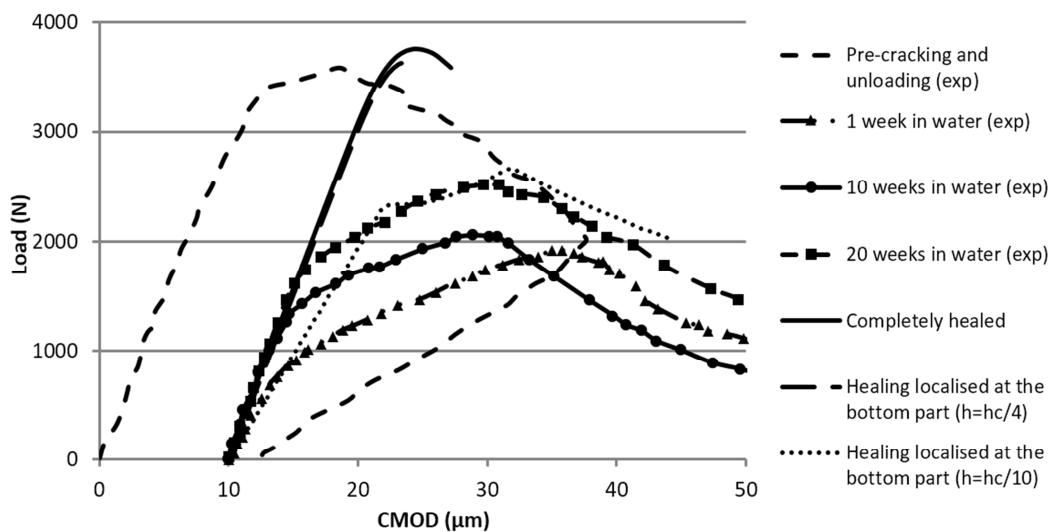


Fig 4: Experimental and numerical loading curves. Numerical curves from the mesoscopic model display various shapes depending on the localisation of the healing products.

Apart from these mechanical considerations, reactive transport models have recently been introduced for permeability preoccupations [31]. Though these models can be classified as mesoscale models, their aim is to describe the healing phenomenon in single cracks by taking into account the different phases, however they may be developed for multiple cracks. For this reason, they could also be classified as macroscale models. Considering calcite precipitation as the main responsible agent for reducing the permeability associated with healing, this model focuses on the reaction between calcium ions leaching out of concrete and carbonate species located in the water penetrating into the crack. Thus, the main interest of a reactive transport model for self-healing, and more generally for civil engineering, is to consider the relation between a structure and its environment. Self-healing may be described as a phenomenon decreasing transport properties (permeability, porosity, diffusivity). The authors have shown that the compositions of both the concrete and the water are of importance regarding ionic species susceptible to react. This type of model seems very promising as it can describe some key features observed experimentally such as the end of healing (which can be attributed to a drastic local porosity decrease stopping ionic diffusion) and the eventual redissolution of healing products under specific conditions such as water flow.

## Routes to multi-scale modelling of the healing phenomenon

Several paths emerge to further develop numerical characterisation by developing multi-scale approaches. Homogenisation of hydration-based micromechanical regains may be relatively

straightforward and could be compared with both mesoscopic models fitting experimental curves and, eventually, micromechanical tests performed on cement pastes. However, as predicted by mesoscopic models and observed experimentally, healing is highly space-dependent: calcite precipitates mainly at the surface of specimen, whereas other healing products responsible for mechanical regains can precipitate inside the crack. Therefore, even if coupling hydration and calcite formation seems highly desirable, experimental work is still needed to determine the influence of calcite precipitation on mechanical regains, differentiating between compressive and tensile or bending in terms of strength and stiffness. Finally, geometrical preoccupations may be an issue not only for the localisation of the healing products but also their geometrical architecture and development which may influence their bond with the original matrix (for example long plate-like portlandite sheets bond with the matrix is relatively fragile [43]).

## Conclusions and perspectives

In this study, recent insights concerning the self-healing phenomenon from novel experimental techniques have been briefly presented. Their relevance concerning modelling has been highlighted. Modelling techniques applied to self-healing have then been reviewed, differentiating hydration-based models and mesoscopic regains-oriented models. Despite their promising results, this study also points to some of their deficits due to the experimental shortcomings. Finally, some routes have been proposed for future self-healing modelling, developing fully coupled permeability-mechanics models.

## Acknowledgements

The authors gratefully acknowledge the financial support provided during Benoit Hilloulin's thesis by GIS LIRGeC and France's Loire Valley Regional Council. Special thanks are due to Odile Abraham, Jean-Baptiste Legland, Vincent Tournat and Olivier Durand for the design and development of nonlinear coda wave interferometry non-destructive tests; Michel Grasset and Laurent Gaillet (MAST, IFSTTAR Nantes) for their collaboration performing 3D microscopic measurements.

## References

- [1] Mario De Rooij, Kim Van Tittelboom, Nele De Belie, and Erik Schlangen (Eds). *Self-Healing Phenomena in Cement-Based Materials*. Springer Netherlands, 2013.
- [2] Klaas van Breugel. Self-healing concepts in civil engineering for sustainable solutions: Potential and constraints. In *Proceedings of the Second International Conference on Self-Healing Materials*, 2009.
- [3] S. Granger, A. Loukili, G. Pijaudier-Cabot, and G. Chanvillard. Experimental characterization of the self-healing of cracks in an ultra high performance cementitious material: Mechanical tests and acoustic emission analysis. *Cement and Concrete Research*, 37(4):519 – 527, 2007.
- [4] Haoliang Huang, Guang Ye, and Denis Damidot. Characterization and quantification of self-healing behaviors of microcracks due to further hydration in cement paste. *Cement and Concrete Research*, 52(0):71 – 81, 2013.
- [5] Benoit Hilloulin, Frédéric Grondin, Mohammed Matallah, and Ahmed Loukili. Numerical modelling of autogenous healing and recovery of mechanical properties in ultra-high performance concrete. In *Proceedings of the Fourth International Conference on Self-Healing Materials (Ghent)*, pages 414–417, 2013.
- [6] C. A. Clear. The effect of autogenous healing upon leakage of water through cracks in concrete. Technical report, *Cement and Concrete Association*, 1985.
- [7] Carola Edvardsen. Water permeability and autogenous healing of cracks in concrete. *ACI Materials Journal*, 96(4):448–454, July-August 1999.

- [8] C. Aldea, W. Song, J. Popovics, and S. Shah. Extent of healing of cracked normal strength concrete. *Journal of Materials in Civil Engineering*, 12:92–96, 2000.
- [9] Hans-Wolf Reinhardt and Martin Jooss. Permeability and self-healing of cracked concrete as a function of temperature and crack width. *Cement and Concrete Research*, 33(7):981 – 985, 2003.
- [10] Carolyn Dry and William McMillan. Three-part methylmethacrylate adhesive system as an internal delivery system for smart responsive concrete. *Smart Materials and Structures*, 5(3):297, 1996.
- [11] Victor C Li, Yun Mook Lim, and Yin-Wen Chan. Feasibility study of a passive smart self-healing cementitious composite. *Composites Part B: Engineering*, 29(6):819 – 827, 1998.
- [12] Hirozo Mihashi, Yoshio Kaneko, Tomoya Nishiwaki, and Koji Otsuka. Fundamental study on development of intelligent concrete characterized by self-healing capability for strength. *Transactions of the Japan Concrete Institute*, 22:441–450, 2000.
- [13] Kim Van Tittelboom, Nele De Belie, Denis Van Loo, and Patric Jacobs. Self-healing efficiency of cementitious materials containing tubular capsules filled with healing agent. *Cement and Concrete Composites*, 33(4):497 – 505, 2011.
- [14] Benoit Hilloulin, Kim Van Tittelboom, Elke Gruyaert, Nele De Belie, and Ahmed Loukili. Design of polymeric capsules for self-healing concrete. *Cement and Concrete Composites*, 55(0):298 – 307, 2015.
- [15] Virginie Wiktor and Henk M. Jonkers. Quantification of crack-healing in novel bacteria-based self-healing concrete. *Cement and Concrete Composites*, 33(7):763 – 770, 2011.
- [16] J.Y. Wang, H. Soens, W. Verstraete, and N. De Belie. Self-healing concrete by use of microencapsulated bacterial spores. *Cement and Concrete Research*, 56(0):139 – 152, 2014.
- [17] Stefan Jacobsen and Erik J. Sellevold. Self healing of high strength concrete after deterioration by freeze/thaw. *Cement and Concrete Research*, 26(1):55 – 62, 1996.
- [18] Nynke Ter Heide. Crack healing in hydrating concrete. Master’s thesis, Delft University of Technology, 2005.
- [19] Nynke Ter Heide and Erik Schlangen. Self healing of early age cracks in concrete. In *Proceedings of the First International Conference on Self Healing Materials, Noordwijk aan Zee, The Netherlands, 18-20 April 2007*, 2007.
- [20] Kim Van Tittelboom, Elke Gruyaert, Hubert Rahier, and Nele De Belie. Influence of mix composition on the extent of autogenous crack healing by continued hydration or calcium carbonate formation. *Construction and Building Materials*, 37(0):349 – 359, 2012.
- [21] Daisuke Fukuda, Yoshitaka Nara, Daisuke Hayashi, Hideo Ogawa, and Katsuhiko Kaneko. Influence of fracture width on sealability in high-strength and ultra-low-permeability concrete in seawater. *Materials*, 6(7):2578–2594, 2013.
- [22] Chi-Won In, R. Brett Holland, Jin-Yeon Kim, Kimberly E. Kurtis, Lawrence F. Kahn, and Laurence J. Jacobs. Monitoring and evaluation of self-healing in concrete using diffuse ultrasound. *NDT & E International*, 57(0):36 – 44, 2013.
- [23] Benoit Hilloulin, Yuxiang Zhang, Odile Abraham, Ahmed Loukili, Frédéric Grondin, Olivier Durand, and Vincent Tournat. Small crack detection in cementitious materials using nonlinear coda wave modulation. *NDT & E International*, 68(0):98 – 104, 2014.
- [24] Zhong Lv and Huisu Chen. Modeling of self-healing efficiency for cracks due to unhydrated cement nuclei in hardened cement paste. *Procedia Engineering*, 27:281 – 290, 2012.

- [25] Zhong Lv and Huisu Chen. Self-healing efficiency of unhydrated cement nuclei for dome-like crack mode in cementitious materials. *Materials and Structures*, pages 1–12, 2013.
- [26] Benoit Hilloulin, Damien Hilloulin, Frédéric Grondin, Ahmed Loukili, and Nele De Belie. Mechanical regains due to self-healing in cementitious materials: Experimental measurements and micro-mechanical model. *Cement and Concrete Research*, 80:21 – 32, 2016.
- [27] Haoliang Huang and Guang Ye. Simulation of self-healing by further hydration in cementitious materials. *Cement and Concrete Composites*, 34(4):460 – 467, 2012.
- [28] Haoliang Huang, Guang Ye, and Denis Damidot. Effect of blast furnace slag on self-healing of microcracks in cementitious materials. *Cement and Concrete Research*, 60(0):68 – 82, 2014.
- [29] B. Hilloulin, F. Grondin, M. Matallah, and A. Loukili. Modelling of autogenous healing in ultra high performance concrete. *Cement and Concrete Research*, 61(0):64 – 70, 2014.
- [30] Benoit Hilloulin, Frédéric Grondin, Ahmed Loukili, and Odile Abraham. Cinétique et potentiel d’auto-cicatrisation des matériaux cimentaires: expériences et modèle de transport réactif. In *Proceedings of 32nd Rencontres Universitaire de Génie Civil (AUGC 2014)*, Orléans, France, 4 - 6 June 2014.
- [31] B. Hilloulin, F. Grondin, A. Soive, and A. Loukili. Investigation of self-healing phenomenon by calcite precipitation using reactive transport modelling and microscopic observation. In *Proceedings of the 15th Euroseminar on Microscopy Applied to Building Materials*, 2015.
- [32] Benoit Hilloulin, Jean-Baptiste Legland, Elisabeth Lys, Odile Abraham, Ahmed Loukili, Frédéric Grondin, Olivier Durand, and Vincent Tournat. Monitoring of autogenous crack healing in cementitious materials by the nonlinear modulation of ultrasonic coda waves, 3d microscopy and x-ray microtomography. *Construction and Building Materials*, 123:143 – 152, 2016.
- [33] Jeroen Van Stappen, Tom Bultreys, Francisco A. Gilabert, Xander K.D. Hillewaere, David Garoz Gomez, Kim Van Tittelboom, Jelle Dhaene, Nele De Belie, Wim Van Paepegem, Filip Du Prez, and Veerle Cnudde. The microstructure of capsule containing self-healing materials: A micro-computed tomography study. *Materials Characterization*, 119:99 – 109, 2016.
- [34] Yahia Abdel-Jawad and Rami Haddad. Effect of early overloading of concrete on strength at later ages. *Cement and Concrete Research*, 22(5):927 – 936, 1992.
- [35] Eunjong Ahn, Hyunjun Kim, Sung-Han Sim, Sung W. Shin, and Myoungsu Shin. Principles and applications of ultrasonic-based nondestructive methods for self-healing in cementitious materials. *Materials*, 10:278, 2017.
- [36] F. Bernard, S. Kamali-Bernard, and W. Prince. 3d multi-scale modelling of mechanical behaviour of sound and leached mortar. *Cement and Concrete Research*, 38(4):449 – 458, 2008.
- [37] C.-J. Haecker, E.J. Garboczi, J.W. Bullard, R.B. Bohn, Z. Sun, S.P. Shah, and T. Voigt. Modeling the linear elastic properties of portland cement paste. *Cement and Concrete Research*, 35(10):1948 – 1960, 2005.
- [38] Huan He, Zhan-Qi Guo, Piet Stroeven, Martijn Stroeven, and Lambertus Johannes Sluys. Self-healing capacity of concrete - computer simulation study of unhydrated cement structure. *Image Analysis & Stereology*, 26:137–143, 2007.
- [39] Huan He, Zhanqi Guo, Piet Stroeven, and Martijn Stroeven. Numerical assessment of concrete’s self-healing potential for promoting durability. *International Journal of Modelling, Identification and Control*, 7:142–147, 2009.

- [40] Adriana Silviana Chitez and Anthony Duncan Jefferson. A coupled thermo-hygro-chemical model for characterising autogenous healing in ordinary cementitious materials. *Cement and Concrete Research*, 88:184 – 197, 2016.
- [41] P. Verpaux, T. Charras, and A. Millard. Castem 2000: une approche moderne du calcul des structures. *Calcul des structures et intelligence artificielle (J.M. Fouet and P. Ladevèze and R. Ohayon)*, pages 261–271, 1988.
- [42] Sébastien Granger. *Caractérisation expérimentale et modélisation du phénomène d'auto-cicatrisation des fissures dans les bétons*. PhD thesis, Ecole Centrale de Nantes, 2006.
- [43] Benoit Hilloulin. *Méthodes avancées et analyses multi-échelles pour l'étude de l'auto-cicatrisation des fissures dans les matériaux cimentaires*. PhD thesis, Ecole Centrale de Nantes - Université de Gand, 2015.

# Modelling mechanical interactions in granular media with generalized continua: towards granular metamaterials

F. Dell'Isola

*Università di Roma "La Sapienza"*  
*fdellisola@icloud.com*

**Part I:** Modelling reality: some general introductory thoughts

**Part II:** Modelling granular materials with generalised continua

**Part III:** Mass-spring systems for modelling material degradation

**Part IV:** Granular metamaterials

## Part I

### Nature *versus* Technology or (rather) Paradigms vs Evolving Science?

Until very recent times, mathematical modelling has been limited to the description of pre-existing materials. The simplifying assumptions which were the basis of engineering in the Industrial Revolution became a paradigm of scientific and technological thought.

The assumptions conjectured by the founders of modern engineering sciences (Cauchy, Poisson, Navier, Maxwell, Piola, etc.) were so deeply rooted in the minds of scientists and engineers that they became first basic doctrine and then paradigms.

**MISSION STATEMENT:** to select the desired behaviour of a material by means of the choice of its governing equations, and subsequently to synthesise and manufacture a micro-structure or a complex multiphysics system whose behaviour is suitably described by the chosen equations.

### EXAMPLES OF POSSIBLE IMPLEMENTATIONS OF THE MISSION STATEMENT:

- To find a material which is able to damp mechanical vibrations by means of a granular microstructure or by transforming mechanical energy into electromagnetic energy via piezoelectric transduction.
- To find a material which exhibits, at least in some directions, a large ratio between weight and fracture toughness.
- To find a deformable porous material saturated by an electrically or magnetically active nematic fluid, to enhance Darcy dissipation to control the propagation of electro- or magneto-nematic waves.
- To find an adaptive material endowed with an embedded sensing system activating variations in mechanical constitutive parameters; for example: a beam with a section moment of inertia that can be modified by the actuation driven by mechanical wave propagation or by an electrical signal, or other kinds of smart materials for bone fracture repair purposes.
- To design a multi-scale fabric constituted by a beam-like substructure whose deformation energy depends on n-th gradient of displacement field, and to exploit these structural elements to form materials exhibiting non-standard dispersion effects, possibly including frequency band gaps.
- To find a material constituted by nearly inextensible fibers which is able to resist shear and elongation by storing deformation energy in the form of fiber bending energy.

## Scientific paradigms

As stated by Thomas Kuhn [1], scientific theories experience periodically a stagnation phase in which they are stuck dealing with paradigms that have to be overcome to correctly describe novel phenomenological evidence.

The exclusive use of either discrete or continuous models, depending on the context (the former for granular systems), may well be one of these paradigms.

## Continuum mechanics, in turn, has its own paradigms:

- The paradigm of continuum models
- The subparadigm of Cauchy continua
- The sub-sub paradigm of hyperelastic continua
- The sub-sub-sub paradigm of linear elasticity

A more general paradigm is that of Microstructured Continua, introduced by Piola [2], and developed by scientists such as Cosserat, Mindlin, Eringen, Sedov.

## An unavoidable question

Today, we are used to the following procedure: developing the homogenised form of microstructured systems and then discretizing them again in order to perform numerical investigations. Computational advantages are crucial.

There is no scientific designing without accurate quantitative previsions.

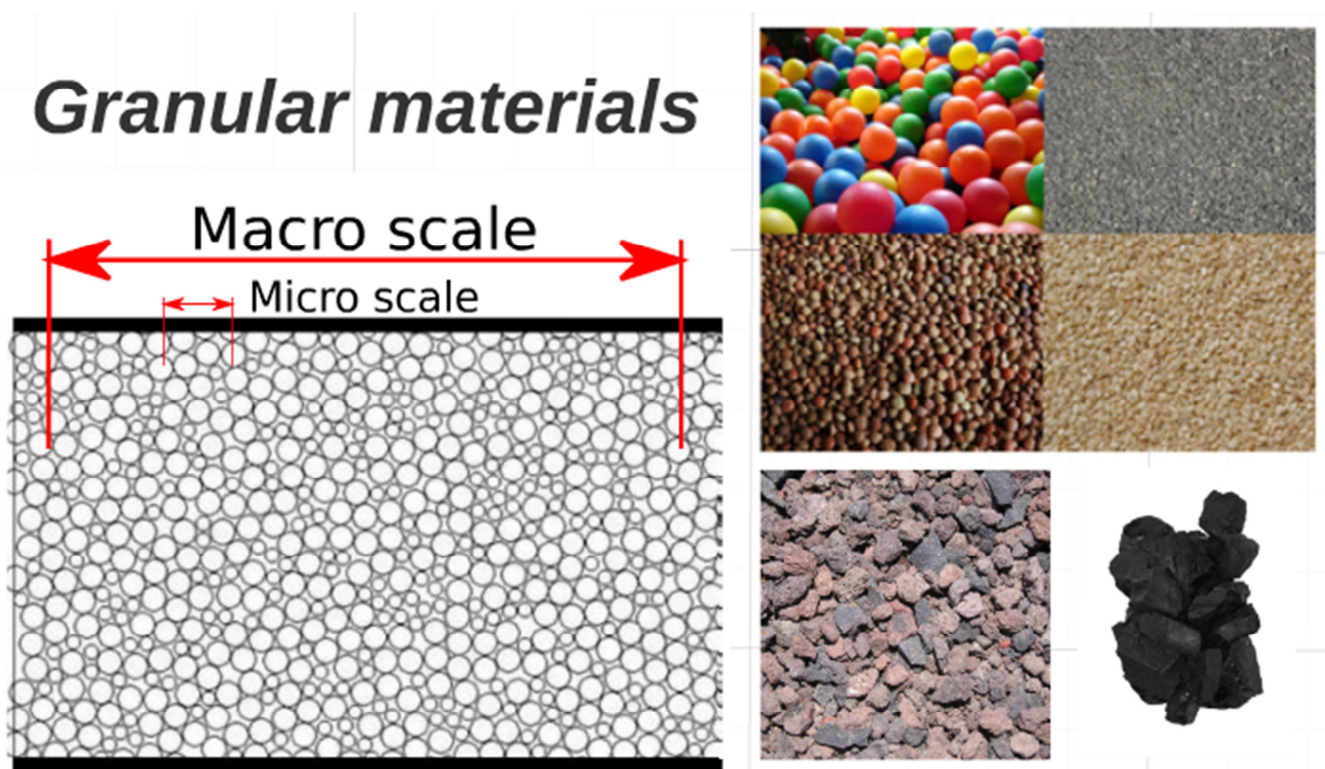
Therefore, a model producing equations theoretically correct but practically impossible to solve is technologically (and scientifically!) of little significance.

## A celebrated example

Copernican system was not more accurate than Ptolemaic system: they both made assumptions of circular orbits and in principle were kinematically equivalent.

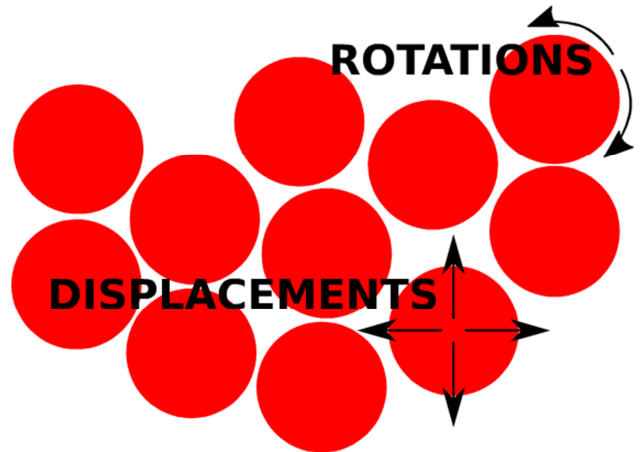
But Copernicus' algorithm was simpler! ([3,4])

## Part II



### **Generalised Continua and Granular Materials**

The macro-scale behaviour of granular materials is significantly influenced by the behaviour at the micro-scale. The latter involves not only displacements of the centroid of the grains but also their rotation [5].



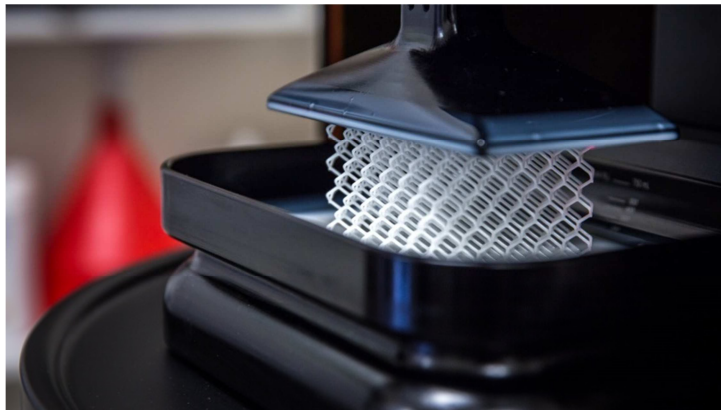
### **Generalised Continua and Granular Materials**

As usually occurs when there are different interacting length-scales, granular materials can be adequately described by means of generalised continuum models, i.e.: models in which the deformation energy depends on the objective part of higher gradients of the placement.

### **Computer-aided experimental validation**

Computer-aided manufacturing can be used to design and perform experiments for model validations and verification.

In particular, 3D-printing allows a very high precision and reliability at the micro-scale while being relatively cheap.



**This can be exploited in two ways:**

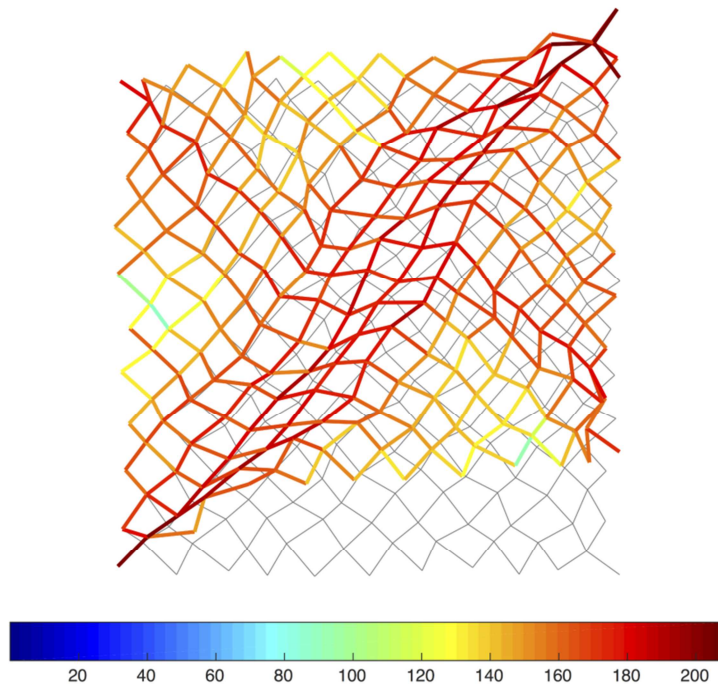
#### **1. 3D-printed disk assembly**

3D-printed disk assembly can be realised in order to reproduce the experiments performed in [6]. This will fasten the testing process, and will allow great flexibility in the choice of disk sizes and shapes (circular, elliptical and polygonal), and disk-pair interfacial behaviour controlled by overlap/spacing.

#### **2. Randomly distributed mass-spring systems**

A promising use of 3D-printing is connected with the randomly distributed systems of masses and springs studied in [7]. Grains interaction potentials, close to the reference configuration, can be reproduced in this way also when very highly nonlinear local potentials have to be considered. The 3D printer can indeed produce sheets in which grains are linked with rods of suitable length, thickness and shape, so as to produce the desired local potential.

Numerical shear test on a randomly distributed system of masses and springs (strain energy density is shown in color map).



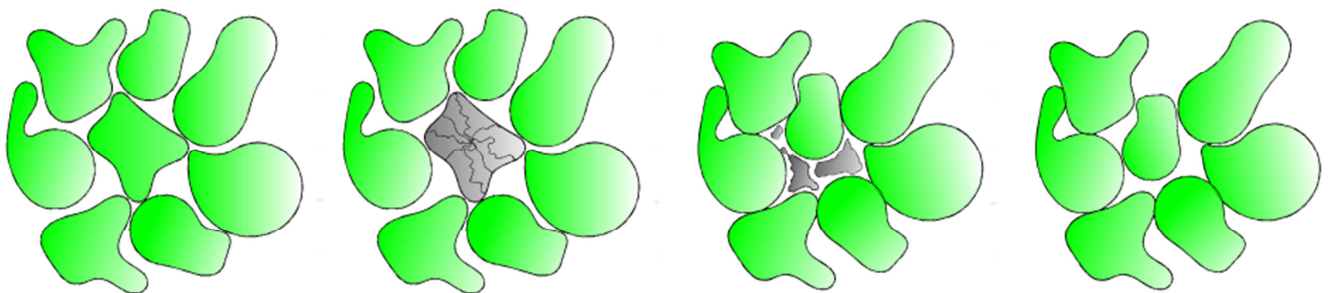
### PART III

Improving the mass-spring model: mass-spring systems can be enriched in order to enlarge their range of applicability to granular materials.

Indeed, if the springs are always in place, the model is able to just account for small deformations around a configuration in which grains are pre-compressed.

Instead, if one includes the possibility that both linear and rotational springs disappear as a consequence of the deformation, the model can account for a larger class of kinematic behaviours, including cases in which the contact inter-grain interaction is lost.

#### Destruction of a grain:



#### Losing interactions leads to a second gradient model

The homogenised limit of a lattice system in which all first neighbours are interacting is a classical Cauchy continuum model.

It is interesting to notice that, whether interactions are lost in a certain (selective) way, what remains has a homogenised limit which is a pantographic second gradient continuum model [8].

## References

- [1] Kuhn, T. S., & Hawkins, D. (1963). The structure of scientific revolutions. *American Journal of Physics*, 31(7), 554-555.
- [2] dell'Isola, F., Maier, G., Perego, U., Andraus, U., Esposito, R., & Forest, S. (2014). *The complete works of Gabrio Piola: volume I*. Cham, Switzerland: Springer.
- [3] Price, D. J. D. S. (1959). Contra-Copernicus: A critical re-estimation of the mathematical planetary theory of Ptolemy, Copernicus, and Kepler. *Critical problems in the history of science*, 197-218.
- [4] Lattis, J. M. (2010). Between Copernicus and Galileo: Christoph Clavius and the collapse of Ptolemaic cosmology. *University of Chicago Press*.
- [5] Misra A, Jiang H. Measured kinematic fields in the biaxial shear of granular materials. *Computers and Geotechnics* 1997;20:267-85; Doi 10.1016/S0266-352x(97)00006-2.
- [6] Misra A, Poorsolhjouy P. Identification of higher-order elastic constants for grain assemblies based upon granular micromechanics. *M&MoCS* 2015;3:285-308;
- [7] Turco E, Rizzi NL. Pantographic structures presenting statistically distributed defects: numerical investigations of the effects on deformation fields. *Mechanics Research Communications* 2016;77:65-9
- [8] Turco, E., Dell'Isola, F., Cazzani, A., & Rizzi, N. L. (2016). Hencky-type discrete model for pantographic structures: numerical comparison with second gradient continuum models. *Zeitschrift für angewandte Mathematik und Physik*, 67(4), 1-28.

## List of participants

ACHOUR	Mohamad	mohamad.achour@eleves.ec-nantes.fr	GeM
AIT MOKHTAR	Karim	karim.ait-mokhtar@univ-lr.fr	LASIE
ALAM	Yasir	Syed-Yasir.Alam@ec-nantes.fr	GeM
ALONSO	Eduardo	eduardo.alonso@upc.edu	Universitat Polytecnica de Catalunya
AMIRI	Ouali	ouali.amiri@univ-nantes.fr	GeM
BUI	Tuan Anh	Tuan-Anh.Bui@univ-nantes.fr	GeM
DAOUADJI	Ali	ali.daouadji@insa-lyon.fr	SMS-ID
DARVE	Félix	felix.darve@3sr-grenoble.fr	3SR
DELL' ISOLA	Francesco	fdellisola@gmail.com	Universita di Roma
DESRUES	Jacques	jacques.desrues@3sr-grenoble.fr	3SR
DINÇ	Ozge	saziye-ozge.dinc@univ-lorraine.fr	ENSG
FROIIO	Francesco	francesco.froiio@ec-lyon.fr	Ecole Centrale de Lyon
GRONDIN	Frédéric	frederic.grondin@ec-nantes.fr	GeM
HATTAB	Mahdia	mahdia.hattab@univ-lorraine.fr	LEM3
HICHER	Pierre-Yves	pierre-yves.hicher@ec-nantes.fr	GeM
HILLOULIN	Benoit	benoit.hilloulin@ec-nantes.fr	GeM
HU	Lianxin	lianxin.hu@insa-lyon.fr	SMS-ID
HUANG	Shun	shun-s.huang@edf.fr	EDF
JRAD	Mohamad	mohamad.jrad@univ-lorraine.fr	LEM3
KY	Sambath	Sambath.Ky@insa-rennes.fr	LGCGM
LEVIN	Friedrich	friedrich.levin@tum.de	TU Munchen
LI	Xia	Xia.Li@nottingham.ac.uk	University of Nottingham
LOUKILI	Ahmed	Ahmed.Loukili@EC-Nantes.fr	GeM
LUU	Li-Hua	li-hua.luu@irstea.fr	IRSTEA
MAROT	Didier	didier.marot@univ-nantes.fr	GeM
MARTINEZ	Juan	Juan.Martinez@insa-rennes.fr	LGCGM
MILLET	Olivier	olivier.millet@univ-lr.fr	LASIE
NGYUEN	Ngoc-Son	ngocson.nguyen@univ-nantes.fr	GeM
NICOT	François	Francois.Nicot@irstea.fr	IRSTEA
SANAHUJA	Julien	julien.sanahuja@edf.fr	EDF
SCHOLTÈS	Luc	luc.scholtes@univ-lorraine.fr	ENSG
SCIARRA	Giulio	giulio.sciarra@ec-nantes.fr	GeM
SELVADURAI	Patrick	patrick.selvadurai@mcgill.ca	McGill University
SIBILLE	Luc	luc.sibille@3sr-grenoble.fr	3SR
SILVANI	Claire	claire.silvani@insa-lyon.fr	SMS-ID
SOIVE	Anthony	anthony.soive@ec-nantes.fr	GeM/CEREMA
SOULI	Hanène	hanene.souli@enise.fr	ENISE
VEYLON	Guillaume	guillaume.veylon@irstea.fr	IRSTEA
WAN	Richard	wan@ucalgary.ca	University of Calgary
WAUTIER	Antoine	antoine.wautier@irstea.fr	IRSTEA
YANG	Jie	jie.yang@eleves.ec-nantes.fr	GeM
YIN	Zhenyu	zhenyu.yin@ec-nantes.fr	GeM
ZHANG	Yuqi	yuqi.zhang@univ-lorraine.fr	LEM3
ZHAO	Chaofa	chaofa.zhao@ec-nantes.fr	GeM